

# **Electrochemical deposition of Graphene Oxide- metal nano-composite on Pencil-Graphite Electrode for the high sensitivity detection of Bisphenol A by Adsorptive Stripping Differential Pulse Voltammetry**

A thesis submitted in fulfillment of the requirements for the degree of

**Master Science in Nanoscience (Chemistry)**

Department of Chemistry: SensorLab

University of the Western Cape

The logo of the University of the Western Cape, featuring a stylized classical building with columns and a pediment, with the text 'UNIVERSITY of the WESTERN CAPE' below it.  
UNIVERSITY of the  
WESTERN CAPE

Supervisor: Prof. N. Jahed

Co-supervisor: Prof. E. I. Iwuoha

By

**Nastaran Ghaffari**

BSc (Hons) Chemistry (University of the Western Cape)

# KEY WORDS:

Differential Pulse Voltammetry

Pencil Graphite Electrode

Graphene

Nanocomposite

Bisphenol A

Electrodeposition



## ABSTRACT

Electrochemical platforms were developed based on pencil graphite electrodes (PGEs) modified electrochemically with reduced graphene oxide metal nanoparticles (ERGO–metalNPs) composite and used for the high-sensitivity determination of Bisphenol A (BPA) in water samples. Synergistic effects of both reduced Graphene Oxide sheets and metal nanoparticles on the performance of the pencil graphite electrode (PGE) were demonstrated in the oxidation of BPA by differential pulse voltammetry (DPV). A solution of graphene oxide (GO) 1 mg mL<sup>-1</sup> and 15 ppm of metal stock solutions (1,000 mg L<sup>-1</sup>, atomic absorption standard solution) (Antimony or Gold) was prepared and after sonication deposited onto pencil graphite electrodes by cyclic voltammetry reduction. Different characterization techniques such as FT-IR, HR-SEM, XRD and Raman spectroscopy were used to characterize the GO and ERGO–metalNPs. Parameters that influence the electroanalytical response of the ERGO–SbNPs and ERGO–AuNPs such as, pH, deposition time, deposition potential, purging time were investigated and optimized. Well-defined, reproducible peaks with detection limits of 0.0125 μM and 0.062 μM were obtained for BPA using ERGO–SbNPs and ERGO–AuNPs respectively. The rGO-metalNPs–PGE was used for the quantification of BPA in tap water sample and proved to be suitable for the detection of BPA below USEPA prescribed drinking water standards of 0.087 μM.

# DECLARATION

I declare that the study **“Electrochemical deposition of Graphene Oxide- metal nano-composite on Pencil-Graphite Electrode for the high sensitivity detection of Bisphenol A by Adsorptive Stripping Differential Pulse Voltammetry”** has not been submitted for any degree or examination in any university and is my own work.

Nastaran Ghaffari

April 2018





# ACKNOWLEDGEMENTS

Firstly I would like to thank God the Almighty for endless opportunities, encouragement and strength he provided for me.

I would like to express my sincere gratitude to my supervisor Prof. Nazeem Jahed for the continuous support of my Masters study, for his guidance, patience, endless insight and motivation. I could not have imagined having a better supervisor and mentor for this study. Without his precious support it would not be possible to conduct this research.

I would like to extend my gratitude to Prof. Emmanuel Iwuoha and SensorLab members as well as UWC Chemistry Department Staff for the opportunity and trust placed in me.

My sincere thanks also goes to Keagan Pokpas for his insightful comments and encouragement. His guidance helped me in all the time of research and writing of this thesis.

Last but not the least, I would like to thank my family: my parents and to my sister and her husband, Amir Afrogheh for all the sacrifice, encouragement, and supporting me throughout writing this thesis and my life in general. Without them this accomplishment would not have been possible.

# TABLE OF CONTENTS

KEYWORDS

ABSTRACT

DECLARATION

ACKNOWLEDGMENT

TABLE OF CONTENTS

LIST OF ABBREVIATIONS

**CHAPTER ONE:** Introduction to the study

1.1. Problem Statement

1.1.1. Bisphenol A Toxicity

1.1.2. Environmental Monitoring

1.2. Motivation of the Study

1.3. Objectives

1.4. Research Questions

1.5. Hypothesis

1.6. Research Approach

1.7. Scope and Delimitations

1.8. Thesis Outline

1.8.1. Chapter One: Introduction to the study



- 1.8.2. Chapter Two: Literature review
- 1.8.3. Chapter Three: Experimental approach
- 1.8.4. Chapter Four: Morphological and Structural Characterization of Graphene and reduced Graphene Oxide- metal nano-composite
- 1.8.5. Chapter Five: Batch preparation of ERGO-Metal NPs-PGE
- 1.8.6. Reduced Graphene Oxide metal nanoparticles Pencile Graphite Electrode (rGO–metalNPs-PGE)
- 1.8.7. Chapter Six: Conclusion and Future Work

**CHAPTER TWO:** Literature Review

- 2.1. Introduction
- 2.2. Electrochemical Techniques for BPA Detection
  - 2.2.1. General Basis of Voltammetry
  - 2.2.2. Common Voltammetric Techniques
    - 2.2.2.1. Cyclic Voltammetry
    - 2.2.2.2. Differential Pulse Voltammetry
- 2.3. Pre-concentration Voltammetry Techniques (Stripping Voltammetry)
  - 2.3.1. Anodic Stripping Voltammetry
  - 2.3.2. Cathodic Stripping Voltammetry
  - 2.3.3. Adsorptive Stripping Voltammetry
- 2.4. Bisphenol A

## 2.5. Nanoscience

## 2.6. Graphene

### 2.6.1. Carbon Allotropes

### 2.6.2. Introduction of Graphene

### 2.6.3. Discovery of Graphene

### 2.6.4. Structure of Graphene

### 2.6.5. Properties of Graphene

#### 2.6.5.1. Electrical Properties of Graphene

#### 2.6.5.2. Optical Properties of Graphene

#### 2.6.5.3. Mechanical Properties of Graphene

### 2.6.6. Synthesis of Graphene

### 2.6.7. Applications of Graphene

## 2.7. Metal Nanoparticles

### 2.7.1. Antimony Nanoparticles

### 2.7.2. Gold Nanoparticles

### 2.7.3. Nanomaterial electrochemical sensors for bisphenol A (BPA) detection

## 2.8. Pencil Graphite Electrodes

## 2.9. Characterization Techniques

### 2.9.1. Fourier Transformed- Infrared (FT-IR) Spectroscopy

- 2.9.2. X-ray Diffraction (XRD)
- 2.9.3. Raman Spectroscopy
- 2.9.4. High Resolution Scanning Electron Microscopy (HRSEM)
- 2.10. Summary

### **CHAPTER THREE:** Experimental Approach

- 3.1. Introduction
- 3.2. Apparatus
- 3.3. Reagents
- 3.4. BPA Solution
- 3.5. Phosphate buffer solution (Electrolyte solution)
- 3.6. Acetate buffer solution
- 3.7. Nitric acid solution
- 3.8. Hydrochloric acid solution
- 3.9. Synthesis of Graphene Oxide (GO)
- 3.10. Preparation of graphene oxide metal nanoparticles (GO–MetalNPs) nanocomposite solution for electrochemical reduction
- 3.11. Preparation of pencil graphite electrodes (PGE)
- 3.12. Preparation of the multiple electrochemically reduced graphene oxide metal nanoparticles pencil graphite electrode (ERGO-MetalNPs-PGE)
- 3.13. Procedure DPV analyses



- 3.14. Quantitation
- 3.15. Sample preparation
- 3.16. Characterization techniques
  - 3.17.1. Fourier Transformed- Infrared (FT-IR) Spectroscopy
  - 3.17.2. X-ray Diffraction (XRD)
  - 3.17.3. Raman Spectroscopy
  - 3.17.4. High Resolution Scanning Electron Microscopy (HRSEM)

**CHAPTER FOUR:** Morphological and Structural Characterization of Graphene and reduced Graphene Oxide- metal nano-composite

- 4.1. Introduction
- 4.2. Fourier Transformed- Infrared (FT-IR) Spectroscopy
- 4.3. Raman Spectroscopy
- 4.4. X-ray Diffraction (XRD)
- 4.5. High Resolution Scanning Electron Microscopy (HRSEM)

**CHAPTER FIVE:** Batch preparation method of electrochemically reduced graphene oxide –metal nanoparticles pencil graphite electrodes (ERGO-Metal NPs-PGEs)

- 5.1. Reproducibility
- 5.2. Conclusion

**CHAPTER SIX: Reduced Graphene Oxide Metal Nanoparticles Pencil Graphite Electrode (rGO–MetalNPs-PGE)**

6.1. Introduction

6.2. Effect of different ERGO-MetalNPs nanocomposite surface on electrochemical oxidation of BPA

6.3. Electrochemically reduced graphene oxide antimony nanoparticles pencil graphite electrode (ERGO-SbNPs-PGE)

6.3.1. Influence of the electrodeposition method of GO-SbNPs onto the PGE

6.3.2. Influence of the number of GO-SbNPs electrodeposition cycles

6.3.3. Effect of the concentration of the antimony

6.3.4. The effect of the electrodeposition time of GO-SbNPs

6.3.5. Microscopic Characterization of Electrodeposited Graphene- SbNPs Modified Pencil Electrode ERGO-SbNPs-PGE

6.3.6. Antimony nanoparticles on the ERGO-SbNPs-PGE

6.3.7. Electrochemical characterization of ERGO-SbNPs-PGE in Ferrocyanide solution

6.3.7.1. Impedimetric analysis

6.3.7.2. Electrochemical improvement of the pencil graphite electrode after the modification

6.3.7.3. The effect of scan rate

6.3.8. The synergetic effect of graphene sheets and antimony nanoparticles in electrochemical response of BPA

6.3.9. The fouling effect of BPA

6.3.10. Electrochemically cleaning of the ERGO-SbNPs-PGE in PBS

6.3.11. Reproducibility

6.3.12. Preconcentration time optimization

6.3.13. Effect of scan rate on the electrocatalytic oxidation of BPA at ERGO-SbNPs-PGE

6.3.14. pH optimization

6.3.15. Interference studies

6.3.16. Detection limit

6.3.17. Analytical application of ERGO-SbNPs-PGE

6.4. Electrochemically reduced graphene oxide gold nanoparticles pencil graphite electrode (ERGO-AuNPs-PGE)

6.4.1. Electrochemical characterization of ERGO-AuNPs-PGE in Ferrocyanide solution

6.4.2. Impedimetric analysis

6.4.3. The effect of scan rate

6.4.4. Influence of the number of GO-AuNPs electrodeposition cycles



- 6.4.5. Effect of the concentration of the gold
- 6.4.6. The effect of the electrodeposition time of GO-AuNPs
- 6.4.7. Microscopic Characterization of Electrodeposited Graphene- AuNPs Modified Pencil Electrode (ERGO-AuNPs-PGE)
- 6.4.8. Effect of the ERGO-AuNPs nanocomposite surface on electrochemical oxidation of BPA
- 6.4.9. Pre-concentration time optimization
- 6.4.10. Effect of scan rate on the electrocatalytic oxidation of BPA at ERGO-AuNPs-PGE
- 6.4.11. pH optimization
- 6.4.12. Interference studies
- 6.4.13. Detection Limit
- 6.4.14. Analytical application of ERGO-AuNPs–PGE



## 6.5. Conclusion

## **CHAPTER SEVEN: Conclusion and Future Work**

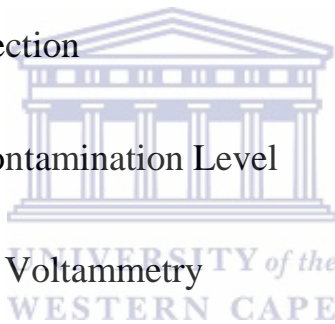
## Bibliography

# LIST OF ABBREVIATIONS

2D	Two Dimensional
3D	Three Dimensional
ABS	Acetate Buffer Solution
AdDSV	Adsorptive Stripping Voltammetry
AE	Auxiliary Electrode
ASV	Anodic Stripping Voltammetry
ATR	Attenuated Total Reflectance
BPA	Bisphenol A
CE	Counter Electrode
CNT	Carbon Nanotube
CSV	Cathodic Stripping Voltammetry
CV	Cyclic Voltammetry
*CVD	Chemical Vapor Deposition
D.L.	Detection Limit

*DNA	Deoxyribonucleic Acid
*DPP	Differential Pulse Polarography
DPV	Differential Pulse Voltammetry
DPSV	Differential Pulse Stripping Voltammetry
EC	Electrochemical
EDCs	Endocrine Disrupting Chemicals
*EDS	Energy Dispersive X-Ray Spectroscopy
EG	Electrodeposited Graphene
*EPA	Environmental Protective Agency
Eqn.	Equation
*FAAS	Flame Atomic Absorption Spectrophotometry
*FET	Field-Effect Transistor
FT_IR	Fourier Transformed Infrared
GCE	Glassy Carbon Electrode
GE	Gold Electrode

GFAAS	Graphite Furnace Atomic Absorption Spectroscopy
GO	Graphene Oxide
HRSEM	High Resolution Scanning Electron Microscopy
*ICP	Inductively Coupled Plasma Spectroscopy
*ICP-MS	Inductively Coupled Plasma Mass Spectroscopy
*ICP-OES	Inductively Coupled Plasma Optical Emission Spectroscopy
L.O.D	Limit of Detection
*MCL	Maximum Contamination Level
NPV	Normal Pulse Voltammetry
PG	Pencil Graphite
PGE	Pencil Graphite Electrode
PBS	Phosphate Buffer Solution
ppb	Parts Per Billion
ppm	Parts Per Million
RE	Reference Electrode



ERGO–SbNPs-PGE Electrochemically reduced Graphene oxide Antimony  
Nanoparticles Pencil Graphite Electrode

ERGO–AuNPs-PGE Electrochemically reduced Graphene oxide Gold  
Nanoparticles Pencil Graphite Electrode

RSD Relative Standard Deviation

\*SECM Scanning Electrochemical Microscopy

SV Stripping Voltammetry

SW Square Wave

SWASV Square Wave Anodic Stripping Voltammetry

\*SWCNT Single Wall Carbon Nanotube

SWV Square Wave Voltammetry

\*US United States

\*USEPA United States Environmental Protection Agency

WE Working Electrode

XRD X-ray Diffraction

# CHAPTER ONE

## Introduction to the Study

### 1.1. Problem Statement

#### 1.1.1. Bisphenol A Toxicity

A wide range of substances, both natural and man-made, that can exhibit hormone-like properties, may interfere with the body's endocrine system. These substances that are man-made can alter the functions of endocrine system and consequently increases the risk of adverse health effects are generally called endocrine disruptors. A plethora of reports has demonstrated in the past two decades that sub- $\mu\text{g/L}$  concentrations of endocrine disrupting chemicals (EDCs) are ubiquitous contaminants in wastewater effluents [1].

Bisphenol A (BPA), a major industrial chemical is being used in a huge number of industrial processes; for example it is a commonly used raw material in the production of epoxy resins, polycarbonate plastics, and coatings which are used in food packaging, etc [2,3]. Most phenolic compounds like BPA are toxic and can be present in the environment due to the degradation products of plastics or manufacturing processes [4–6]. As regards toxicity, BPA has been identified as an endocrine disruptor that can cause negative effects on the functioning of the endocrine system of humans and wildlife by mimicking oestrogen, a female hormone that is directly linked to development, reproduction and growth of humans [7–9]. A correlation was found between BPA and an increase in cancer rate, heart diseases, a decrease in semen quality, diabetes, reduce immune function and elevation of levels of some serum liver enzymes.

## 1. 1. 2. Environmental Monitoring

A considerable increase in the demand for clean water as the most essential natural resource for guaranteeing the basic quality of human life have been evident for some time. In order to secure wastewater treatment and product quality the water policies need to be focused on automatic monitoring and continuous surveillance aspects. Chinese Health Standard (GB 13116-91, GB 14942-94) has set a maximum contamination level of  $0.05 \text{ mg kg}^{-1}$  of BPA to protect water quality and human health [10].

Nowadays, there is a growing interest in the development of methodologies for detection, remediation and quantification of endocrine disruptors such as BPA among environmental communities. The determination of BPA has mostly been carried out using either high-performance liquid chromatography (HPLC), fluorimetry or gas chromatography-mass spectrometry (GC-MS) techniques [4,5,11]. However, these methods are expensive, need qualified staff, and time-consuming. BPA can be determined by electrochemical sensors thanks to its two electrochemical-active phenolic hydroxyl groups. As a result, electrochemical methods are very promising in determination of BPA due to their excellent sensitivity, fast response time, low power consumption, automation, and low cost equipment. However, direct determination of BPA using bare electrodes is difficult because of the relatively high oxidation potential of phenolic compounds and poor response of traditional electrochemical sensors to BPA. Moreover, the electrochemical oxidation analyte molecules containing phenolic groups may inactivate the electrode surface as the result of the deposition of electropolymerization films and this drawback is a challenge for the BPA determination because it contains two phenolic moieties [12]. To overcome these limitations, novel sensing materials and modification of electrode surfaces using different approaches have been investigated recently.

## 1.2. Motivation to the study

One analytical technique which has shown to be capable of meeting the demand of determining bisphenol A is that of electrochemical stripping voltammetry [13]. Electrochemical stripping voltammetry is a powerful technique for the measurement of BPA at trace and ultratrace concentration levels due to the inherent preconcentration step, relative simplicity, low-cost instrumentation and possibility of system integration and miniaturization. In particular, adsorptive stripping voltammetry (AdSV) is one of the most useful methods in this field due to its capability of electrolytically accumulating bisphenol A at the surface of an appropriate electrode, resulting in high sensitivity and low detection limits [14].

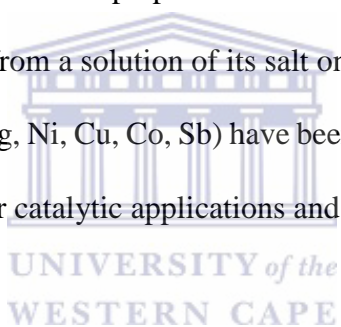
A crucial factor in assuring a favorable performance in an AdSV procedure is to find a suitable material for the working electrode. Carbon based solid materials has been utilized as an electrode substrate material in different applications due to their wide potential window and low background current [15]. The pencil graphite electrode (PGE) as a new type of carbon electrode has been used in numerous electroanalytical applications in recent years [16,17]. Pencil-graphite electrode (PGE) offers many attractive features compare to other carbon-based electrodes such as good electroconductivity, low cost, no need for time-consuming pretreatments, disposability, low background current, and availability [18]. The electrochemical reactivity and surface area of a PGE can be easily improved by surface modification and electrochemical treatments [19]. To eliminate the fouling effect from the oxidation of BPA, single-use pencil graphite electrode can be used as an alternative to the modified and unmodified glassy carbon electrodes.

The use of graphene and reduced graphene oxide as a material to modify carbon based electrodes has attracted lots of attention due to its intrinsic properties such as high surface area, high



mechanical strength, excellent conductivity, and ease of functionalization [20,21]. Graphene-based electrodes exhibit superior detection properties as chemical and biological sensors for environmental analysis [18]. Graphene oxide can be directly electrochemically reduced onto the electrode surface to develop a highly sensitive working electrode for determination of BPA using AdSV.

Metal nanoparticles have been incorporated to improve the sensitivity for bisphenol A analysis. The catalytic properties of metal-nanoparticles make them suitable for catalyzing the redox process of some molecules with analytical interest which can be studied using electroanalytical methods [22]. An increasingly attractive route for the preparation of metal-nanoparticles modified electrode is the electrodeposition of a metal from a solution of its salt onto the electrode surface [23]. Some metal-nanoparticles (e.g., Au, Pt, Ag, Ni, Cu, Co, Sb) have been the subject of innumerable studies in producing electrode materials for catalytic applications and electrochemical biosensing.



### 1.3. Objectives

The objectives of this project are:

- To investigate and understand the differential pulse adsorptive stripping voltammetry technique
- To synthesize graphene oxide and characterize it using FT-IR, Raman spectroscopy and XRD
- To electrochemically reduce graphene oxide-metal nanocomposite onto pencil graphite to give the ERGO-MetalNPs-PGE
- To investigate the ERGO-MetalNPs-PGE responses towards BPA

- To optimize instrumental parameters and determine the analytical parameters of the ERGO-MetalNPs-PGE for BPA determination
- To develop an analytical procedure for the determination of BPA in water samples using the ERGO-MetalNPs-PGE

## 1.4. Research Questions

- Would pencil graphite electrodes be suitable for use in bisphenol A analysis?
- Would coating of the electrode with electrochemically reduced graphene oxide-metal nanocomposite improve electrode sensitivity for BPA determination?

## 1.5. Hypothesis

It is possible to modify the PGE electrochemically for the first time with reduced graphene oxide metal nanoparticles (rGO–MetalNPs) composite to have high-sensitive single use rGO–MetalNPs-PGE for determination of BPA in water samples using differential pulse adsorptive stripping voltammetry (AdSV). The study will introduce a very simple electrochemically method to modify PGE as a cheap decomposable electrode with nanocomposite.

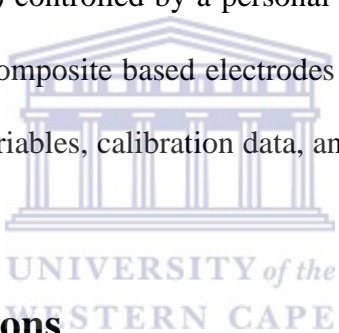
## 1.6. Research Approach

Experiments were designed to understand the effect of:

- Methods of Graphene synthesis;
- Coating techniques of PGEs;
- Instrumental parameters on stripping voltammetry process;
- Electrochemically reduced Graphene-Metal nanocomposite pencil graphite electrodes for improved sensitivities and detection limits towards Bisphenol A;

- Standard addition method on recovery studies;
- Real samples analysis of electrochemically reduced Graphene-Metal nanocomposite pencil graphite electrodes.

In this study, real water sample was collected from tap water from Bellville Municipality area in Cape Town South Africa and graphite powder was obtained from Sigma-Aldrich. The quality of synthesized graphene was evaluated using morphological and structure characterization techniques including FT-IR, Raman spectroscopy, XRD and HRSEM. Differential pulse adsorptive stripping voltammetric measurements were performed using 797 VA COMPUTRACE instrument (Metrohm, Switzerland) controlled by a personal computer to evaluate the enhanced detection of graphene-metal nanocomposite based electrodes towards the detection of bisphenol A. Investigation of instrumental variables, calibration data, and real water samples was led to this evaluation.



## **1.7. Scope and Delimitations**

The study involves the synthesis of starting reagents obtained from Sigma Aldrich and using the tap water of Bellville Municipal region in Cape Town, South Africa. Bisphenol A was investigated using water samples.

The cost effective and environmentally friendly pencil-graphite can show an increasing improvement in the sensitivity towards bisphenol A at parts per billion range when it coated with graphene-metal nanocomposite providing good results during voltammetry in the tap water samples.

The pencil graphite electrodes were *Pentel* 0.5 mm HB black lead with HI polymer as they show good stability and reproducibility.

To produce good quality and reproducible graphene- metal nanocomposite pencil graphite electrodes without the need for inexpensive instrumentation electrochemical synthesis approach were applied.

## **1.8. Thesis Outline**

The thesis to follow includes six chapters which cover various aspects of the work.

### **1.8.1. Chapter One: Introduction to the study**

A brief introduction to the toxicity and detection of bisphenol A as an endocrine disrupter has provided in the chapter one. Moreover, the motivation of utilized techniques in the study, main objectives, scope and delimitation, research approach and hypothesis were discussed.

### **1.8.2. Chapter Two: Literature review**

Chapter two provides a comprehensive survey of relevant literature to the study. Literature on the development of cost effective electrode alternatives have been reviewed with emphasis on the choice of materials, analytical techniques and applications of the graphene-metal nanocomposite pencil-graphite electrode with consideration to many parameters, like, the sensitivity, environmental impact, detection limit, peak height, deposition time, potential, electrode rotation speed, etc. The review is concluded to a summary which will help to understand the reasons behind every decision that has been made in this study.

### **1.8.3. Chapter three: Experimental Approach**

The equipment and techniques that have been applied in the work has outlined in chapter three. Sample preparation and detailed descriptions of sample collection are provided as well as synthesis, characterization, and protocols for analysis are highlighted.

### **1.8.4. Chapter four: Morphological and Structural Characterization of Graphene and reduced Graphene Oxide- metal nano-composite**

The morphological and structural changes along the chemical synthesis routs of graphite, graphene oxide and graphene-metal nanocomposite demonstrated in chapter four. The formation of good quality few-layer reduced graphene oxide-metal nano- composite as sensing platform for the determination of bisphenol A was investigated using spectroscopic and microscopic techniques.

### **1.8.5. Chapter five: Batch preparation of ERGO-Metal NPs-PGE**

Chapter five introduces a multiple prepared electrochemically reduced graphene oxide metal nanoparticles pencil graphite electrode. The preparation steps of multiple ERGO-MetalNPs-PGE is demonstrated. The advantages of multiple preparation of ERGO-MetalNPs-PGE is discussed.

### **1.8.6. Chapter six: Reduced Graphene Oxide Metal Nanoparticles Pencil Graphite Electrode (rGO–MetalNPs-PGE)**

Chapter six provides results and discussion related to reduced graphene oxide metal nanoparticles pencil graphite electrode (rGO–MetalNPs-PGE). The characterization of electrochemical and microscopic aspects of the rGO–MetalNPs-PGE is demonstrated. The concept is proved by

conducting recovery studies and calibration curves on known concentration of test solutions. The potential and suitability of ERGO-MetalNPs-PGE for real water sample analysis is shown.

### **1.8.7. Chapter seven: Conclusion and Future Work**

In this chapter results and discussion verify the hypothesis of this study. Conclusions and future work arising from the results of the work is specified.



# CHAPTER TWO

## Literature Review

### 2.1. Introduction

This chapter introduces the materials utilized for the application and preparation of electrochemical sensors for the determination of bisphenol A. It focuses on the use of nanocomposites specifically graphene-metal nanocomposites and various electroanalytical techniques for enhanced modified sensors.



### 2.2. Electroanalytical Techniques for Bisphenol A Detection

#### 2.2.1. General Basis of Voltammetry

Electrochemical techniques are of a great interest to researchers for detection of several analytes (organic and inorganic) as they offer good sensitivity, cheap instrumentation, rapid measurements, and a wide linear concentration range [24]. Voltammetry is a section of electrochemistry developed from the discovery of polarography, which is a class of voltammetry where a hanging mercury drop is the working electrode discovered in 1922 by the Czech chemist Jaroslav Heyrovsky. Voltammetric techniques monitor the current resulting from an applied potential difference between electrodes [25–27].

Voltammetry measurements are performed in an electrochemical cell consists of a working electrode (WE), reference electrode (RE), auxiliary electrode or counter electrode (AE or CE) and a non-reactive electrolyte (Figure 2.1) [28]. The working electrode, at which the oxidation and reduction of analyte under investigation occurs offers the surface for electron transfer [29]. The reference electrode which is usually the silver/silver chloride (Ag/AgCl) or the saturated calomel electrode (SCE) is kept under constant potential to measure the working electrode potential [29]. The counter electrode which is commonly made of noble metals or carbon/ graphite, makes an electrical connection to the electrolyte to act as a counter reaction to the working electrode [25].

Voltammetric analysis determines the quantity of various compounds by applying a potential to the working electrode that changes the concentration of the electroactive species at the electrode surface. The change in concentration of the analyte will result in the mass transport and current to occur [25].

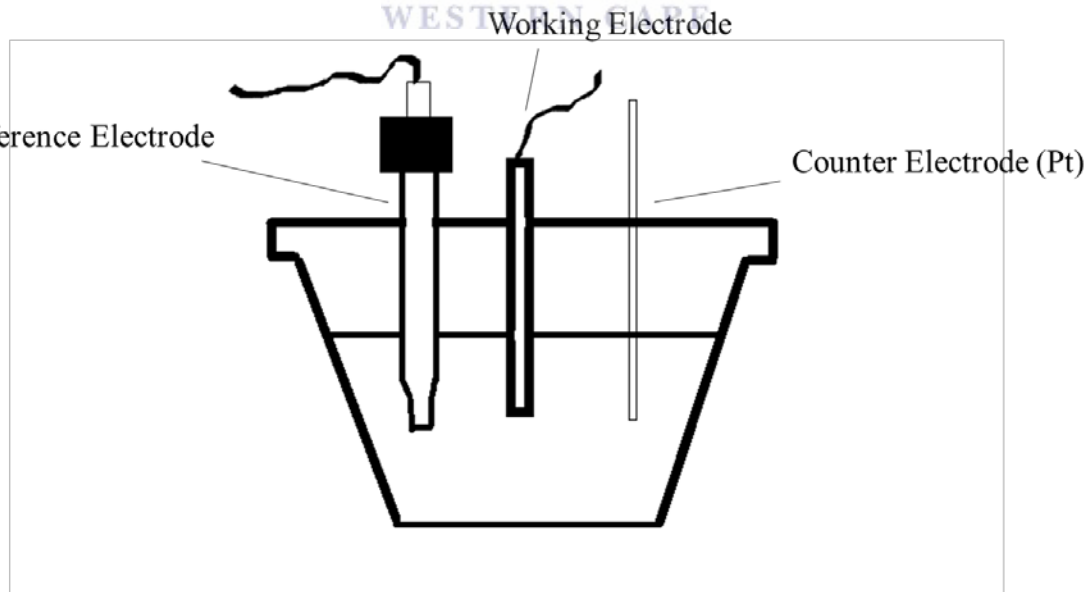


**Figure 2.1:** Three electrode system for voltammetry



## **2.2.2. Common Voltammetric Techniques**

This section provides a brief discussion of a wide range dynamic voltammetric techniques that have been developed to overcome various limiting factors of voltammetry including pulse methods, cyclic voltammetry as well as different pre-concentration methods.

### **2.2.2.1. Cyclic Voltammetry**

Cyclic voltammetry is a suitable electroanalytical technique for providing information of both oxidation and reduction half-cell reactions [28]. The potential start from an initial potential and the direction of the potential scan reverses after ramping the potential to the switching potential. The forward part of the CV is oxidation if the potential is scanned from negative values. The type of electrode reaction and the number transfer electrons can be concluded by the shape of the cyclic voltammograms [28]. Reversible and irreversible reactions have equal and unequal oxidation and reduction peaks, respectively. The peak current increases with increasing the concentration of the analyte [30].

### **2.2.2.2. Differential Pulse Voltammetry**

Differential pulse voltammetry (DPV) technique uses a series of potential pulses in which each potential pulse is fixed of small amplitude (10 to 100 mV) and is superimposed on a staircase-wave form [25]. The current measurement is made at two points for each pulse, before and after the application of each pulse; this differences are plotted against the base potential. DPV offers enhanced sensitivity due to its slow scan rate which makes it attractive for analysis where long

deposition time is required [29]. Inexpensive instrumentation and improved signal-to-background response makes it a suitable measurement technique [31].

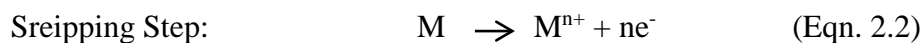
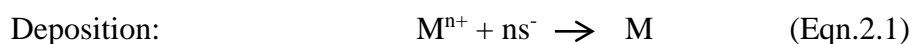
### **2.3. Pre-concentration Voltammetric Technique (Stripping Voltammetry)**

Stripping voltammetry technique aims to determine ultra-low levels of trace analyte in order to provide lower detection limits, good selectivity and good sensitivity. The ability of multi-element analysis, available instrumentation, very low detection limit, *in-situ* applications, small size, and a low power demand make the stripping technique a quick and robust technique [32]. The stripping voltammetry analysis consists of three steps as following: the deposition or pre-concentration step, the equilibrium step or rest period, and the stripping step [33].

The accumulation of the analyte onto the working electrode occurs by applying a constant potential for a definite time under reproducible hydrodynamic condition at the pre-concentration step [34]. During the accumulation step the solution is stirred at a fixed rate so that more analyte concentrate onto the working electrode. In the second step, the stirring is stopped and a rest period is employed to allow the homogeneous dispersal of the analyte to occur and form a uniform concentration for the restoration of calm solution conditions to return. The final step (stripping step) involves re-oxidizing of the analyte from the working electrode back into solution [34]. The current observed during the stripping step is proportional to the concentration of the analyte. The basis of pre-concentration voltammetric techniques are as following: anodic stripping voltammetry (ASV), cathodic stripping voltammetry (CSV), adsorptive stripping voltammetry (AdSV) [34].

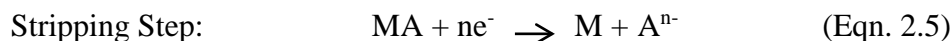
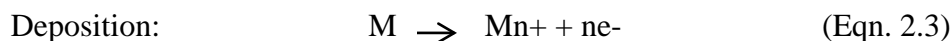
### 2.3.1. Anodic Stripping Voltammetry

Anodic stripping voltammetry (ASV) is one of the most sensitive voltammetric techniques commonly used in heavy metal detections. A negative potential is applied to reduce the analyte onto the working electrode followed by scanning in a positive direction to strip out anodically the analyte back into the solution [35]. Peak currents of subsequent voltammograms are related to the amount analyte present in the solution. The two-step mechanism is illustrated as follows:



### 2.3.2. Cathodic Stripping Voltammetry

Cathodic stripping voltammetry (CSV) is a very sensitive technique to use in a wide range of organic and inorganic compounds. The deposition potential in the CSV is opposite to the ASV procedure meaning the oxidizing potential of the analyte is applied to the working electrode at the accumulation step. Potential then sweeps positively to strip the oxidized species [35]. The deposited film is reduced into the solution when the potential scan in the negative direction. The mechanism can be represented as follows:



### 2.3.3. Adsorptive Stripping Voltammetry

The adsorptive stripping voltammetry (AdSV) is an extremely sensitive technique and is characterized by the non-electrolyte nature of the accumulation process; it can be used for the analysis of a wide variety of compounds where adsorption plays an important role in the pre-concentration step. The accumulated compound by adsorption will be oxidized or reduced if an appropriate potential is applied [36].

## 2.4. Bisphenol A

Bisphenol A [2,2-bis (4-hydroxyphenyl) propane, BPA] is an organic compound that widely used in the industrial manufacture of polycarbonate plastics and phenolic resins for coating of food and beverage containers, dental sealants and nursing bottles, optical lenses and powder paints. In vitro experiments, BPA leached into product has shown estrogenic activity and some antiandrogenic activity even at concentration as low as 1 ng/l level [13,37–39]. BPA as an endocrine disrupter can behave in a similar way to estrogen and other hormones in the human body making it possible to impact human health in various ways. BPA exposure can cause reproductive disorders and interfere with egg maturation and endocrine function of hypothalamus and the pituitary gland leading to infertility [3,7–9,40]. Findings suggest that even low-dose BPA exposure could trigger cardiovascular problems, including heart attack, coronary artery heart disease, hypertension, angina, and peripheral artery disease [40]. Researches have linked BPA exposure to insulin resistance and therefore diabetes type 2 [40]. Studies have shown that exposure to BPA before birth could increase the risk of breast, prostate, and other cancers [40]. Therefore, different analytical methods have been developed for determination of BPA.

To date, various methods have been developed for BPA detection, such as fluorimetry [41–43], high performance liquid chromatography (HPLC) [44–48], enzyme-linked immunosorbent assay (ELISA) [49], and gas chromatography coupled with mass spectrometry (GC/MS) [41,50,51]. These instrument-based techniques have high sensitivity and low detection limit, but they are expensive, complicated and time-consuming. In recent years, electrochemical methods have attracted considerable attention due to the advantages of their high sensitivity, cheap instrument, low cost, excellent selectivity, fast response, timesaving and simple operation. Furthermore, to enhance the sensitivity and selectivity often modifications have been applied on the bare electrode. For instance, glassy carbon electrode modified with gold nanoparticles, silk fibroin, and PAMAM dendrimers have been investigated for BPA determination [52]. Ling Zhou et al. prepared an electrochemical aptasensor based the electrochemical behavior of BPA on gold nanoparticles dotted graphene modified glassy carbon electrode for label-free detection of bisphenol A in milk with a low limit of detection of 5 nM [10]. Xiuli Niu et al. reported a novel electrochemical sensor of bisphenol A based on stacked graphene nanofibers/gold nanoparticles composite modified glassy carbon electrode with a visual detection limit of 30.5 nM [14]. Fernando C. Moraes et al. studied the effect of the surface organization with carbon nanotubes on the electrochemical detection of bisphenol A [53]. Lorena Athie Goulart et al. investigated the influence of the different carbon nanotubes on the development of electrochemical sensors for bisphenol A with a limit of detection of 84.0 nM [54]. Though some satisfactory results have been obtained, the fouling of electrode surface by BPA oxidation product is still a challenge for the BPA determination. To overcome these limitations, novel sensing materials and modification of electrode surfaces using different approaches have been investigated recently. For example, Ali Ozcan investigated the synergistic effect of lithium perchlorate and sodium hydroxide in the preparation of

electrochemically treated pencil graphite electrodes for selective and sensitive bisphenol A detection in water samples using singled used pencil electrodes [11]. Sujitra Poorahong et al. prepared amperometric sensor for detection of bisphenol A using a pencil graphite electrode modified with polyaniline nanorods and multi-walled carbon nanotubes [55].

## 2.5. Nanoscience

Recently, a great deal of attention has been place on nanotechnology and nanoscience as a popular area of science. Its application in a large number of fields has attracted many researchers from chemistry, physics, biotechnology, and engineering fields to dedicate a large amount of funding in public and private sectors to research in this science field [56]. Scientists use biomimetics to imitate the nanaomaterials naturally occurring in nature.

Nanotechnology is the science area where design, application, production and characterization of structures, materials and systems is taking place at the nanometer scale and dimension. Manipulating the size and structure of nanomaterials poses beneficial properties for a large number of applications.

The ultra-small size of materials and structures in nanotechnology enable it to deliver a range of important benefits such as modification and coating of surfaces with transparent, thin or minimal materials.

Size confinement, quantum mechanics and dominance of interfacial phenomena, are the intrinsic phenomena of nanoscale [57].

The quantum effects at the nanoscale are responsible for unique properties of nanostructures through four quantum mechanics:

- Quantum confinement: when the material is sufficiently small (less than 10 nm) the optical and electronic properties change due to the bandgap increase resulted from electrons and holes being squeezed into a critical quantum dimension called the exciton Bohr radius [58].
- Entanglement: the linkage of quantum effects of two or more objects meaning one cannot be described without mentioning of the other.
- Superposition: the mathematical probability of constructive and destructive interference waves overlapping each other.
- Discretization: particles can have only defined energy levels.

Two main approaches are used to synthesize nanomaterial: Top- down and bottom- up approaches.

Top- down: To make nanostructures materials are etched into bulk structures.

Bottom-down: in order to produce self- assembled nano-sized materials atomic and molecular building blocks are bringing together by non-covalent and covalent interactions [59].

## 2.6. Graphene

### 2.6.1. Carbon Allotrope

Carbon is one of the most fascinating elements in the periodic table. Carbon can exist in many different forms (allotropes). Some common examples of carbon allotropes are diamond, graphite, fullerene, graphene and carbon nanotubes, or CNTs. Due to the distinct properties of nanoscale forms of carbon, they have attracted lots of attention [60].

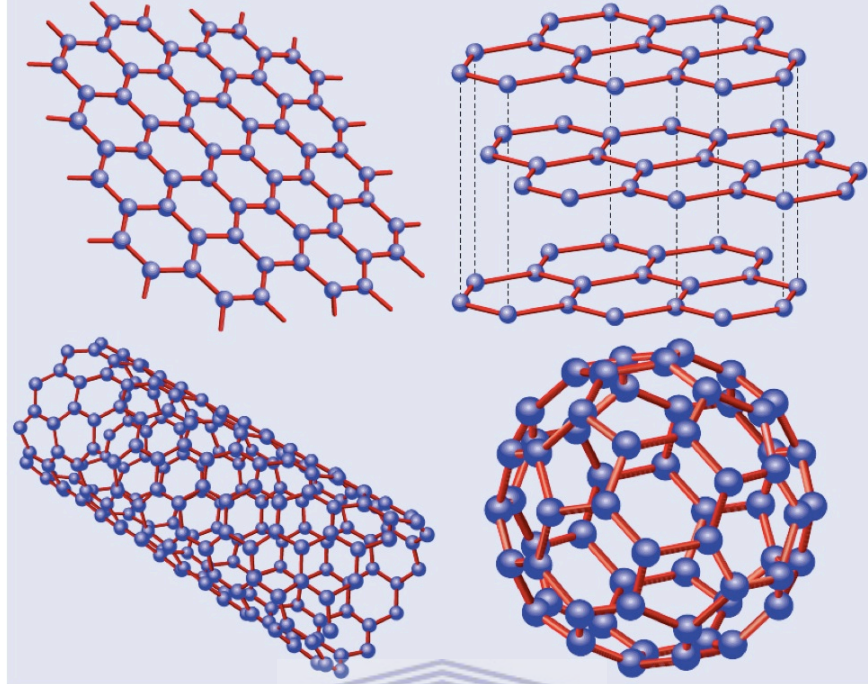


**Figure 2.2:** Structures of selected carbon allotropes[61].

### **2.6.2. Introduction to Graphene**

Graphite is the most common form of carbon, which consists of stacked hexagonal sheets of carbon held together by Van de Waals force. A single layer of graphite is what we call graphene. Graphene is two-dimensional allotrope of carbon with a number of remarkable properties such as, being stronger than steel and very stretchable and it also has very high thermal and electrical conductivity, which can make it a flexible conductor. These properties make it interesting for both fundamental studies and device applications [62,63]. Graphene's amazing properties as the lightest and strongest material, compared with its ability to conduct heat and electricity better than anything else, makes this two dimensional material applicable in numerous disciplines, but not limited to: bioengineering, composite materials, electronics, energy technology and nanotechnology [64].



### 2.6.3. Discovery of Graphene

In 2004, graphene was first produced by Andre Geim and Kostya Novoselov using scotch tape to peel away layers of graphite [65]. Graphene has attracted lots of attention because of its role in the significant improvement to the sensitivity of various applications due to its rapid electron transfer and high surface to volume ratio.

### 2.6.4. Structure of Graphene

Graphene is a quasi-two-dimensional sheet of carbon atoms with an atomic-scale honeycomb lattice made of  $sp^2$  bonded carbon atoms that are densely packed [60,66]. It takes at least 10 such sheets to resemble graphite by stacking on top of each other [67]. The length of carbon-carbon bond is 0.142 nm. The area of two carbon atoms of the unit hexagonal cell of graphene is approximately  $0.052 \text{ nm}^2$ .

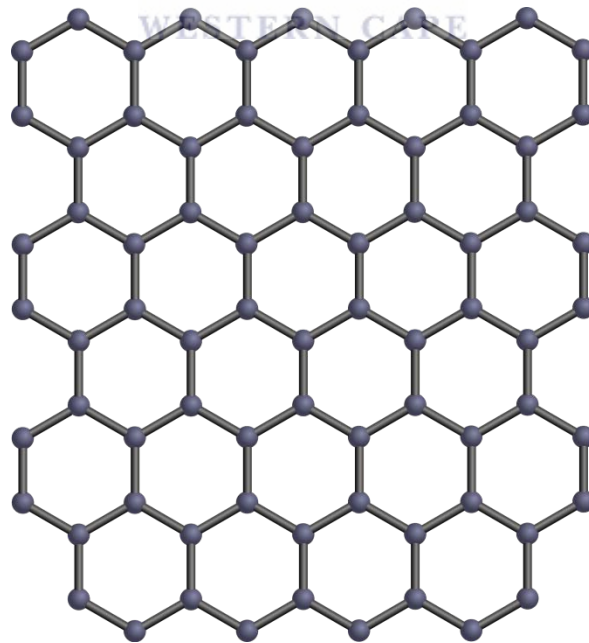


*Figure 2.3:* Diagram representing the graphene lattice unit cell [68].

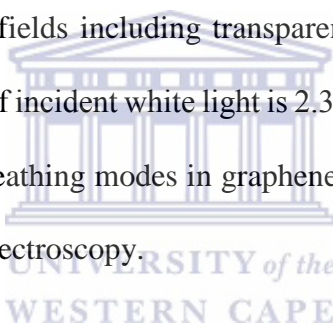
## **2.6.5. Properties of Graphene**

### **2.6.5.1. Electrical Properties of Graphene**

Graphene is a zero-gap semiconductor theoretically [65]. The transport mechanism changes entirely in graphene due to not overlapping of the valance and conduction bands at the Fermi level [69]. The linear dispersion relation of charge carriers in graphene behaving like massless relative particles was led to the quantum Hall Effect discovery in 1980 [70].

### **2.6.5.2. Optical Properties of Graphene**

Graphene has been used in many fields including transparent displays in electronics due to its transparency. The absorption rate of incident white light is 2.3 % or  $\pi\alpha$  where  $\alpha$  is the fine structure constant [71]. Compressing and breathing modes in graphene produce the optical bands of the D and G respectively using Raman spectroscopy.



### **2.6.5.3. Mechanical Properties of Graphene**

Graphene is known as one of the lightest materials while being extremely strong with a breaking strength of  $42 \text{ Nm}^{-1}$ . The breaking strength of graphene is 100 times greater than steel; it weighs  $0.77 \text{ mg m}^2$ . Atomic force microscopy (AFM) has been applied to measure the tensile strength of single graphene sheet.

## **2.6.6. Synthesis of Graphene**

A wide range approach for the synthesis of graphene based on the use of instrumentation, efficiency, cost of material and production have been studied in modern times.

The first and simplest method with an inexpensive instrumentation that has developed to prepare thin graphene sheet is the scotch tape method by Geim *et al.* [63]. The thin sheets of graphite exfoliated using scotch tape. The transparent sheets are observed after repeated folding of scotch tape and then they are transferred to silicon wafers for analysis.

Three principle methods present a simple chemical approach for the preparation of graphene from graphene oxide, which are reported as inexpensive, massively scalable, facile and fast methods are: Brodie [72], Hummers [73] and Staudenmeier [74]. Complete exfoliation of GO into graphene oxide sheets, followed by their reduction to reduced graphene oxide nanoplatelets is done by many different routes. The reduction of graphene oxide to graphene can be done by chemical reduction, photoreduction, thermal reduction, electrochemical reduction etc. The major drawback of this approach is the formation of defects in the graphene structure.

The method that promises the production of high quality single graphene sheets is chemical vapor deposition (CVD). The CVD can be employed to produce single sheets of graphene with high quality on a large scale [75]. The graphene sheets resulted from CVD do not need further treatments and can grow on arbitrary surfaces using transition metal catalysts [76].

### **2.6.7. Application of Graphene**

Graphene has attracted lots of attention as an alternative to existing materials such as electrode materials in laboratories and thanks to its novel electrical, mechanical, thermal and optical properties it has been used in a wide range of applications. It is being employed as inexpensive display screens in mobile devices [77], fuel cells [78], hydrogen storage [79], lithium-ion batteries [80], solar cells, ultracapacitors, light weight gas tanks, electrodes in electrochemical sensors [20,66,81].

The use of graphene and reduced graphene oxide as a material to modify carbon based electrodes has attracted lots of attention due to its intrinsic properties such as high surface area, high mechanical strength, excellent conductivity, and ease of functionalization. Graphene-based electrodes exhibit superior detection properties as chemical and biological sensors for environmental analysis such as heavy metal detection and organic and inorganic materials determination.

## **2.7. Metal Nanoparticles**

The synthesis and characterization of nanosized of metals have received great interests in the fields of chemistry, biology, physics, medicine, and material science and their different interdisciplinary fields due to their unusual physical (structural, electronic, magnetic and optical) and chemical (catalytic) properties [82,83]. Catalysis is the most important electrochemical application of metal-nanoparticles that have received increasing attention due to their high ratio of surface atoms with free valences to the cluster of total atoms and the facilitation of the electronic transfer [82,83]. The catalytic properties of metal-nanoparticles make them suitable for catalyzing the redox process of some molecules with analytical interest which can be studied using electroanalytical methods. Begon et al. have reviewed the electroanalytical applications of various metal-nanoparticles in electrochemical sensors [83].

An increasingly attractive route for the preparation of metal-nanoparticles modified electrode is the electrodeposition of a metal from a solution of its salt onto the electrode surface. Some metal-nanoparticles (e.g., Au, Pt, Ag, Ni, Cu, Co, Sb) have been the subject of innumerable studies in producing electrode materials for catalytic applications and electrochemical biosensing [23,84].

### **2.7.1. Antimony nanoparticles**

In the recent years metals, such as Antimony have been applied for the modification of surface electrodes. In 2007 the antimony film electrode in situ on a glassy carbon (SbFE/GC) was introduced for the first time as another alternative that approaches the electroanalytical performance of mercury- and bismuth-based electrodes featuring some interesting characteristics, such as higher hydrogen overpotential, favorably negative overvoltage of hydrogen evolution, a wider useful potential window, convenient performance in more acidic media ( $\text{pH} \leq 2$ ), mechanical stability, easily renewable surface, effective preconcentration in stripping procedures and low stripping signal for antimony itself [12,16]. Hocevar et al. investigated the use of antimony film electrode for electrochemical stripping analysis for the first time [16]. Cesarino et al. reported a glassy carbon sensor modified with reduced graphene oxide antimony nanoparticles for estriol hormone detection [85]. The reduced-graphene oxide-antimony nanocomposite can be prepared by a direct electrochemical reduction method at pencil graphite electrode surface making it possible to control film thickness; the nanocomposite may expand the application area of graphene and offers great opportunities for new functions due to the synergistic effects of the component materials.

### **2.7.2. Gold nanoparticles**

Gold nanoparticles (AuNPs) have attracted electroanalytical chemists from a fundamental and practical point of view because of their high surface-to-volume ratio, excellent conducting capability, and good biological compatibility. Although Au is known to be a poor catalyst in the bulk form nanometer-sized Au particles show extraordinary catalytic activity originated from the quantum scale dimensioned the presence of active sites on the fine particles [82]. Haruta and co-

workers demonstrated the use of highly dispersed, nanometer-sized Au particles in many important reactions.

### **2.7.3. Nanomaterial electrochemical sensors for bisphenol A (BPA) detection**

Electrodes modified with different nanomaterials such as graphene have been used in various studies for BPA detection. Goulart's group have demonstrated the use of carbon nanotubes films to develop a high-sensitivity determination of bisphenol A using CV [54]. Ntsendwana et al. reported a glassy carbon electrode modified with graphene for determination of BPA [86]. Wensheng Huang investigated voltammetric determination of bisphenol A using a carbon paste electrode based on the enhancement effect of cetyltrimethylammonium bromide (CTAB) [39]. However the sensitivity of the electrochemical sensor for detection of BPA exhibit improved by using carbon nanotubes or graphene metal nanocomposites due to synergistic effect of graphene sheets and metal nanoparticles. The use of carbon-based electrodes modified by carbon nanotubes and antimony nanoparticles to detect BPA using DPV was reported by Moraes et al. [87]. Tu et al. evidenced the use of multiwalled carbon nanotubes-gold nanoparticles film for bisphenol A determination using CV [38]. Niu et al. introduced an electrochemical sensor based on stacked graphene nanofibers (SGNF) and gold nanoparticles (AuNPs) composite modified glassy carbon electrode (GCE) for determination of bisphenol A (BPA) [14]. Yin et al. reported the electrochemical behavior of bisphenol A at glassy carbon electrode modified with a composite made from gold nanoparticles and silk fibroin and PAMAM dendrimers [52]. A label-free electrochemical aptasensor for bisphenol A (BPA) detection in milk samples on gold nanoparticles dotted graphene modified glassy carbon electrode was developed by Zhou et al. [10]. Tu et al. developed a sensitive electrochemical method for electroanalysis of Bisphenol A at a glassy carbon electrode (GCE) modified with a multiwalled carbon nanotubes (MWCNTs)-gold nanoparticles

(GNPs) hybrid film [38]. Li et al. coated glassy carbon electrode with carboxylated multi-walled carbon nanotubes for voltammetric determination of bisphenol A [37].

The above mentioned carbon-based electrodes modified with nanomaterials exhibit significant improved sensitivity towards detection of BPA and support the use of nanocomposites for enhanced detection capabilities.

## 2.8. Pencil Graphite Electrodes

Carbon based solid materials has been utilized as an electrode substrate material in different applications due to their wide potential window and low background current. The pencil graphite electrode (PGE) as a new type of carbon electrode has been used in numerous electroanalytical applications in recent years [17,88]. Pencil-graphite electrode (PGE) offers many attractive features compare to other carbon-based electrodes such as good electro-conductivity, low cost, no need for time-consuming pretreatments, disposability, low background current, and availability [18]. The electrochemical reactivity and surface area of a PGE can be easily improved by surface modification and electrochemical treatments. Commonly used coating methods to improve the electrochemical activity of electrode surfaces to create sensitive high performance sensor are drop casting, passive adsorption and dip coating of chemically reduced graphene oxide solutions [64,66,89,90]. Electrochemical reduction of graphene oxide onto the electrode surface as a fast and green synthesis approach is an alternative to the reduction of graphene oxide chemically [91–94]. A method of direct electrochemical reduction of graphene oxide onto electrode surfaces have been proposed by Guo et al, and Chen et al. in order to limit the structural defects of graphene sheets and control film thickness [91,92]. To eliminate the fouling effect from the oxidation of BPA, single-use pencil graphite electrode can be used as an alternative to the modified and

unmodified glassy carbon electrodes. Ali Ozcan developed a sensitive and selective method for determination of BPA using pencil graphite electrodes were activated electrochemically in the presence of different supporting electrolytes [11].

## **2.9. Characterization Techniques**

The understanding of the properties of synthesized graphene sheets is imperative in evaluating the quality of graphene oxide (GO) and produced graphene. The purity and defects of graphene, reduced graphene oxide and reduced graphene oxide-metal nanocomposite is investigated using various characterization techniques including Fourier transformed infrared spectroscopy (FT-IR), x-ray diffraction (XRD), Raman spectroscopy and high resolution electron microscopy (HRSEM). A brief discussion of these techniques is listed below.

### **2.9.1. Fourier Transformed-Infrared (FT-IR) Spectroscopy**

The quantitative and qualitative features of functional groups in organic and inorganic solid, liquid and gas samples are investigated by the FT-IR spectroscopy. FT-IR as an inexpensive and rapid detection method measures the absorbed light of a specific wavelength when interference wave interacts with the sample [95,96].

### **2.9.2. X-ray Diffraction (XRD)**

XRD determines the molecular and atomic structure of crystals. The molecular structure is determined by measuring the angles and intensities of the diffracted X-ray light beam caused by the sample. The crystallographic and chemical composition of materials can be obtained [97].

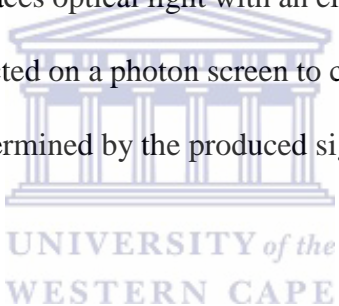


### **2.9.3. Raman Spectroscopy**

In Raman spectroscopy, the interaction between light and matter is investigated. Samples absorb and re-emit photons of the laser light. The change of re-emitted photons frequency in response to the original frequency is measured. The information of functional groups and changes in the structure of the sample can be provided by the obtained spectra [98].

### **2.9.4. High Resolution Scanning Electron Microscopy (HRSEM)**

Scanning electron microscopy replaces optical light with an electron beam to interact with sample producing photons which are collected on a photon screen to create an image. The sample surface topography and composition is determined by the produced signals.



## **2.10. Summery**

From what has reviewed in the literature it can be deduced that: Stripping voltammetry is a widely used method for determination of bisphenol A. The cost effective and environmentally friendly pencil-graphite electrode modified with graphene-metal nanocomposite may be used as a high sensitive electrode providing good results during voltammetry. The literature presented shows that the study done for this thesis would be successful and produce positive results.

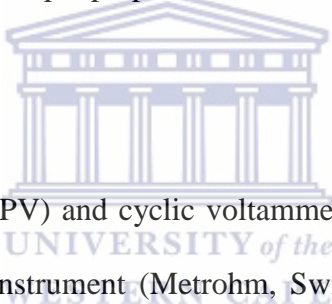
# CHAPTER THREE

## Experimental Approach

### 3.1. Introduction

The experimental procedures and instrumentations applied to obtain the relevant data utilized in this study including electrode and sample preparation has been detailed in this section.

### 3.2. Apparatus



Differential pulse voltammetry (DPV) and cyclic voltammetry (CV) experiments were applied using 797 VA COMPUTRACE instrument (Metrohm, Switzerland) controlled by a personal computer. The technique employed three electrode system consisting of an electrochemically reduced graphene oxide metal (antimony and gold) nanoparticles pencil-graphite electrode (ERGO-SbNPs-PGE and ERGO-AuNPs-PGE) served as the working electrode. A platinum wire and Ag/AgCl (saturated KCl) served as the counter and reference electrodes, respectively. All experiments were performed in a one compartment 20 mL voltammetric cell at room temperature.

Fourier Transform Infrared (FT-IR) spectra were recorded using a (Perkin Elmer Spectrum 100) coupled to an Attenuated Total Reflectance (ATR) sample holder. FT-IR was used to gain information and confirmation on graphene oxide. Scanning Electron Microscopy (SEM) measurements were utilized using a LEO 1450 SEM 30 kV instrument equipped with Electronic

Data System (EDS) and Windows Deployment Services (WDS); images were taken using the secondary electron detector. Before SEM observations, the samples were dried in a vacuum oven and deposit on the silicon grid surface. XRD measurements were employed using a Bruker AXS D8 Advance diffractometer from BRUKER-AXS Germany with Cu-K $\alpha$  radiation and Raman spectroscopy was obtained using a Dilor XY Raman spectrometer with a Coherent Innova 300 Argon laser with a 514.5 nm laser excitation.

### **3.3. Reagents**

All chemicals used in this study are of analytical reagent grade purity. 1,000 mg L<sup>-1</sup> atomic absorption standard solution from Sigma-Aldrich was provided and diluted as required. Bisphenol A (BPA, 99%) was purchased from Aldrich. Phosphate buffer solution (0.1 M, pH 7) was prepared by mixing dipotassium hydrogen phosphate and potassium dihydrogen phosphate solutions followed by diluting the solution with ultra-pure distilled water (Millipore), this solution was served as the supporting electrolyte. In order to verify the pH of the supporting electrolyte (phosphate buffer solution), a pH meter (Metrohm 827 pH Lab.) was used.

### **3.4. BPA solution**

Bisphenol A solution was prepared by dissolving it in ethanol and was diluted with ethanol.

### **3.5. Phosphate buffer solution (Electrolyte solution)**

Appropriate amounts of dipotassium hydrogen phosphate and potassium dihydrogen phosphate were mixed with ultrapure water in order to prepare 0.01 M phosphate buffer solution (PB).

### **3.6. Acetate buffer solution**

Acetate buffer solution (0.1 M, pH 4.6) was prepared by mixing glacial acetic acid and sodium acetate followed by diluting the solution with ultra-pure distilled water (Millipore). Acetate buffer solution (ABS) was used as the solvent for graphene oxide GO solution.

### **3.7. Nitric acid solution**

In order to prepare 3 M Nitric acid solution on a volume to volume basis, Nitric acid (55%) was diluted with distilled water. The prepared solution was used for glassware and electrode cleaning.

### **3.8. Hydrochloric acid solution**

HCl (32%) was diluted with high purity distilled water to prepare 1 M hydrochloric acid solution.

### **3.9. Synthesis of graphene oxide (GO)**

Graphite oxide was synthesized from graphite powder according to the Hummers method [68] with some modifications. Graphite powder (2 g) and sodium nitrite (1 g) were mixed with sulfuric acid (50 mL) in a clean dry conical flask and stirred at room temperature for 30 minutes, followed by subsequent mixing in an ice bath for 20 min. Potassium permanganate (7 g) was added gradually over a 30 minutes period with constant stirring. The resulting solution was allowed to reach room temperature prior to being placed in a water bath set at 35 °C and, left to stir for 2 hours. The flask was returned to the ice bath with constant stirring. Ultra-pure water, 150 mL, was added before the addition of approximately 5 mL hydrogen peroxide until effervescence ceases. The flask was removed from the ice bath and allowed to stir at room temperature overnight and centrifuged for 20 minutes. Three successive acid washes were

performed followed by one with ultra-pure water. The resulting product was dried for 48 hours in a vacuum oven. To prepare a  $1.0 \text{ mg mL}^{-1}$  GO solution, 10 mg of the product (graphite oxide) was exfoliated in 10 mL of ethanol or ultrapure water.

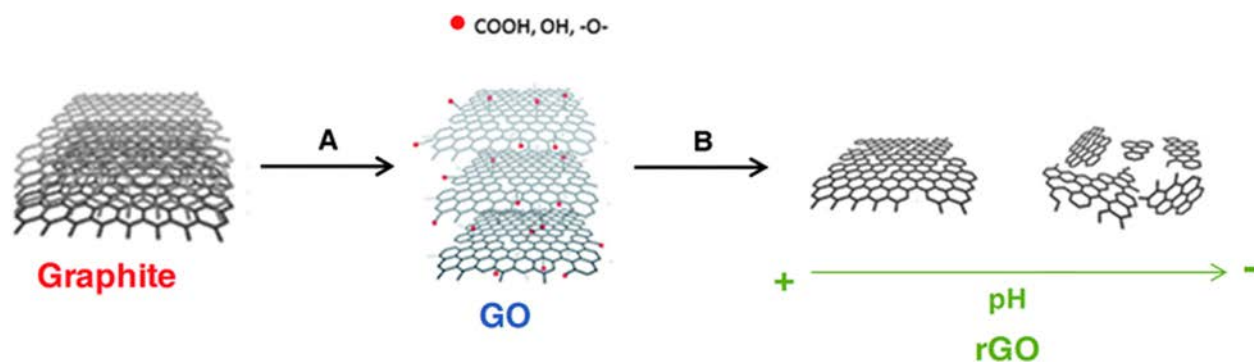
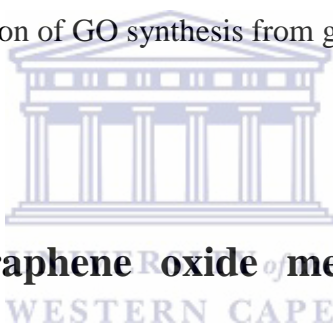


*Figure 3.9.1:* Graphic representation of GO synthesis from graphite powder [99].



### 3.10. Preparation of graphene oxide metal nanoparticles (GO–MetalNPs) nanocomposite solution for electrochemical reduction

After exfoliating the prepared graphite oxide (10 mg) in 10 mL of 0.1 M acetate buffer solution ABS (pH 4.6) by ultrasonication for 1.0 hour to give a  $1.0 \text{ mg mL}^{-1}$  GO solution, 15 ppm standard solution of metal (Sb, Au, Ni, Pd, Co, Cu) was added to the GO solution and was sonicated for 2 hours.

### 3.11. Preparation of pencil graphite electrodes (PGE)

The pencil-graphite rods (Pentel, HB of 0.5 mm in diameter and 6 cm in length) were obtained from the local book store. A copper wire was attached to one end of the pencil rod to establish

electrical connection with the potentiostat and a plastic syringe was used to hold them together into which the pencil rod was inserted into it along with the copper wire exposing 1 cm of the other end of the pencil rod at one end of the syringe. The attached copper wire passed through the top of the syringe.

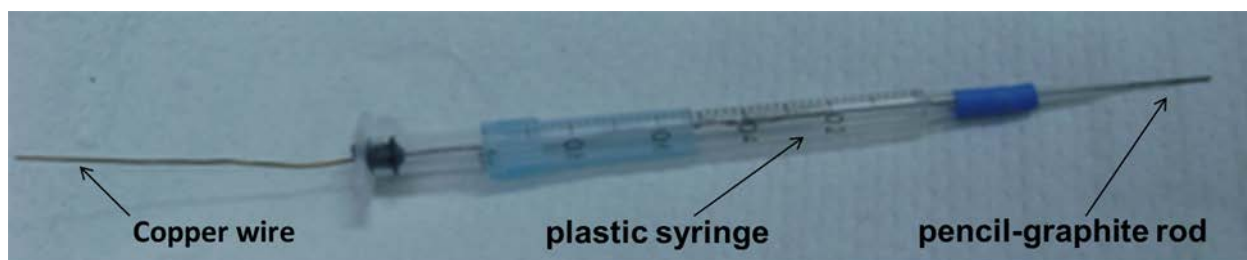


*Figure 3.11.1:* Photograph of pencil graphite electrode (PGE) made from pencil-graphite rod, plastic syringe and copper wire.

### **3.12. Preparation of the multiple electrochemically reduced graphene oxide metal nanoparticles pencil graphite electrode (ERGO-MetalNPs-PGE)**

In order to eliminate the fouling effect from the oxidation of BPA, single-use pencil graphite electrode was used but it was time consuming with less reproducible results to prepare one ERGO-MetalNPs-PGE for each measurement at a time so a new technique was introduced to make multiple ERGO-MetalNPs-PGE at once. The pencil rod's tips were immersed in 10 mL of GO-MetalNPs nanocomposite dispersion ( $1 \text{ mg mL}^{-1}$ ) and cyclic voltammetric reduction of GO-MetalNPs was performed with constant stirring in the fixed potential of (-0.7 V, vs. Ag/AgCl) and then cycling in a range between (-1.5 V, vs. Ag/AgCl) and (+0.3 V, vs. Ag/AgCl) for five successive cycles. The instrumental parameters that were used for the electrodeposition

procedure are as follows; deposition time (120 s), deposition potential (-0.7 V, vs. Ag/AgCl), equilibration time (10 s), sweep rate ( $0.1 \text{ Vs}^{-1}$ ), and voltage step (0.005 V). The ERGO-MetalNPs-PGEs were dried for one hour and then conditioned by applying the potential of (-0.7, vs. Ag/AgCl) V from (0.0 V, vs. Ag/AgCl) to (1.0 V, vs. Ag/AgCl) in phosphate buffer solution (PBS) before each measurement. The multiple preparation technique is explained in detail in chapter 5.

### 3.13. Procedure DPV analyses

The electrodes were immersed (1 cm) into the electrochemical cell containing, 10 mL of phosphate buffer (0.1 M, pH 7), and bisphenol A. The solution was stirred for 60 seconds and after a brief rest period (10 seconds) the potential was scanned from (0.1 V, vs. Ag/AgCl) to (0.9 V, vs. Ag/AgCl) by applying differential pulse voltammetry to the ERGO-MetalNPs-PGE. Experiments repeated three times by applying a new fresh electrode for each measurement.

To investigate the effect of instrumental parameters on the peak heights produced by the current, each one was varied while keeping the remaining ones constant. The optimum instrumental parameters were used for all further experiments.

Before each experiment the electrode was run in PBS without BPA in the cell in order to stabilize the modification on the electrode surface.

Once the preparation of the electrode was developed and an understanding of the technique was achieved, the electrode was applied for tap water analysis.

### 3.14. Quantitation

To determine the concentration of the analyte, standard addition method was used. Each analysis was repeated four times for reproducibility purposes. The standard addition formula for calculation of the analyte concentration is as follows:

$$c(\text{unknown}) = \frac{c(\text{standard}) \times v \times 1000}{(i_1 - i) \times (V + v)}$$

Where,

C (unknown) = concentration of the final unknown solution

C (standard) = concentration of the standard solution

V = volume of the sample solution

v = volume of the standard solution added

i = peak height of the unknown solution

i' = peak height of the unknown solution + standard

### 3.15. Sample preparation

After collection of tap water in our laboratory 9 mL of it was added to 1 mL of 1 M phosphate buffer solution and the analysis was performed as described by the procedure in section 3.14 to determine BPA.



## 3.16. Characterization techniques

### 3.16.1. Fourier Transformed Infrared Spectroscopy (FT-IR)

In order to distinguish between graphene and GO and investigate the presence of oxygen in the graphite structure in the form of oxygenated functionalities, FT-IR spectroscopy was performed. 10 mg of graphite, graphene oxide, and graphene grounded in a pestle and mortar on the Attenuated Total Reflectance (ATR) sample holder and Perkin Spectrum 100 FT-IR spectrometer recorded the FT-IR spectrum.

### 3.16.2. X-ray Diffraction (XRD)

A BRUKER AXS X-ray diffractometer with Cu-K $\alpha$  radiation was utilized to investigate the structural changes in graphite, graphene oxide and graphene. The list of instrumental operating conditions is shown in Table 3.1 below.

**Table 3.1:** Operating parameters for XRD.

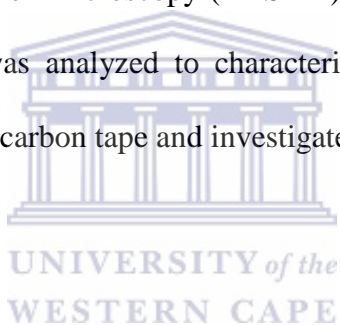
XRD Operating Parameters	
Radiation Sources	Cu-K $\alpha$
Radiation Wavelength	1.506 Å
Tube Voltage	40 kV
Tube Current	40 mA
Variable Slits	0.28 mm

### **3.16.3. Raman Spectroscopy**

A Dilor XYRaman spectrometer with a Coherent Innova 300 Argon laser with a 514 nm laser excitation was used to investigate the change in structure after chemical transformation, from pure graphite to graphene oxide. 1.0 mg mL<sup>-1</sup> solutions of graphite and graphene oxide were exfoliated by ultrasonification and were drop cast onto glass slides in order to form thin film sample for Raman spectroscopy characterization.

### **3.16.4. High Resolution Scanning Electron Microscopy (HRSEM)**

The high resolution scanning electron microscopy (HRSEM) of the bare PGE, ERGO-PGE and ERGO-MetalNPs-PGE surfaces was analyzed to characterize their surface morphology. The graphite electrodes were placed on carbon tape and investigated at various magnifications.

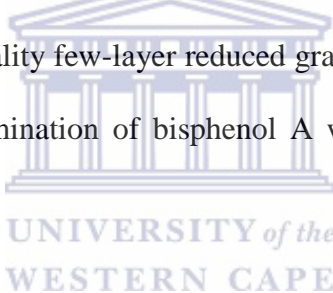


# **Chapter Four:**

## **Morphological and Structural Characterization of Graphene and reduced Graphene Oxide- metal nano- composite**

### **4.1. Introduction**

The morphological and structural changes along the chemical synthesis routes demonstrated in this chapter. The formation of good quality few-layer reduced graphene oxide-metal nano-composite as sensing platform for the determination of bisphenol A was confirmed using FT-IR, XRD, Raman spectroscopy and HRSEM.



### **4.2. Fourier Transformed Infrared Spectroscopy (FT-IR)**

The Fourier Transformed Infrared (FT-IR) spectra of graphite and graphene oxide (GO) are represented in Figure 4. As expected, graphite shows no significant characteristic IR features. However, GO exhibits a large compilation of diffused bands attributed to the presence of oxygen functional groups namely, hydroxyl, epoxides, carbonyl and carboxylic groups [20,100,101]. The peak at  $3117\text{ cm}^{-1}$  is due to O-H stretching vibrations, whereas, the band at  $1760\text{ cm}^{-1}$  is attributed to C=O stretching vibration [102]. The peak at  $1589\text{ cm}^{-1}$  is associated with C=C stretching vibration [101], while the peak at  $1401\text{ cm}^{-1}$  corresponds to the bending C-O-H vibration [101]. The peaks at  $1260\text{ cm}^{-1}$  and  $1026\text{ cm}^{-1}$  are due to the C-O stretching vibration occurring in alcohols and epoxides within the graphite structure [102].

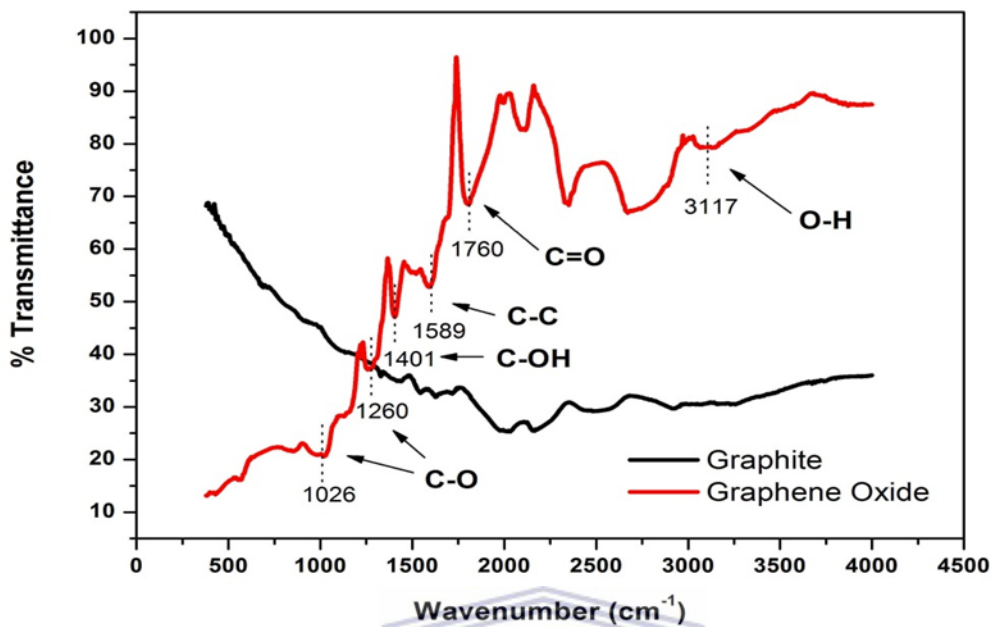


*Figure 4.1:* FT-IR spectra of Graphite and Graphene Oxide (GO)

### 4.3. Raman Spectroscopy

Raman spectroscopy investigated the change in structure after chemical transformation, from pure graphite to graphene oxide. The Raman spectra of graphite and graphene oxide are shown in Figure 5. The Raman spectrum of graphite includes a strong G band at  $1575\text{ cm}^{-1}$ , a significantly weaker D band at  $1350\text{ cm}^{-1}$  and a moderate 2D band at  $2721\text{ cm}^{-1}$ . The strong G band is because of the symmetry of the graphite structure which allows first order scattering of the E<sub>2g</sub> mode (of sp<sup>3</sup> hybridized carbon atoms) to occur in the neatly ordered [103]. The ratio of the intensities of the D and G bands ( $I_D/I_G$ ), measuring defects or disorder within the structure, was calculated as 0.25 for graphite which confirms the highly ordered structure [104].

For GO, the G band is decreased, broadened and shifted to  $1600\text{ cm}^{-1}$  and the D peak at  $1360\text{ cm}^{-1}$  is significantly larger than in graphite. The ratio of the intensities ( $I_D/I_G$ ) for GO is 0.975, depicting an increase in structural disorder. This increase is attributed to the significant reduction in size of the in-plane  $sp^2$  domains caused by oxidation and ultrasonic exfoliation, and somewhat disordered graphite crystal structure of graphene nano-platelets

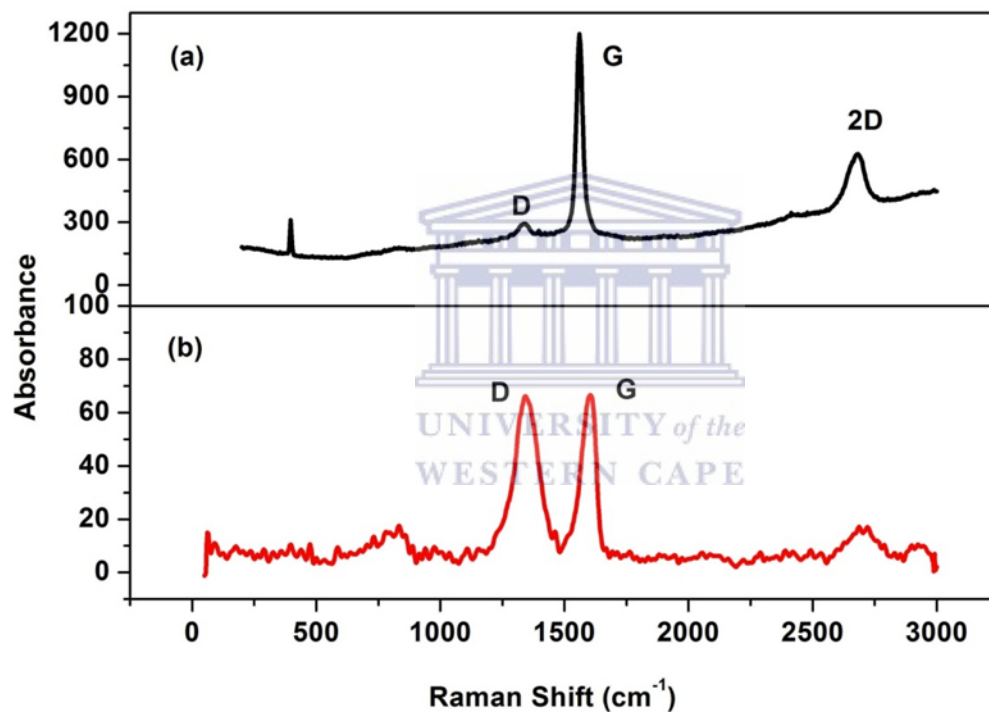


**Figure 4.2:** Raman spectra of Graphite (black) and Graphene Oxide (red).

## 4.4. X-ray Diffraction (XRD)

The XRD analysis of graphite and graphene oxide (GO) are shown in Figure 6. In the XRD spectrum of graphite the presence of the strong, distinguishable 002 peak at  $26.56^\circ$  with interlayer distance of 0.34 nm imply a highly ordered carbon structure while, the peaks indexed as 100 at  $44.54^\circ$  and 004 at  $54.61^\circ$  are indicative of the crystalline structure of graphite [105]. GO shows a sharp, tall 001 peak at  $9.81^\circ$  corresponds to an interlayer spacing of approximately 0.7 nm and confirms the presence of oxygen containing functional groups formed during oxidation which in turn, cause the graphene oxide sheets to stack more loosely [106].

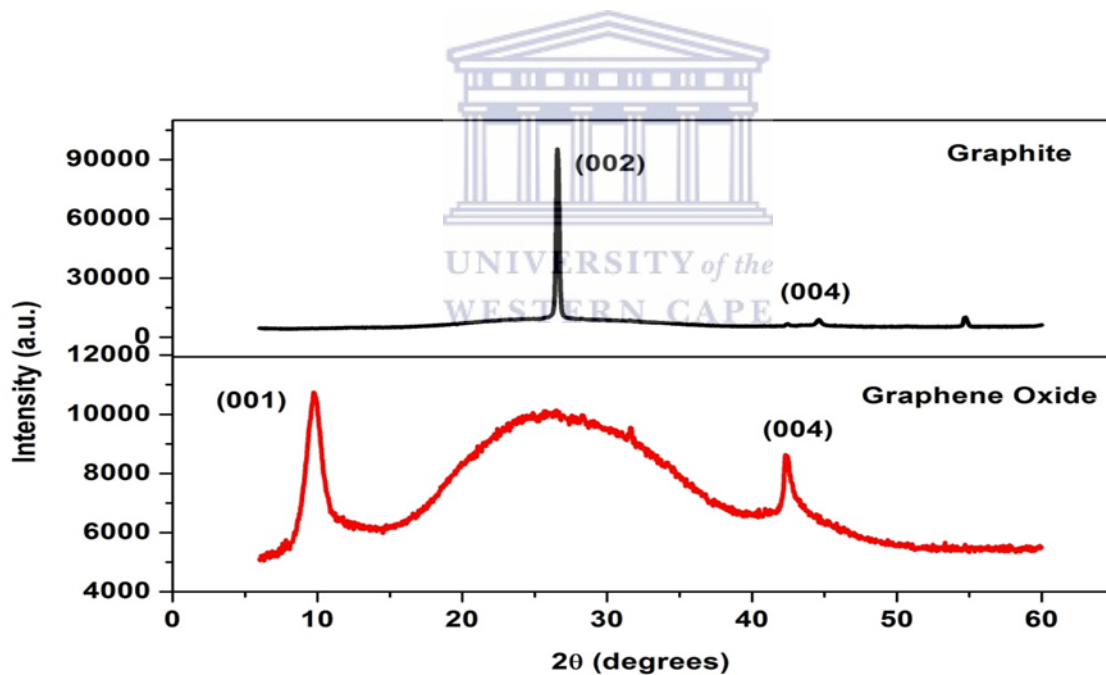


*Figure 4.3:* X-Ray Diffractograms for Graphite and Graphene Oxide.

#### **4.5. The high resolution scanning electron microscopy (HRSEM)**

The high resolution scanning electron microscopy (HRSEM) images of the bare PGE, ERGO-PGE, ERGO-SbNPs-PGE and ERGO-AuNPs-PGE surfaces are shown in Figure 1. Surface roughness with grooves on the surface along the direction of machining can be observed at the bare PGE surface. Following the electrochemical reduction of graphene oxide flakes of wrinkly graphene sheets are observed at the ERGO-PGE surface [103]. Little dots on ERGO-AuNPs-PGE surface image confirm the presence of gold nanoparticles on the electrode surface.



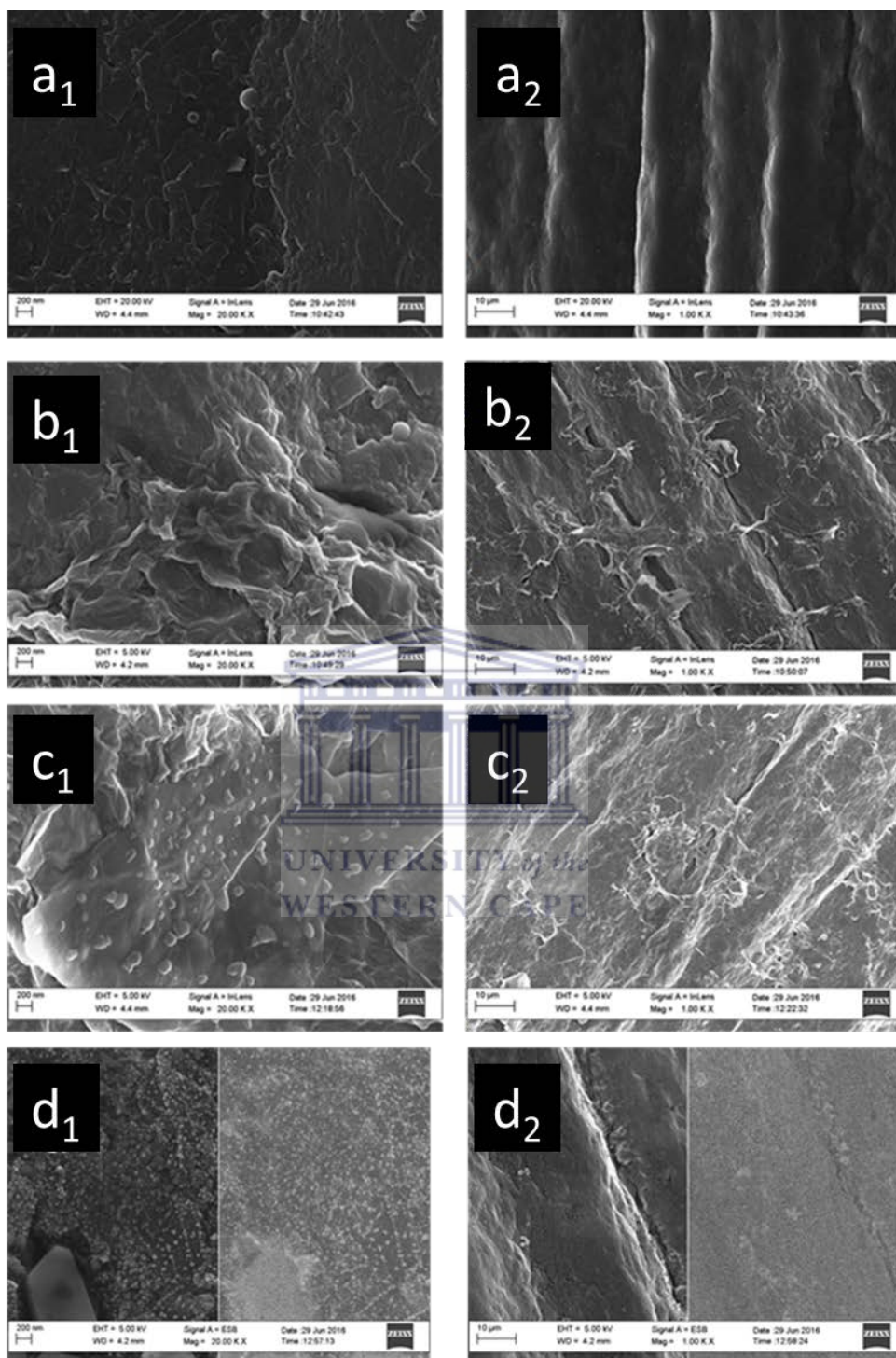


**Figure 4.4:** HRSEM images of bare PGE (a), ERGO-PGE (b), ERGO-SbNPs-PGE (c) and ERGO-AuNPs-PGE (d) at 20.00 K (1) and 1000 times magnification (2).



# Chapter Five

## **Batch preparation method of electrochemically reduced graphene oxide –metal nanoparticles pencil graphite electrodes (ERGO-Metal NPs-PGEs)**

In order to eliminate the fouling effect resulting from the oxidation of BPA, single-use the ERGO-MetalNPs-PGEs were used but their preparation is time consuming since each analysis run required a fresh ERGO-MetalNPs-PGE. Hence, it was for this reason that a method was devised to prepare multiple ERGO-MetalNPs-PGEs batches of eight and simply referred to as the “batch preparation method”.

  
UNIVERSITY of the  
WESTERN CAPE

A plastic container was used to hold the GO-MetalNPs solution and its lid served as a holder into which the reference electrode (Ag/AgCl saturated KCl), counter electrode (platinum wire) and working electrode (8 pencil rods connected to each other with copper wire) were inserted at the holes drilled into it as shown in Figure 5.1.1.

Prior to modification, the PGE electrode surfaces were cleaned with 3M nitric acid, rinsed thoroughly with deionized water and conditioned three times in PBS by applying the potential of -0.7 V from 0.0 V to 1.0 V using differential pulse voltammetry. The pencil rod's tips were immersed in 10 mL of GO–MetalNPs nanocomposite dispersion (1 mg mL<sup>-1</sup> of GO in acetate buffer solution and 15 ppm metal) and cyclic voltammetric reduction of GO-MetalNPs was

performed with constant stirring in the fixed potential of -0.7 and then cycling in a range between -1.5 and +0.3 V for five successive cycles. A small magnetic stirrer bar was placed into the GO–MetalNPs solution stir the solution throughout the deposition process. The instrumental parameters that were used for the electrodeposition procedure are as follows; deposition time (120 s), deposition potential (-0.7 V), equilibration time (10 s), sweep rate ( $0.1 \text{ Vs}^{-1}$ ), and voltage step (0.005 V). The ERGO-MetalNPs-PGEs were dried for one hour and then conditioned by applying the potential of -0.7 V from 0.0 V to 1.0 V in phosphate buffer solution (PB) before each measurement.



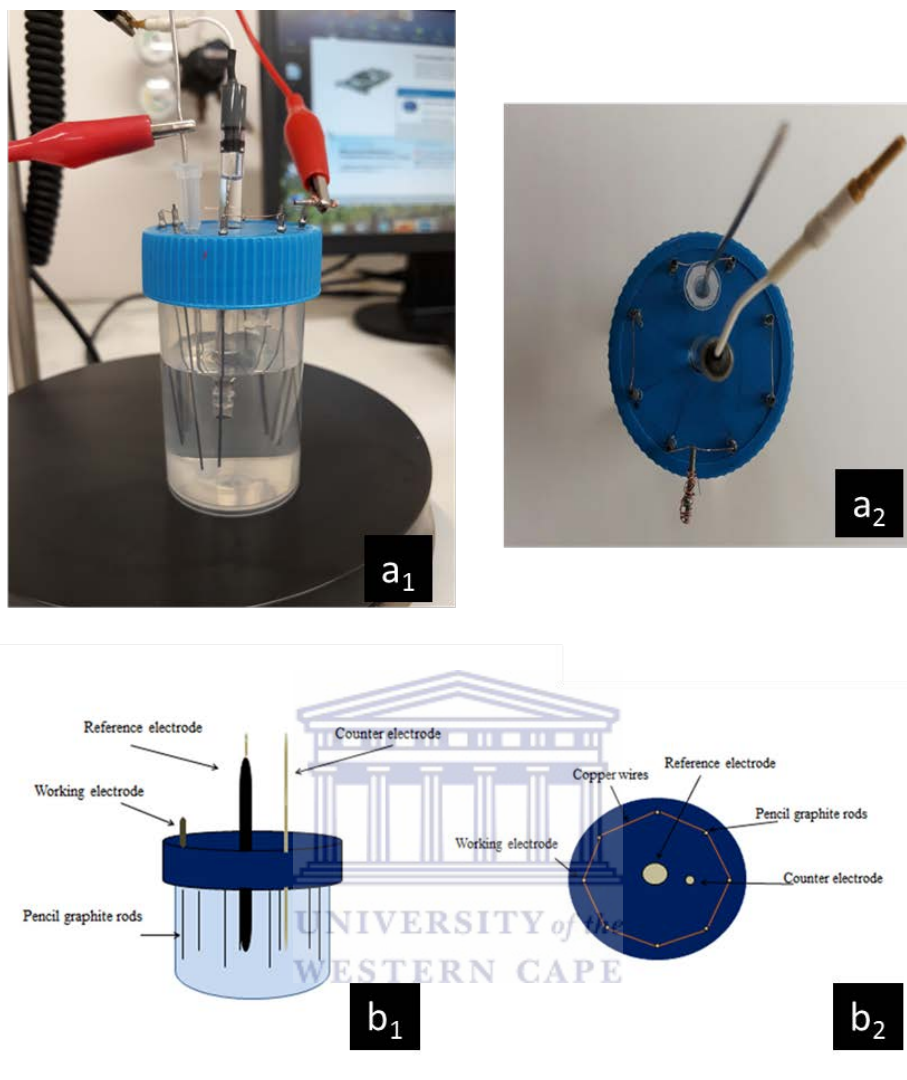


**Figure 5.1.1:** Photograph of apparatus used for coating multiple ERGO-MetalNPs-PGE (a<sub>1</sub>) side view, (a<sub>2</sub>) top view. Graphic representation of apparatus used for coating multiple ERGO-MetalNPs-PGE (b<sub>1</sub>) side perspective, (b<sub>2</sub>) top perspective.

## 5.1. Reproducibility

The reproducibility of the ERGO-MetalNPs-PGEs when they prepared individually and in batch was investigated. Calibration curves obtained for three sets of electrodes prepared individually

shown in and in a batch were compared. It was found that the slopes of the calibration curves for the electrodes prepared in a batch of electrodes were similar in comparison to individually prepared electrodes.

Figure 5.2.1 shows the calibration curves constructed from three sets of individually prepared ERGO-SbNPs-PGEs in BPA whilst The calibration curves of three sets of batch prepared ERGO-SbNPs-PGEs is shown in Figure 5.2.2.

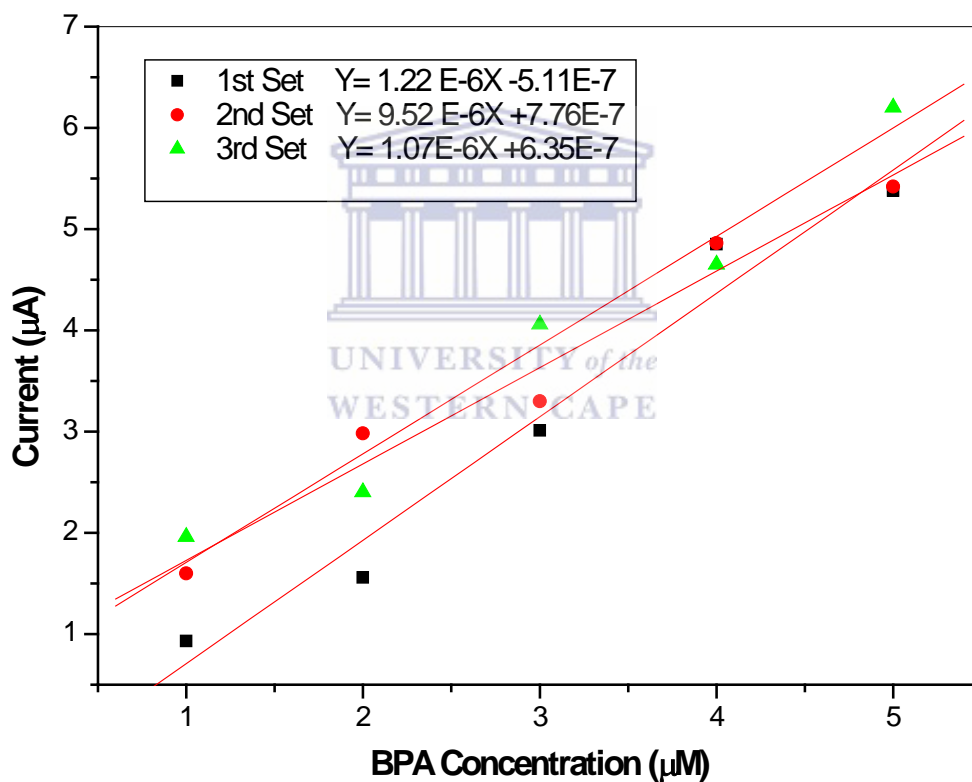


**Figure 5.2.1.** The standard calibration curves for BPA using individually prepared ERGO-SbNPs-PGEs (showing linear dependence of the peak current with BPA concentration ranging from 1.0  $\mu\text{mol L}^{-1}$  to 5.0  $\mu\text{mol L}^{-1}$ .)

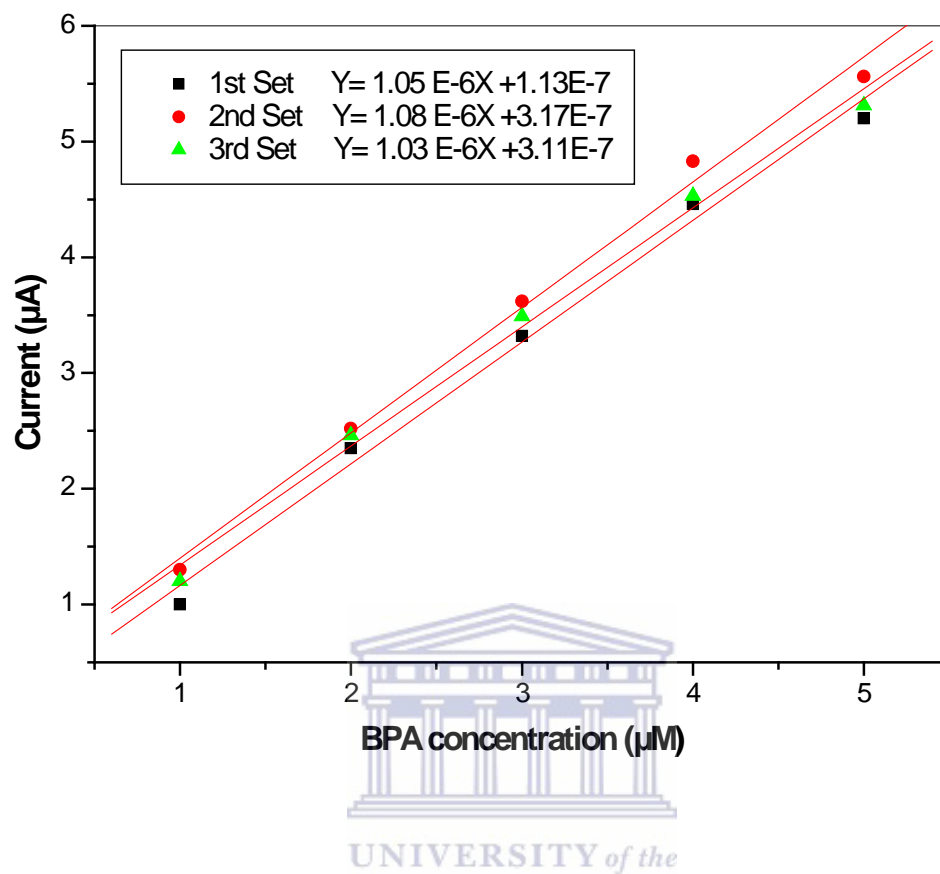


**Figure 5.2.2.** The standard calibration curves for BPA using batch prepared ERGO-SbNPs-PGEs (showing linear dependence of the peak current with BPA concentration ranging from 1.0  $\mu\text{mol L}^{-1}$  to 5.0  $\mu\text{mol L}^{-1}$ .)

It was observed that the slopes of the calibration curves obtained from individually prepared ERGO-MetalNPs-PGEs have a larger variation in comparison to those prepared using the batch method. Table 5.2.1 shows a comparison between the individually and batch prepared ERGO-MetalNPs-PGEs in terms of slopes, correlation coefficient and percentage relative standard deviation (% RSD). It is clear from the results in Table 5.2.1 that the % RSD of the slopes obtained using the batch preparation method was 2.389 % in comparison with the 12.429 % obtained when using individually prepared electrodes. The results clearly demonstrate the high reproducibility of

the batch preparation method with regards to electrode preparation. Furthermore, the reproducibility of the batch prepared electrodes yield calibration curves having linear correlation coefficients much closer to 1 thus highlighting the superiority of the batch preparation method.

**Table 5.2.1:** The correlation and slope of the linear regression equation of the linear plot of current vs BPA concentration for multiple and singled prepared ERGO-MetalNPs-PGEs.

Calibration Curve	Batch Prepared Electrodes		Individually Prepared Electrodes	
	Slope	R <sup>2</sup>	Slope	R <sup>2</sup>
First Set	$1.05 \times 10^{-6}$	0.991	$1.22 \times 10^{-6}$	0.969
Second Set	$1.08 \times 10^{-6}$	0.994	$9.52 \times 10^{-7}$	0.967
Third Set	$1.03 \times 10^{-6}$	0.994	$1.07 \times 10^{-6}$	0.969
RSD %	2.389		12.429	

## 5.2. Conclusion:

A new method for the multiple preparation of ERGO-MetalNPs-PGE was introduced. The batch preparation method not only is less time consuming since 8 pencil graphite electrodes can be modified at once but also improves the reproducibility of the electrodes.

# CHAPTER SIX

## Electrochemically Reduced Graphene Oxide Metal

### Nanoparticles Pencil Graphite Electrode

#### (ERGO–MetalNPs-PGE)

### 6.1. Introduction

The pencil graphite electrode (PGE) as a carbon electrode offers many attractive features compare to other carbon-based electrodes such as good electro-conductivity, low cost, no need for time-consuming pretreatments, disposability, low background current, and availability [17,18]. Moreover, the electrochemical reactivity and surface area of a PGE can be easily improved by surface modification and electrochemical treatments [86].

Recently, Graphene as a versatile material to modify electrode surfaces has attracted lots of attention because of its role in the significant improvement to the sensitivity of various applications due to its rapid electron transfer and high surface to volume ratio and this two dimensional material has become one of the most widely used materials for surface modification to increase the sensitivity, selectivity, and reproducibility of the developed electrochemical sensors [61].

In the recent years metal nanoparticles, such as Antimony, Gold, and Silver have been applied for the modification of surface electrodes for electroanalysis purposes. Metal nanoparticles have shown significant electrocatalytic and electron-conducting characteristics due to their different size, shape, composition, and crystalline structures [10,14,23,37,38,52,80–85].

A one-step direct electrochemical reduction technique was utilized in this chapter to prepare reduced graphene oxide metal nanoparticles pencil graphite electrodes ERGO-MetalNPs-PGEs from colloidal graphene oxide metal nanoparticles solution. The modified pencil electrodes were applied for the determination of bisphenol A (BPA) by adsorptive stripping voltammetry.

## **6.2. Effect of different ERGO-MetalNPs nanocomposite surface on electrochemical oxidation of BPA**

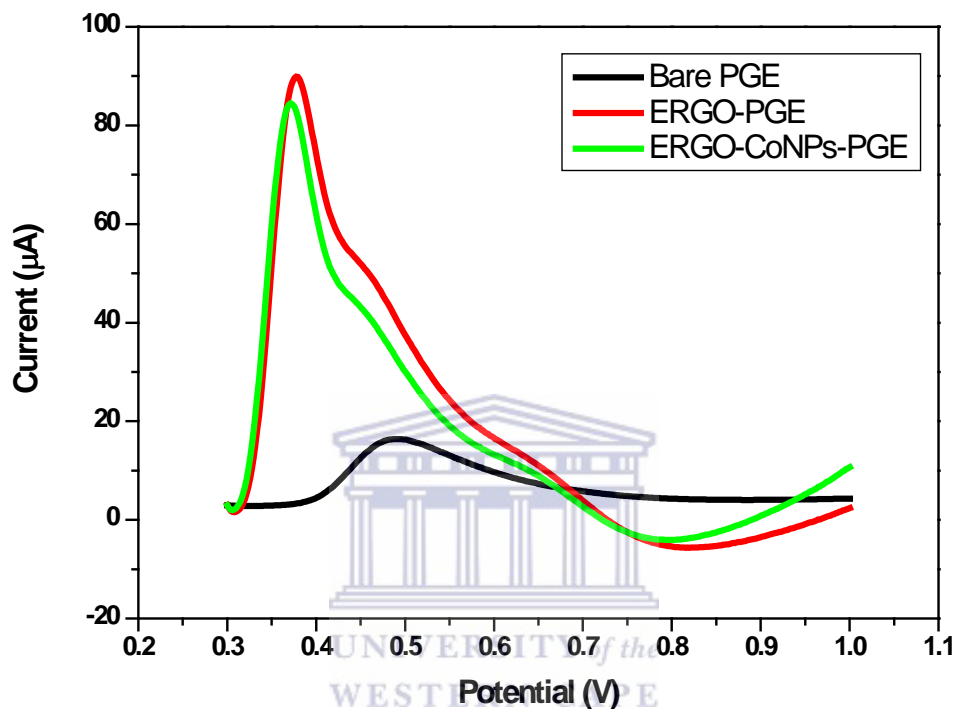
The effect of various metals such as Sb, Au, Ni, Pd, Co and Cu that were used to prepare the ERGO-MetalNPs nanocomposites and investigated for electrochemical oxidation of BPA. The enhancement in the oxidation peak of BPA from bare pencil graphite electrode (PGE) to electrochemically reduced graphene oxide pencil graphite electrode (ERGO-PGE) to electrochemically reduced graphene oxide metal nanoparticles pencil graphite electrode (ERGO-MetalNPs-PGE) was evaluated.

The electrochemical behavior of BPA at the ERGO-MetalNPs-PGE (Metal: Sb, Au, Ni, Pd, Co and Cu) was evaluated in 0.1 mol L<sup>-1</sup> PBS pH 7, containing 50 μM BPA by using differential pulse voltammetry (DPV) experiments with an amplitude of 100 mV, step potential of 2 mV, and an effective scan rate of 5 mV/s. The results are presented in Figures 6.1, 6.2, 6.3, 6.4, 6.5 and 6.6.

Figure 6.1 shows the electrochemical behavior of BPA at the bare pencil graphite electrode (PGE), electrochemically reduced graphene oxide pencil graphite electrode (ERGO –PGE) and electrochemically reduced graphene oxide cobalt nanoparticles pencil graphite electrode (ERGO-

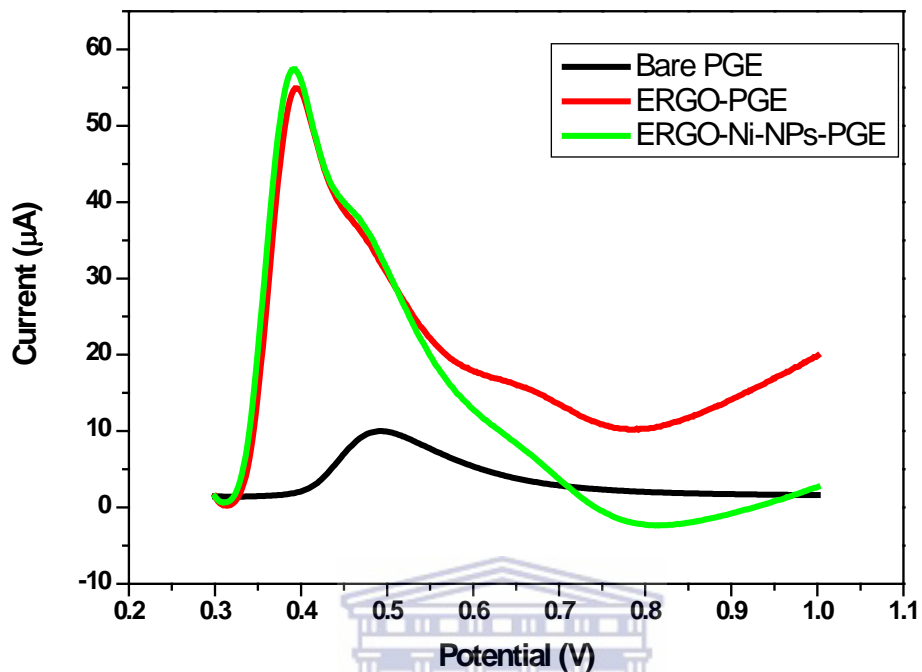


CoNPs-PGE). The electrochemical response shows no improvement from ERGO –PGE to ERGO-CoNPs-PGE.



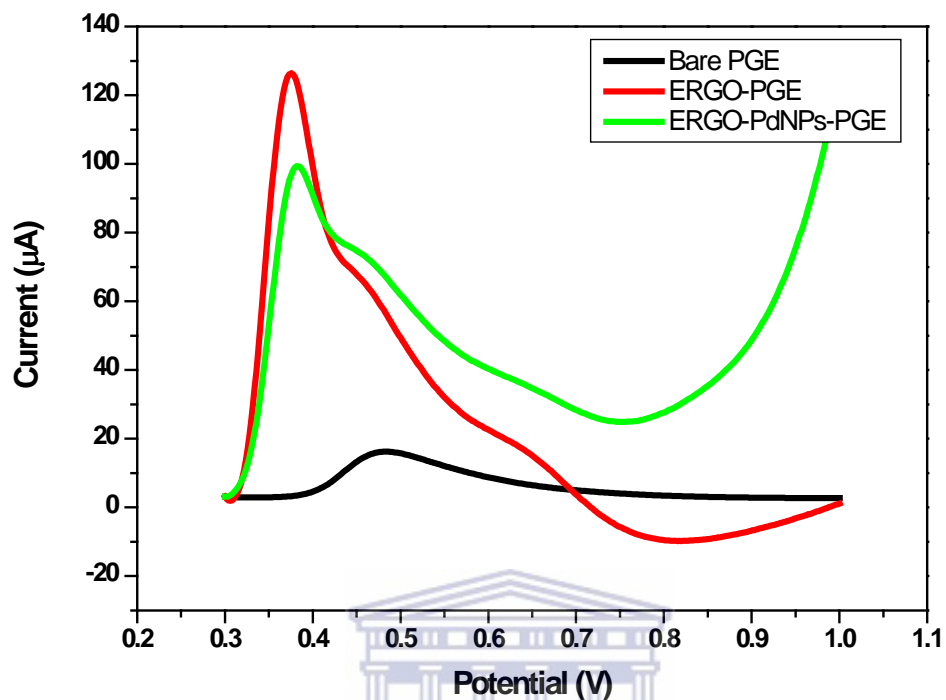
**Figure 6.1:** DPV of  $0.1 \text{ molL}^{-1}$  PBS at pH 7 containing  $50 \mu\text{M}$  BPA for the electrode (black) bare PGE, (red) ERGO-PGE, (green) ERGO-CoNPs-PGE.

The electrochemical behavior of BPA at the bare PGE, ERGO –PGE and ERGO-NiNPs-PGE are shown in Figure 6.2. There is a slight enhancement in the peak height at the ERGO-NiNPs-PGE in comparison to the bare PGE and ERGO –PGE but not significant enough to be used for sensor applications.



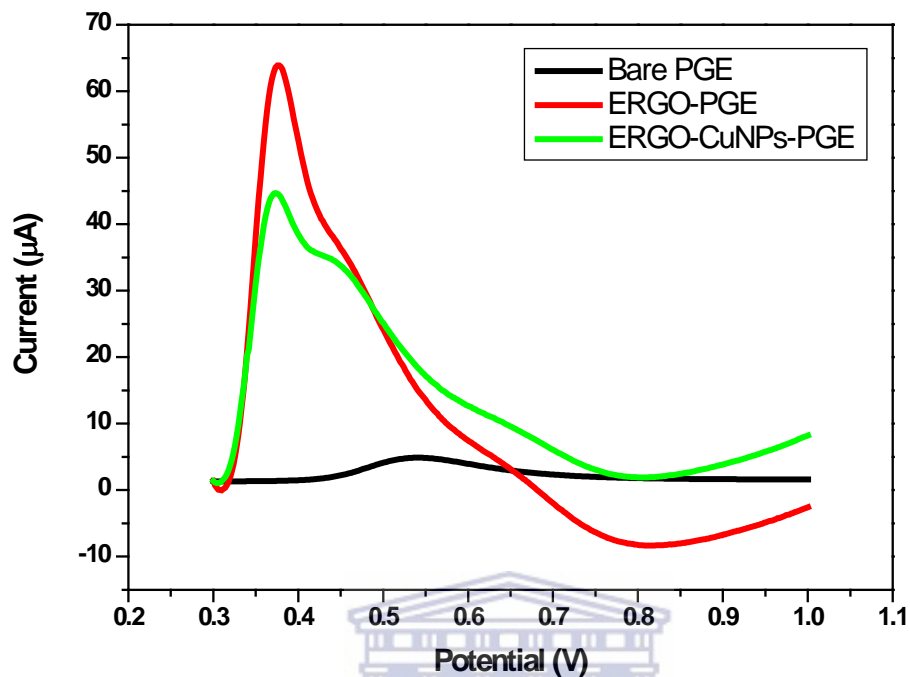
**Figure 6.2:** DPV of  $0.1 \text{ molL}^{-1}$  PBS at pH 7 containing  $50 \mu\text{M}$  BPA for the electrode (black) bare PGE, (red) ERGO-PGE, (green) ERGO-NiNPs-PGE.

Figure 6.3 represents the increase in the BPA oxidation peak at the bare PGE, ERGO –PGE and ERGO-PdNPs-PGE. An increase in the peak height is observed from the bare PGE to the ERGO-PGE. The effect of the synergetic combination of ERGO sheets and Pd nanoparticles yielded to a significant enhancement in the peak height at the ERGO-PdNPs-PGE.



**Figure 6.3:** DPV of  $0.1 \text{ molL}^{-1}$  PBS at pH 7 containing  $50 \text{ }\mu\text{M}$  BPA for the electrode (black) bare PGE, (red) Pd Film-PGE, (green) ERGO -PGE, (blue) ERGO-PdNPs-PGE.

The electrochemical response of PBA oxidation at the bare PGE, ERGO -PGE and ERGO-CuNPs-PGE is represented in Figure 6.4. The peak current has been decreased from ERGO -PGE to ERGO-CuNPs-PGE.



**Figure 6.4:** DPV of  $0.1 \text{ molL}^{-1}$  PBS at pH 7 containing  $50 \text{ }\mu\text{M}$  BPA for the electrode (black) bare PGE, (red) ERGO-PGE, (green) ERGO-CuNPs-PGE.

The electrochemical responses of the bare PGE, ERGO –PGE and ERGO-AuNPs-PGE platforms towards BPA are compared in Figure 6.5. A considerable increase in peak height can be seen at the ERGO-AuNPs-PGE in comparison to the bare PGE and ERGO –PGE. The enhanced conductivity and electron transfer is due to the higher surface area-to-volume ratio of graphene and gold nanoparticles in the nanometer range (1-100 nm) confirmed by the increased stripping peak current from the bare PGE to ERGO –PGE and ERGO-AuNPs-PGE.

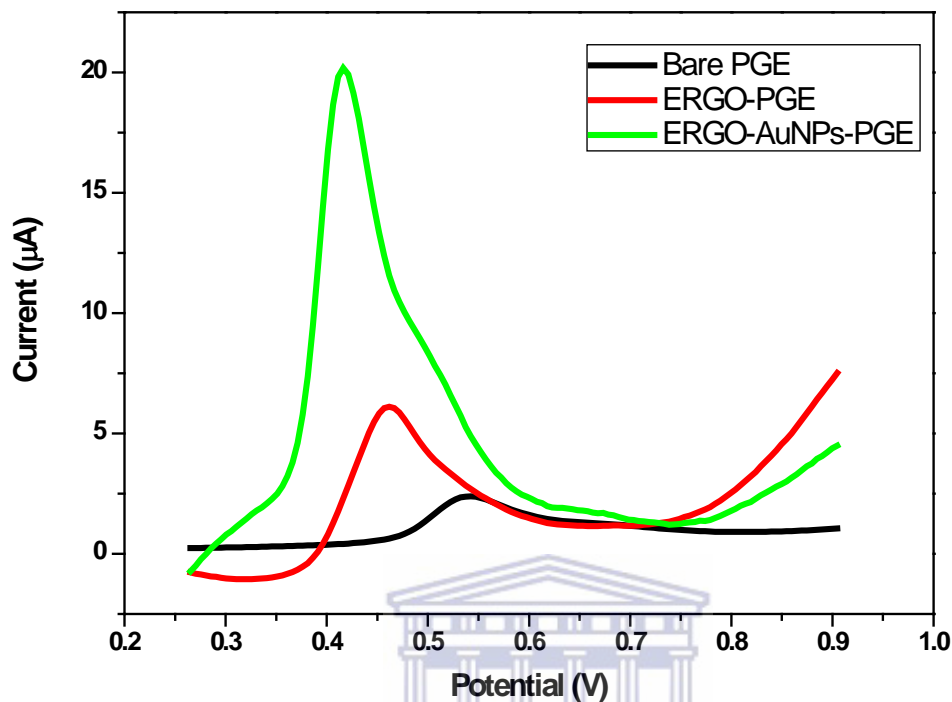


**Figure 6.5:** DPV of  $0.1 \text{ molL}^{-1}$  PBS at pH 7 containing  $50 \mu\text{M}$  BPA for the electrode (black) bare PGE, (red) ERGO-PGE, (green) ERGO-AuNPs-PGE.

The stripping peak current of BPA at the bare PGE, ERGO –PGE and ERGO-SbNPs-PGE is shown in Figure 6.6. The DPV voltammetry shows a negative shift for BPA oxidation peak on bare PGE at 492 mV to 389 mV on ERGO-PGE and ERGO-SbNPs-PGE. Moreover, the BPA oxidation peak on modified ERGO-SbNPs-PGE shows a 12 times bigger current than the bare PGE. The enhancement in the oxidation current peak of PBA at ERGO-SbNPs-PGE reflects the increase of the electroactive surface area by the formed hybrid (rGO–SbNPs).

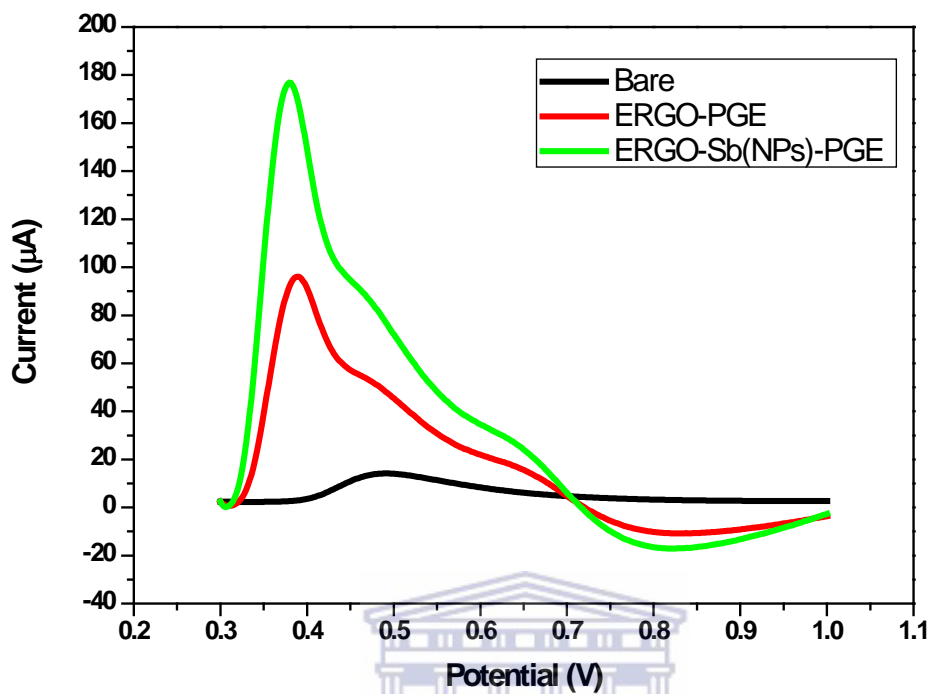


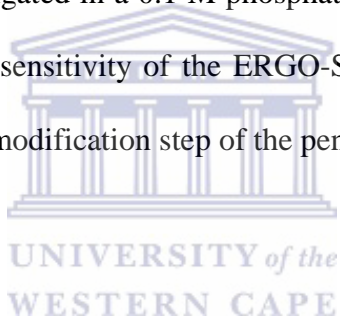
**Figure 6.6:** DPV of  $0.1 \text{ molL}^{-1}$  PBS at pH 7 containing  $50 \text{ }\mu\text{M}$  BPA for the electrode (black) bare PGE, (red) ERGO-PGE, (green) ERGO-SbNPs-PGE.

The electrochemical oxidation of BPA increased significantly when ERGO-SbNPs-PGE and ERGO-AuNPs-PGE were used as the working electrodes; thus the electrochemical characterizations of these two electrodes were conducted to investigate them in more details.

## **6.3. Electrochemically reduced graphene oxide antimony nanoparticles pencil graphite electrode (ERGO-SbNPs-PGE)**

### **6.3.1. Influence of the electrodeposition method of GO-SbNPs onto the PGE**

The electrodeposition of GO-SbNPs onto the pencil graphite electrode was conducted in three different methods: (1) Applying fixed potential for 120 s. (2) Cycling for 5 excessive cycles. (3) Applying fixed potential for 120 s as the conditioning step and then cycling 5 excessive cycles. The effect of electrodeposition method of GO-SbNPs onto the pencil graphite electrode on the oxidation peak of BPA was investigated in a 0.1 M phosphate buffer solution (pH 7) containing 50  $\mu\text{g L}^{-1}$  BPA (Figure 6.7). The sensitivity of the ERGO-SbNPs-PGE improved significantly when the last method used for the modification step of the pencil graphite electrode.



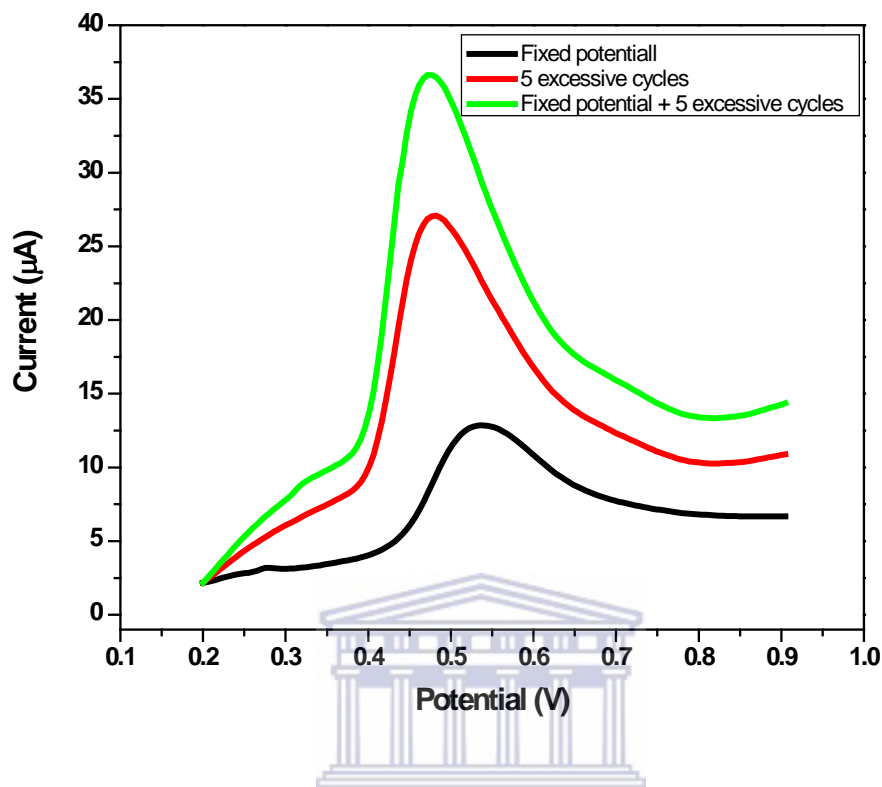


**Figure 6.7:** DPV of 0.1 molL<sup>-1</sup> PBS at pH 7 containing 50 μM BPA for the electrode (black) GO-SbNPs deposited at a fixed potential of -0.7 V, (red) GO-SbNPs deposited by 5 excessive cycles, (green) GO-SbNPs deposited at a fixed potential of -0.7 V and 5 excessive cycles.

### 6.3.2. Influence of the number of GO-SbNPs electrodeposition cycles

The sensitivity and performance of any electrode is influenced by the speed and ease of electron transfer through the deposited film [107]. The influence of the number of GO-SbNPs electrodeposition cycles on the oxidation peak of BPA is shown in Figure 6.8. A deposition of five cycles was selected for the further experiments of detection of BPA at the ERGO-SbNPs-PGE as it showed the biggest peak current. The peak current decreased after 5 cycles because the thickness of the graphene- SbNPs film impedes the flow of electrons to the electrode surface. The advantage



of electrodeposition of the GO-SbNPs onto the pencil electrode using cycling voltammetry is the ability of controlling the film thickness deposited on the electrode surface.

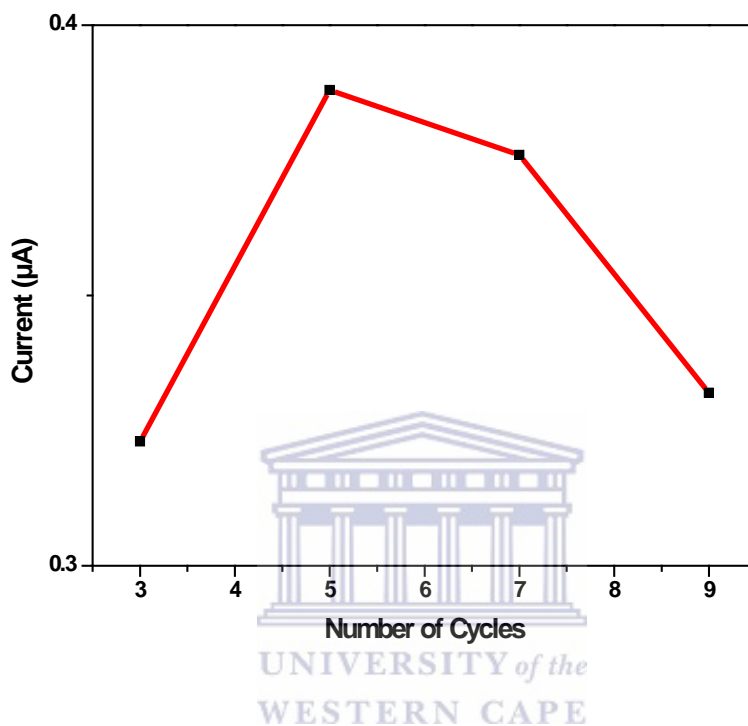


**Figure 6.8:** Effect of number of cycles on the peak currents of BPA at the ERGO-SbNPs-PGE in 0.1 M phosphate buffer solution (pH 7).

### 6.3.3. Effect of the concentration of the antimony

The effect of the antimony concentration in the GO-SbNPs solution was varied from 5 to 20 ppm for the modification of the pencil graphite electrode; the oxidation peak of BPA was investigated in a 0.1 M phosphate buffer solution (pH 7) containing  $50 \mu\text{g L}^{-1}$  BPA (Figure 6.9). The peak currents increased to a maximum with increasing the antimony concentration followed by the decrease in peak current with increasing the concentration. The decrease in the peak height can be due to the enlargement of the antimony nanoparticle sizes as a result of high concentration of the

antimony in the GO-SbNPs solution [80,81,108]. A concentration of 15 ppm was selected as the optimum antimony concentration for the detection of BPA at the EGO-SbNPs-PGE.

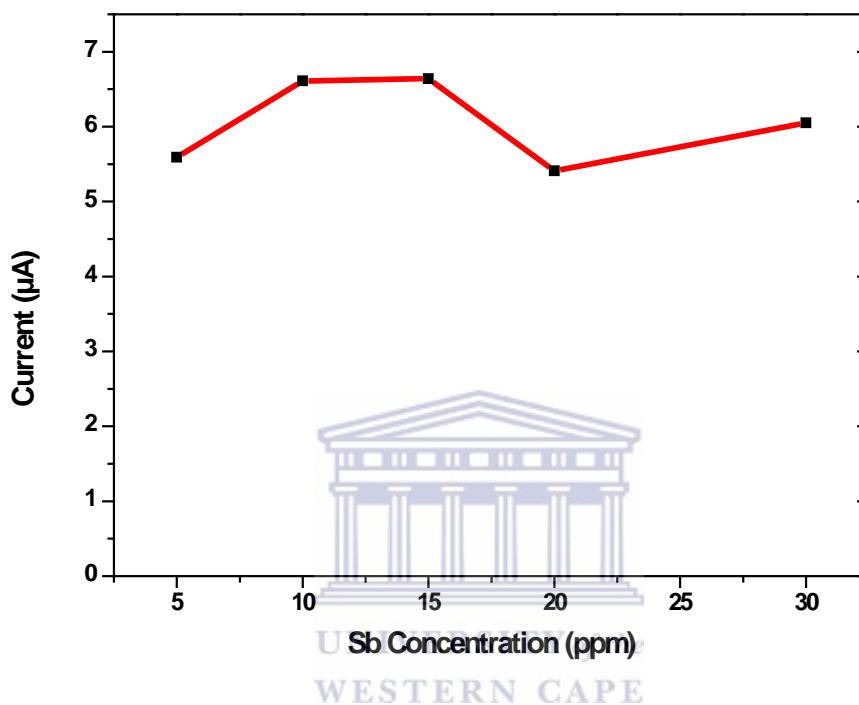


**Figure 6.9:** Effect of antimony concentration in the GO-SbNPs solution for modification of pencil graphite electrode on the oxidation peak of BPA in 0.1 M PBS (pH 7) containing  $50 \mu\text{g L}^{-1}$  BPA.

#### 6.3.4. The effect of the electrodeposition time of GO-SbNPs

The influence of the electrodeposition time of GO-SbNPs in the pencil graphite electrode modification step on the peak current of BPA was studied over the time interval from 60 to 300 seconds (Figure 6.10). The peak current is observed to be increased up to 120 s after which the peak height level off suggesting surface saturation of the electrode. As a consequence of this

behavior a deposition time of 120 s was selected for the developing the electrodeposited GO-Sb NPs-PGE.

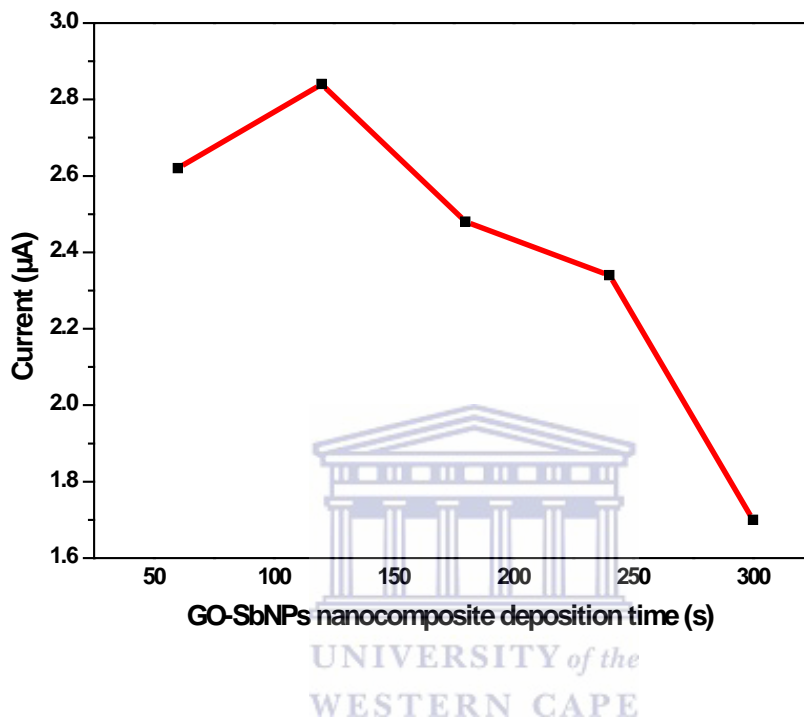


**Figure 6.10:** Effect of the electrodeposition time of GO-SbNPs for modification of pencil graphite electrode on the oxidation peak of BPA in 0.1 M PBS (pH 7) containing  $50 \mu\text{g L}^{-1}$  BPA.

### 6.3.5. Microscopic Characterization of Electrodeposited Graphene- SbNPs Modified Pencil Electrode ERGO-SbNPs-PGE

Figure 6.11 shows the surface morphologies of the bare PGE, EGO-PGE, and ERGO-SbNPs-PGE with high resolution scanning electron microscopy (HRSEM). The grooves along the surface in

the direction of machining was observed at the bare PGE at low magnification, Figure 6.11 (a), while graphene fake sheets at higher magnification are observed at EGO-PGE, and ERGO-SbNPs-PGE, Figure 6.11 (b) and 6.11 (c). Antimony nanaoparticles on top of the graphene sheets can be seen at the ERGO-SbNPs-PGE at higher magnification in Figure 6.11(c).

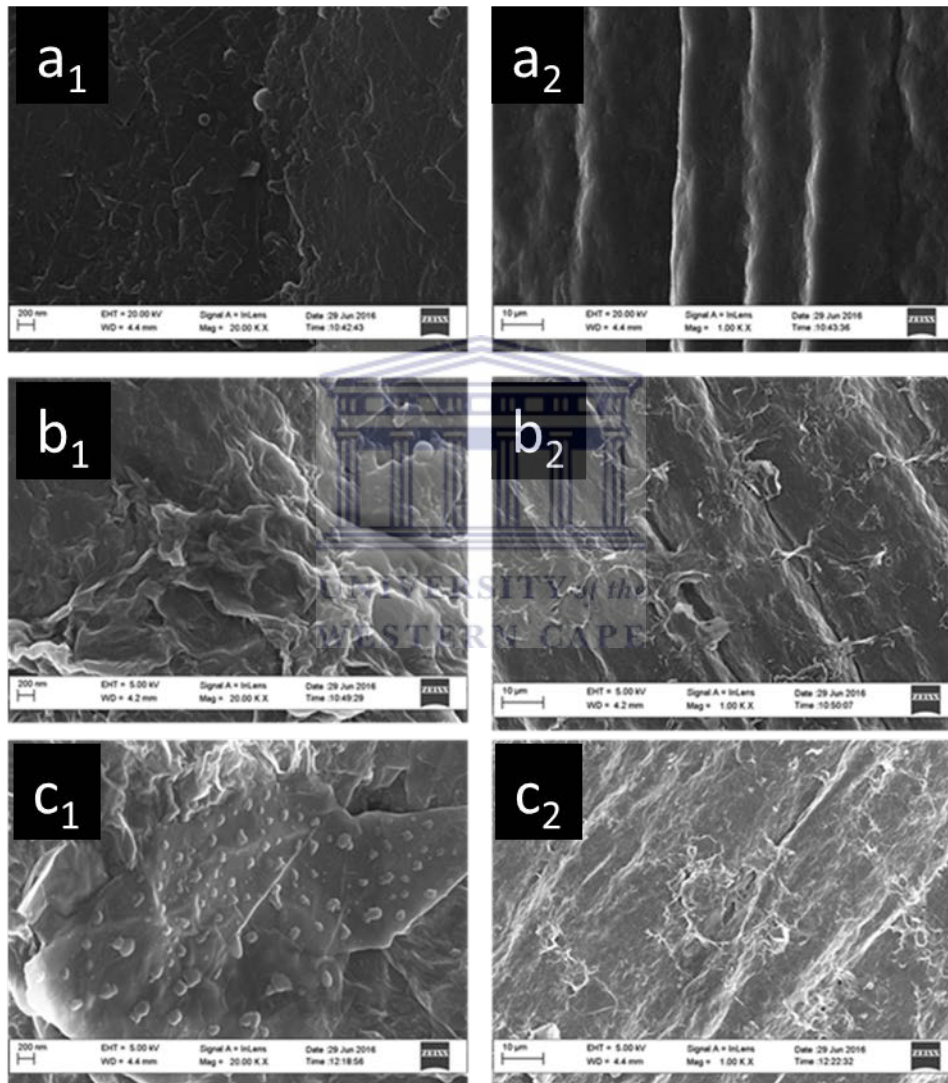


**Figure 6.11:** HRSEM images of bare PGE (a), EGO-PGE (b), and ERGO-SbNPs-PGE (c) at 20.00 k times magnification (1) and 1000 times magnification (2).

### 6.3.6. Antimony nanoparticles on the ERGO-SbNPs-PGE

The presence of the antimony nanoparticles on the electrode surface was investigated electrochemically in HCl solution to confirm the observation in HRSEM images (Figure 6.12). The ERGO-SbNPs-PGE was run in a 1 M HCl solution with differential pulse voltammetry and a big oxidation peak at -0.1 V was observed confirming the presence of antimony nanoparticles on the electrode surface.

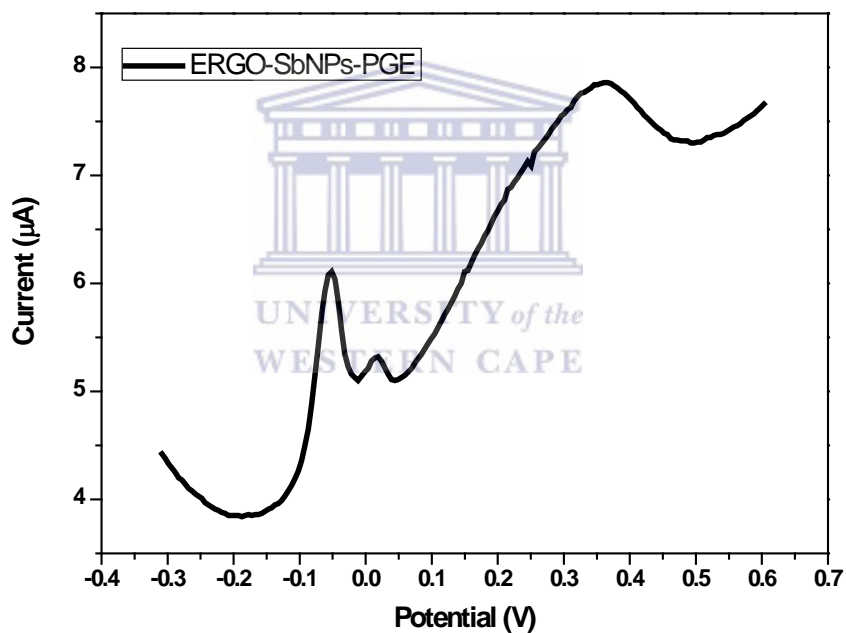


**Figure 6.12:** Stripping voltammetry of antimony nanoparticles in a 1.0 M HCl solution at ERGO-SbNPs-PGE.

### 6.3.7. Electrochemical characterization of ERGO-SbNPs-PGE in Ferricyanide solution

Potassium ferricyanide was used as a redox marker to investigate the electrochemical properties of electrochemically reduced graphene oxide antimony nanoparticles pencil graphite electrode. The measurements of impedance, CV, and effect of scan rate were carried in 0.1 M KCl solution containing 5 mM  $[\text{Fe}(\text{CN})_6]^{-3/4}$ .

#### 6.3.7.1. Impedimetric analysis

Figure 6.13 shows electrochemical impedance analysis of the bare PGE, ERGO-PGE, and ERGO-SbNPs-PGE in 0.1 M KCl solution containing 5 mM  $[\text{Fe}(\text{CN})_6]^{-3/4}$ . The electrochemical properties of the film modified on the pencil graphite electrode are studied by using the associated equivalent circuit model. The semicircle parameters of the Nyquist plots of the bare PGE, ERGO-PGE, and ERGO-SbNPs-PGE correspond to the double layer capacity ( $C_{dl}$ ) of the film and the electron transfer resistance ( $R_{ct}$ ) [109–111]. A semicircle area ( $R_{ct} = 1204 \Omega$ ) is observed at bare PGE which is larger than ERGO film ( $R_{ct} = 269.6 \Omega$ ); this area has decreased at ERGO-SbNPs film ( $R_{ct} = 209.8 \Omega$ ) in comparison to other two electrodes indicating the lower electron transfer resistance at ERGO-SbNPs film which improves the electron-transfer kinetics process as a faster one and more suitable for the electrocatalytic activities, respectively [110,112,113].

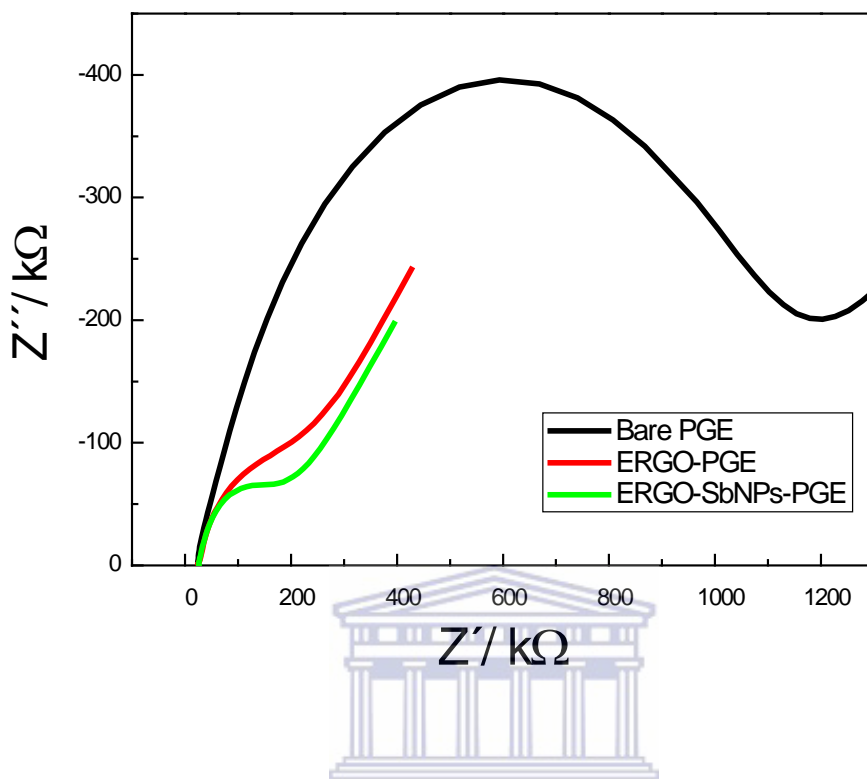


**Figure 6.13:** EIS response of the bare PGE (black), and ERGO-PGE (red), and ERGO-SbNPs-PGE (green) in 0.1 M KCl containing 5 mM  $[\text{Fe}(\text{CN})_6]^{3-/4-}$ .

### 6.3.7.2. Electrochemical characterization of the pencil graphite electrode after the modification

Figure 6.14 shows the electrochemical response of the pencil electrode before and after each modification step in ferricyanide solution. The oxidation and reduction response of 5 mM  $[\text{Fe}(\text{CN})_6]^{3-/4-}$  in 0.1 M KCl solution at bare PGE, ERGO-PGE and ERGO-SbNPs-PGE was measured with cyclic voltammetry at 50 mV s<sup>-1</sup> scan rate. The broad peaks of  $[\text{Fe}(\text{CN})_6]^{3-/4-}$  redox couple at bare pencil graphite electrode can be seen and the separation of anodic and cathodic peaks is 0.71503 V, 0.11582 V, and 0.10071 V for bare PGE, ERGO-PGE, and ERGO-SbNPs-PGE, respectively.

This result is consistent with the decrease in  $R_{ct}$  observed using EIS. There is an enhancement in the peak size after each modification step showing a better sensitivity in the electrode surface due to the higher surface to volume ratio and faster electron transfer [87,107].

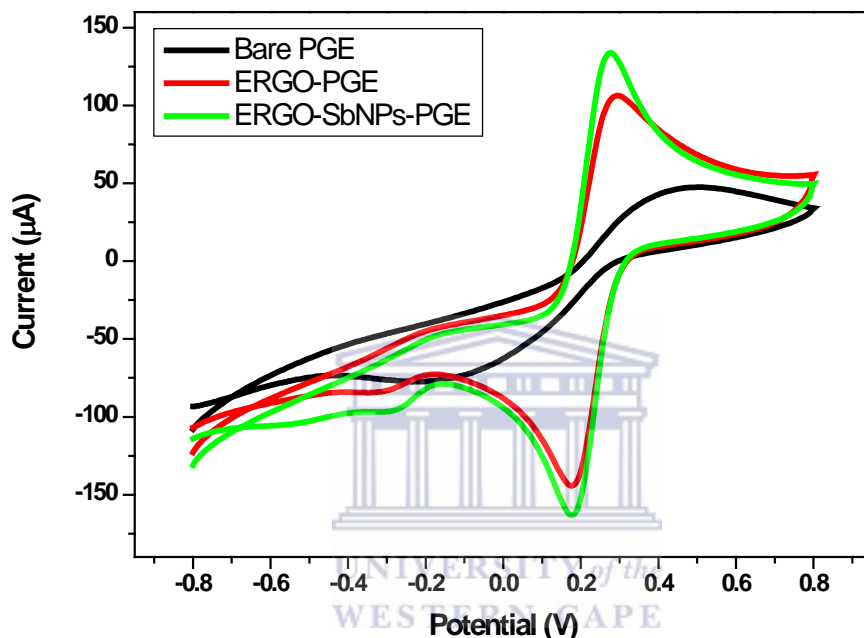


**Figure 6.14:** CV voltammograms of 5 mM  $[\text{Fe}(\text{CN})_6]^{3-/4-}$  in 10 mL of 0.1 M KCl solution at bare PGE (black), ERGO-PGE (red), and ERGO-SbNPs-PGE (green).

### 6.3.7.3. The effect of scan rate

The dependence of peak currents on the scan rate over the  $10 \text{ mV s}^{-1}$  to  $100 \text{ mV s}^{-1}$  range is shown in the Figure 6.15 (a). The oxidation and reduction peak currents exhibit a linear increase with increasing the square root of the scan rate (Fig 6.15 (b)) indicating the process is diffusion controlled. A correlation of 0.996 was obtained for both anodic and cathodic peak current versus the square root of the scan rate.



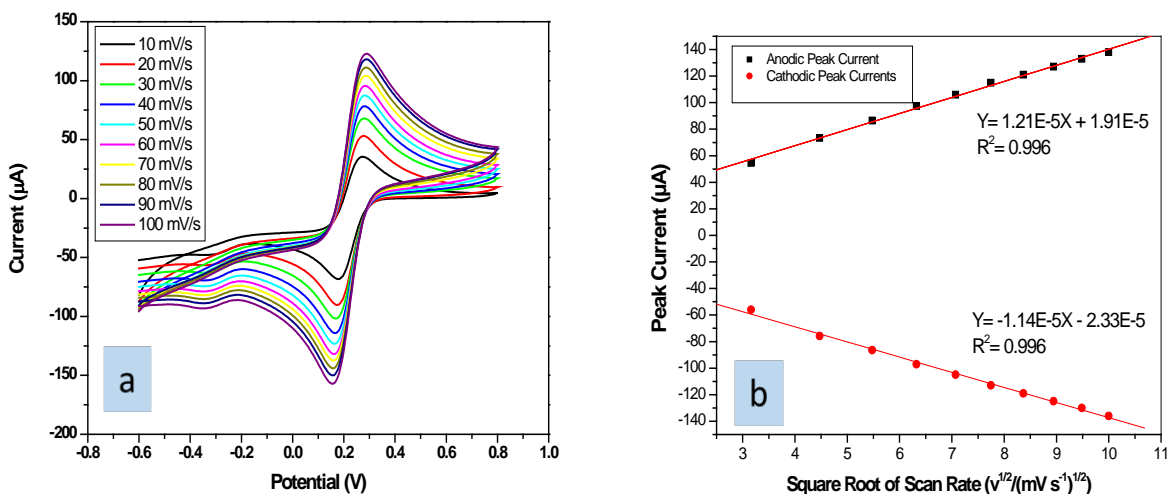


**Figure 6.15:** Cyclic voltammograms overlay at different scan rates from 10 to 100  $\text{mV s}^{-1}$  in 10 mL 0.1 M KCl solution containing 5.0 mM  $[\text{Fe}(\text{CN})_6]^{3-/4-}$  at ERGO-SbNPs-PGE (a) and The plot of peak currents vs square root of scan rate (b).

### 6.3.8. The synergetic effect of graphene sheets and antimony nanoparticles in electrochemical response of BPA

Figure 6.16 shows the change of the oxidation peak height of 50  $\mu\text{M}$  BPA with DPV at bare pencil graphite electrode and modified pencil graphite electrode. There is an improvement in the electrode sensitivity when it is modified with antimony nanoparticles (Figure 6.16 a). There is a chance the antimony is deposited on the electrode surface as a film which can explain why the sensitivity of the electrode is not improved significantly. A big enhancement in the peak height is observed from bare PGE to ERGO-PGE shown in Figure 6.16 b. Figure 6.16 c shows a significant increase in the oxidation peak of BPA when the pencil electrode is modified with both graphene and antimony nanoparticles.

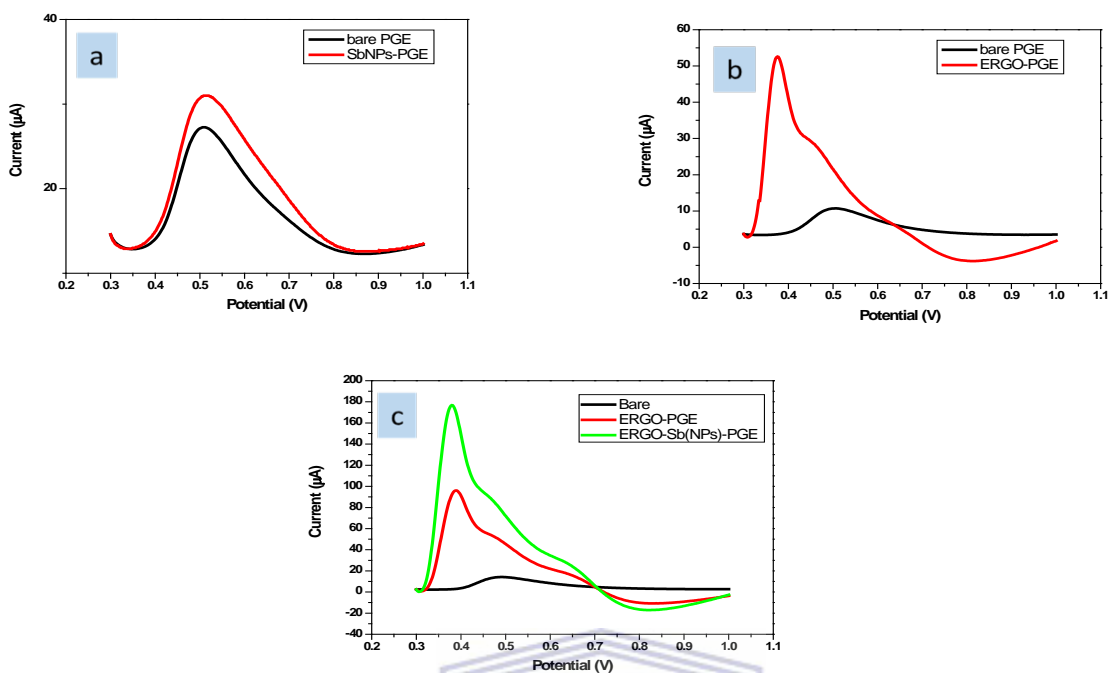


**Figure 6.16:** The comparison of DPV measurements of  $0.1 \text{ mol L}^{-1}$  PBS at pH 7 containing  $50 \mu\text{M}$  BPA at bare PGE and SbNPs-PGE (a), bare PGE and ERGO-PGE (b), and bare PGE, ERGO-PGE and ERGO-SbNPs-PGE (c).

### 6.3.9. The fouling effect of BPA

The adsorption behaviour of BPA was investigated using adsorptive stripping differential pulse voltammetry. Figure 6.17 illustrates 9 differential pulse voltammograms carried out in  $0.1 \text{ mol L}^{-1}$  PBS (pH 7.0) containing  $5.0 \mu\text{mol L}^{-1}$  of BPA, in a potential range between +0.3 and +1.0 V using the same ERGO-SbNPs-PGE for all measurements without electrochemically cleaning of the electrode. The BPA oxidation process decrease by each measurement showing the well-known fouling effect of BPA caused by the phenol group owing to the formation of a polymeric film on the electrode surface [11,12,54]. Attempts were made to clean the ERGO-SbNPs-PGE electrochemically in order to remove fouling from the electrode.

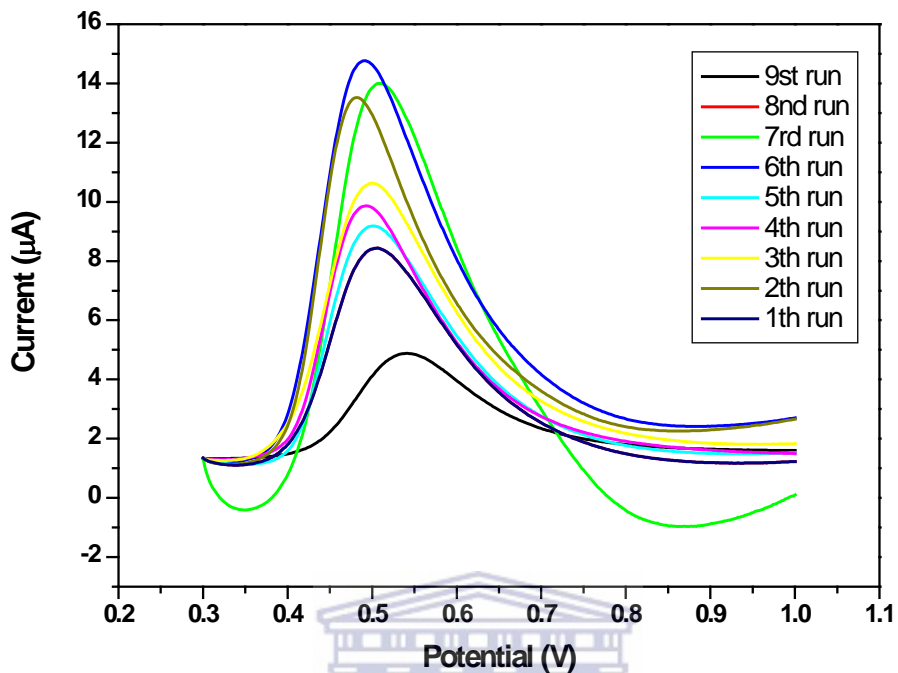


**Figure 6.17:** 9 successive differential pulse voltammograms at ERGO-SbNPs-PGE, in 0.1 mol L<sup>-1</sup> of PBS pH 7.0 containing 5.0 µmol L<sup>-1</sup> of BPA.

### 6.3.10. Electrochemically cleaning of the ERGO-SbNPs-PGE in PBS

The influence of electrochemically cleaning on the recovery of the original response of BPA at ERGO-SbNPs-PGE was investigated using DPV. Figure 6.18 shows the dependence of the oxidation peak of BPA at the same ERGO-SbNPs-PGE on the electrochemically cleaning of the electrode in PBS at -0.2 V. It can be observed in the Figure 6.18 that the oxidation process decreases significantly after the first measurement at the fresh ERGO-SbNPs-PGE and it starts to increase again after the second measurement by applying the cleaning potential to the electrode but the complete recovery was not obtained due to fouling effect of the phenol groups. The single-

use modified pencil graphite electrode was used to overcome these restrictions for the further measurements in the study.

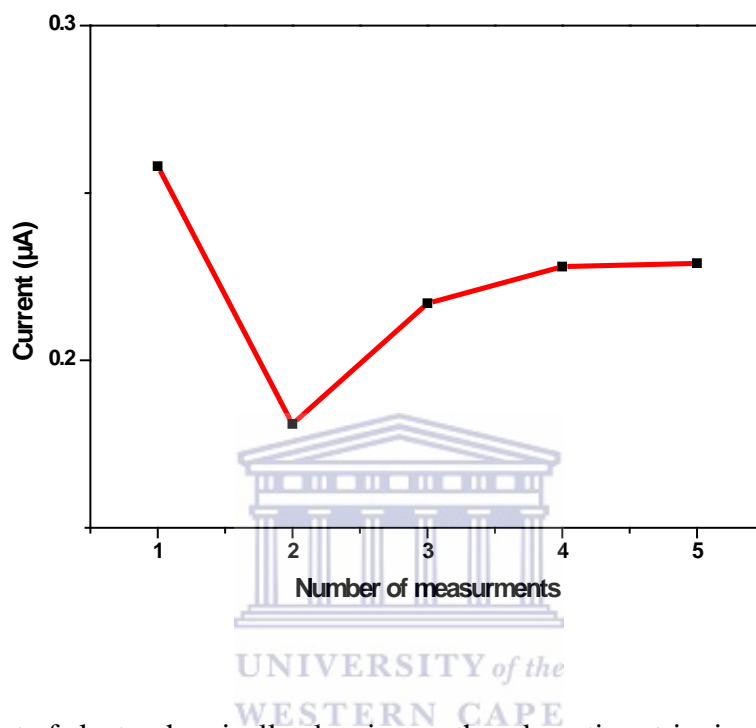


**Figure 6.18:** Effect of electrochemically cleaning on the adsorptive stripping peak current of BPA at the ERGO-SbNPs-PGE in a 0.1 M PBS (pH 7.0) containing 5.0 µM BPA.

### 6.3.11. Reproducibility

Since the complete recovery was not obtained by applying the cleaning potential (-0.2 V) to the ERGO-SbNPs-PGE, the use of a new modified pencil graphite electrode was used each time to overcome the restrictions due to fouling. The oxidation peak current of BPA showed little variation when the batch modification method was used to prepare the ERGO-SbNPs-PGE. The adsorptive differential pulse voltammograms of 50.0 µM BPA in 0.1 M PBS at single-use ERGO-SbNPs-PGE is shown in figure 6.19. The range of relative standard deviation of 2- 5 % was calculated for

the oxidation peak of BPA showing the good reproducibility in preparing the ERGO-SbNPs-PGE.

The modified electrodes were stored in a refrigerator in between the measurements.

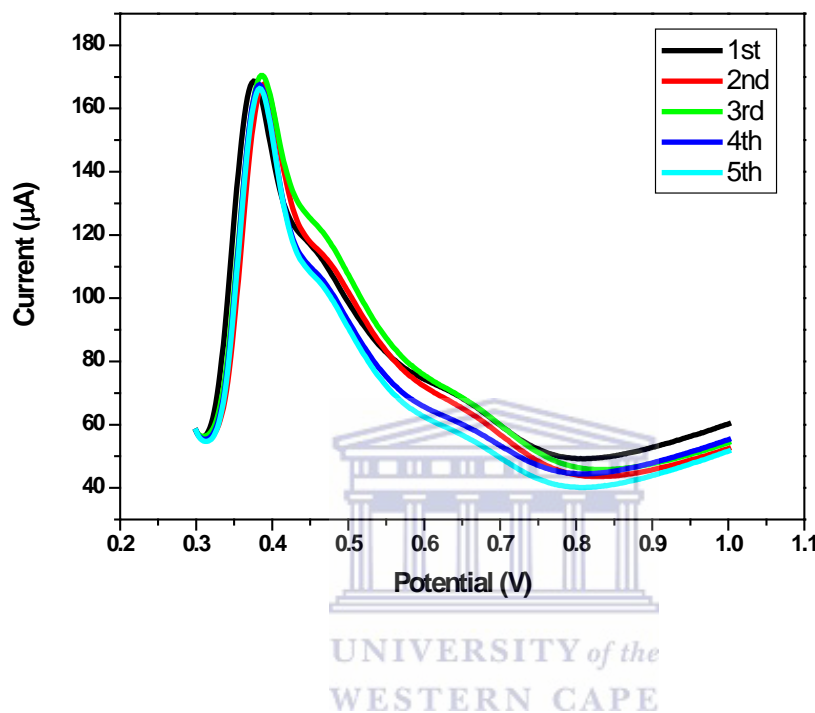


**Figure 6.19:** DPV of  $0.1 \text{ molL}^{-1}$  PBS at pH 7 containing  $50 \text{ }\mu\text{M}$  BPA at single- use ERGO-SbNPs-PGE.

### 6.3.12. Preconcentration time optimization

The influence of pre-concentration time on the peak current of BPA while stirring was investigated over the time interval from 30 to 180 seconds (Figure 6.20). A significant enhancement of adsorptive stripping peaks was observed as the pre-concentration time increased since, a longer time allowed for more BPA to be adsorbed onto the electrode surface. As the peak heights has not increased significantly after 60 seconds a pre-concentration time of 60 s was chosen for further analysis.

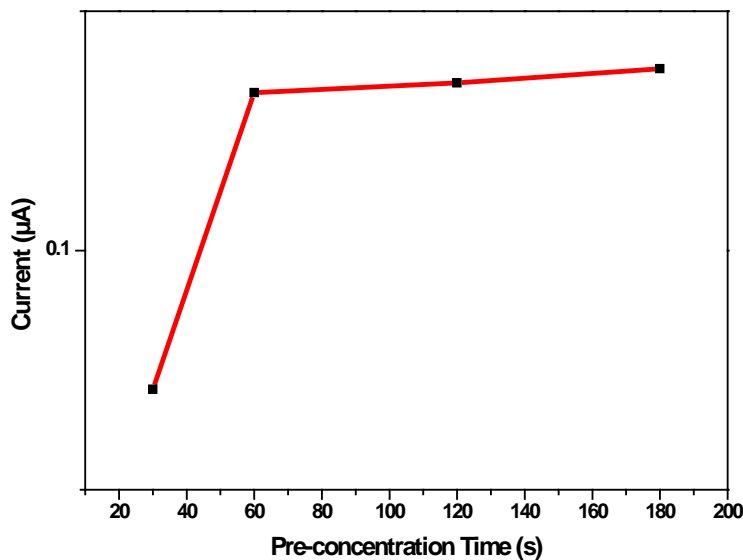


**Figure 6.20:** Effect of pre-concentration time on the peak current of 5.0  $\mu\text{M}$  BPA in 10 mL 0.1 M PBS at ERGO-SbNPs-PGE using DPV.

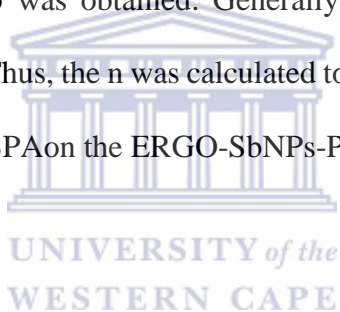
### 6.3.13. Effect of scan rate on the electrocatalytic oxidation of BPA at ERGO-SbNPs-PGE

Figure 6.21 shows the cyclic voltammograms of BPA at the ERGO-SbNPs-PGE when the scan rate ( $\nu$ ) varies from 10 to 100  $\text{mVs}^{-1}$ . As is shown in Fig 6.21 (a), the oxidation peak currents increased linearly in an irreversibly electrode process, indicating that the oxidation of BPA at the ERGO-SbNPs-PGE is adsorption-controlled. Moreover, not linearity of the plot of the peak current ( $I_{pa}$ ) against the square root of scan rate ( $\nu^{1/2}$ ), confirms the adsorption-controlled BPA oxidation (Fig 6.21 (d)) [52,114,115]. The linear regression equations for oxidation peak ( $I_{pa}$ ) current is:  $I_{pa} = 409.44 \nu + 1.6547$  with the correlation coefficients of 0.9984 (Fig 6.21 (b)). As shown in figure 6.21 (c) there is a linear relationship between the peak potential ( $E_p$ ) and the natural logarithm of

scan rate ( $\ln v$ ) for the ERGO-SbNPs-PGE. As for an irreversibly electrode process, the number of electrons involved in the reaction can be estimated according to the Laviron's equation as follows:

$$E_p = E^0 + (RT/\alpha nF) [\ln (RTk_s/\alpha nF) - \ln v] \quad (\text{Eqn. 6.1})$$

Where  $\alpha$  is the electron transfer coefficient,  $k_s$  is the standard rate constant of the surface reaction,  $T$  is the temperature (298 K here),  $v$  is the scan rate,  $R$  the gas constant ( $8.314 \text{ JK}^{-1}\text{mol}^{-1}$ ),  $n$  is the electron transfer numbers,  $F$  the Faraday constant ( $96,480 \text{ C mol}^{-1}$ ) and  $E^0$  the formal redox potential. The  $\alpha n$  value can be calculated from the slope of the linear regression equation of the linear plot of  $E_p$  with respect to  $\ln v$  of  $E_p = 0.0248 \ln(v) + 0.4649$ ,  $R^2 = 0.998$ .  $RT/\alpha nF$  was 0.0248 here, then the value of  $\alpha n = 1.035$  was obtained. Generally, for a totally irreversible electron transfer,  $\alpha$  was assumed to be 0.5. Thus, the  $n$  was calculated to be 2.07 showing that two electrons were involved in the oxidation of BPA on the ERGO-SbNPs-PGE.



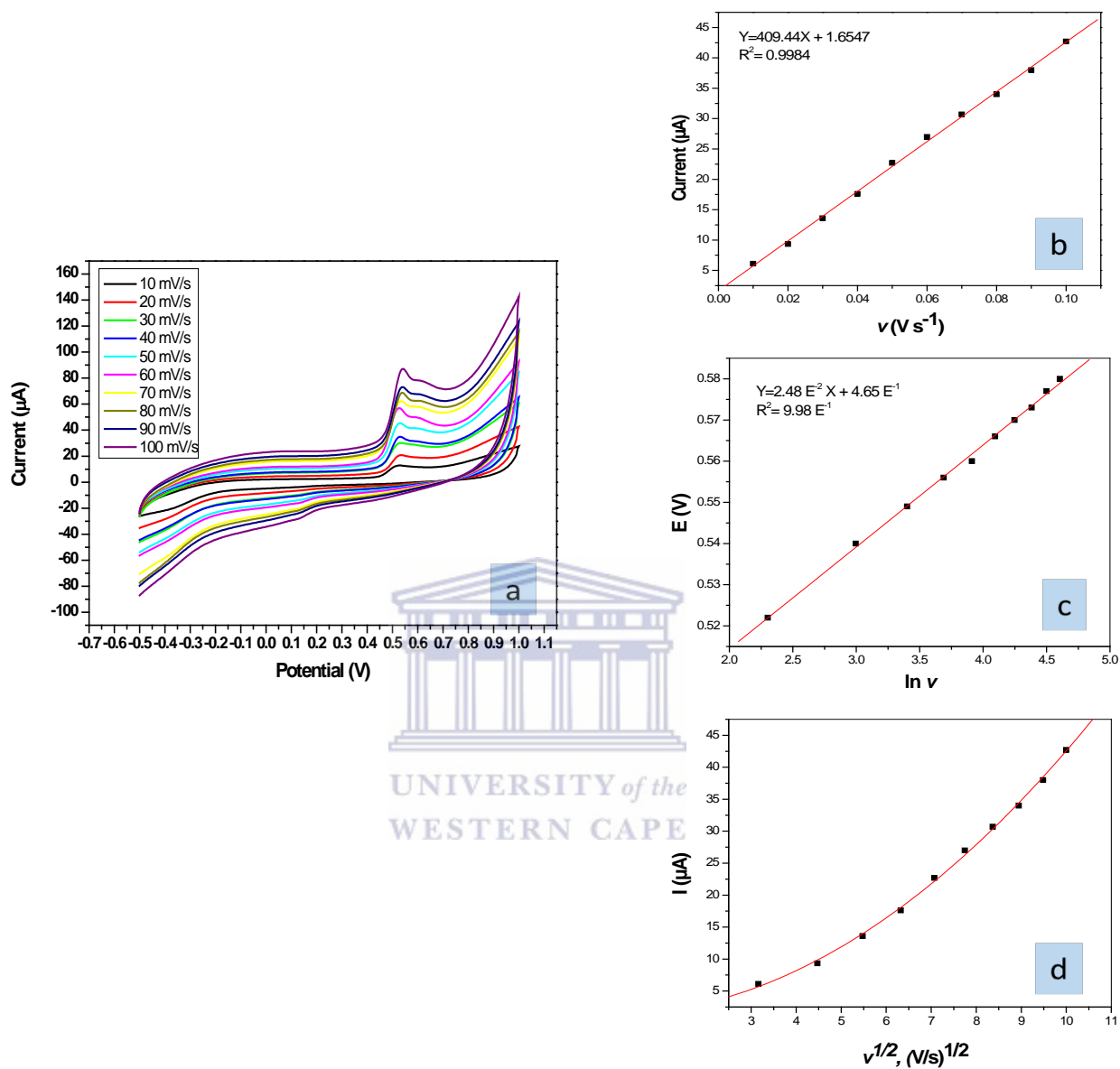


**Figure 6.21:** (a) Cyclic voltammetric responses of 10  $\mu\text{M}$  BPA at ERGO-SbNPs-PGE in 0.1 M PBS (pH= 7.0) at scan rates, (inner to outer) 10, 20, 30, 40, 50, 60, 70, 80, 90, 100  $\text{mVs}^{-1}$ . (b and d) The plots of peak currents vs scan rate and square root of scan rate, respectively. (c) The variation of peak potential vs  $\ln v$ .



### 6.3.14. pH optimization

The effect of pH on the adsorptive stripping peak current ( $I_p$ ) and peak potential was studied by differential pulse voltammetry measurements at pH ranging from 5 to 10 containing 5.0  $\mu\text{M}$  BPA (Figure 6.22). The highest peak current ( $I_p$ ) was observed at 7.04. Therefore pH 7.04 was chosen as the optimum pH for use in subsequent BPA measurements. The linear shifting of the peak potential to more negative values with increasing pH with a slope of  $-61.24 \text{ mV/pH}$  which was close to the theoretical value  $57 \text{ mV/pH}$  indicates equal number of protons and electrons are involved in the BPA oxidation (a two-electron-two-proton process) [11,86,115].

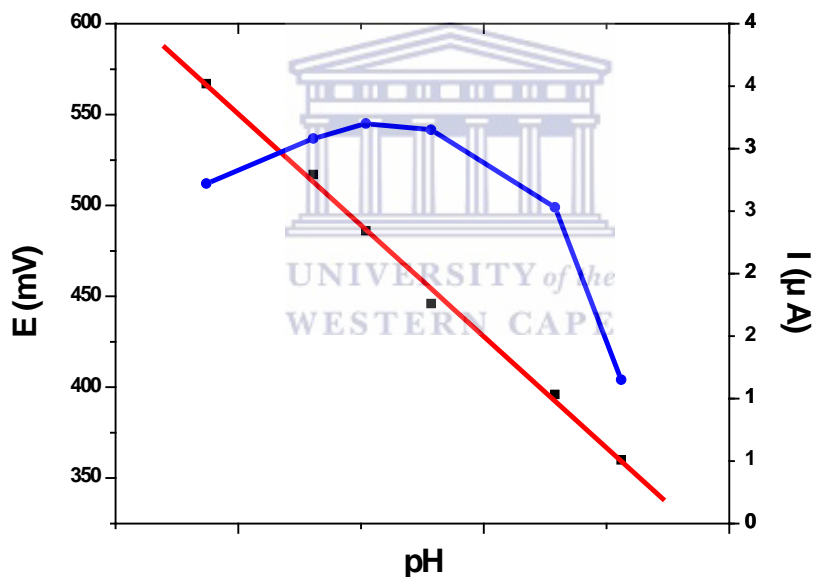


**Figure 6.22:** Effect of pH on the peak current (blue) and peak potential (red) of 1.0  $\mu\text{M}$  BPA in 10 mL 0.1 M PBS at ERGO-SbNPs-PGE using DPV.

### 6.3.15. Interference studies

The effect of various possible interfering molecules was examined on the determination of 50  $\mu\text{M}$  bisphenol A by DPV measurements in the absence and presence of the interferences (Figure 6.23). The electroinactive molecules that were tested were as following: O-Nitrophenol, Potassium Chloride, Cerium (III) nitrate hexahydrate, sodium chloride, 4-cumylphenol. As it shown in the Figure 8 no electroactivity and change was found in the voltammetric response of 50  $\mu\text{M}$  BPA in the presence of two-time excess concentration (100.0  $\mu\text{M}$ ) of these species except 4-cumylphenol. The oxidation peak response of the BPA increased significantly in the presence of 4-cumylphenol indicating the interfering effect of 4-cumylphenol on electrode response towards BPA measurement.



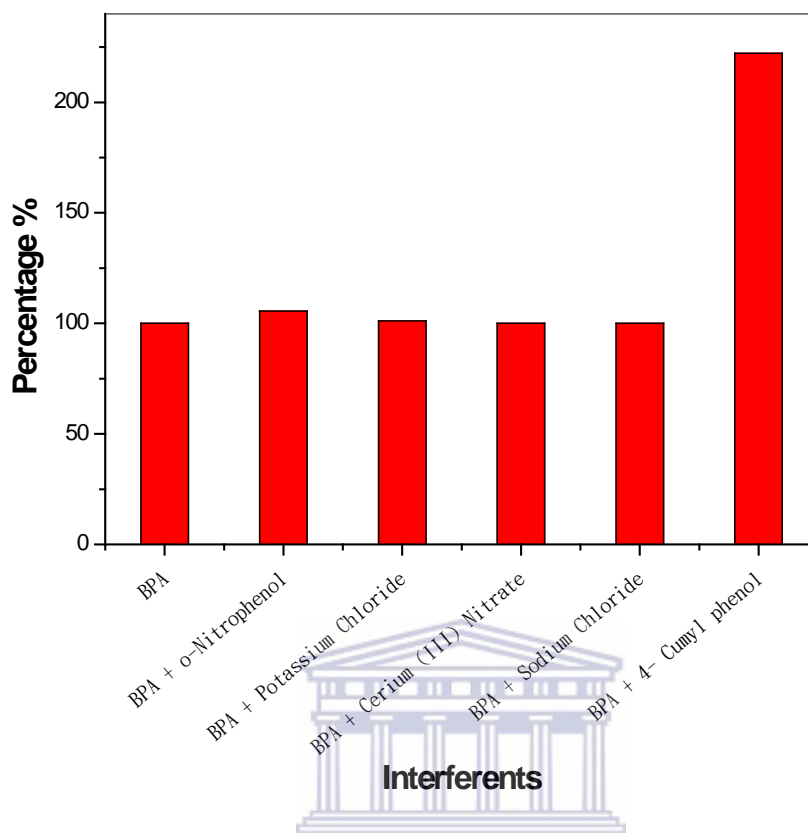


**Figure 6.23:** Percentages of the oxidation peak current of 50  $\mu\text{M}$  of the BPA in absence and presence of 100  $\mu\text{M}$  O-Nitrophenol, Potassium Chloride, Cerium (III) nitrate hexahydrate, sodium chloride, 4-cumylphenol.

### 6.3.16. Detection limit

The detection limit was calculated from BPA calibration curve using the DPV optimized conditions as previously described at the rGO-SbNPs-PGE electrode to investigate its electrochemical response as a function of the BPA concentration (0.4  $\mu\text{M}$  to 5.0  $\mu\text{M}$ ). As it was shown in Figure 6.24 there was a linear relationship between the BPA concentration and peak current with a correlation coefficient of 0.999 ( $n = 9$ ).

The linear regression equation of the average of calibration curves (n=5) was used to calculate the detection limit as the following equation:

$$I(\mu\text{A}) = 1.1 (\mu\text{A } \mu\text{mol L}^{-1}) [\text{BPA}] (\mu\text{mol L}^{-1}) + 0.0715 (\mu\text{A}) \quad (\text{Eqn. 6.2})$$

The detection limit was determined to be 0.012415  $\mu\text{M}$  using a  $3\sigma/\text{slope}$  ratio, where  $\sigma$  is the standard deviation of the mean value for 10 voltammograms of the blank.

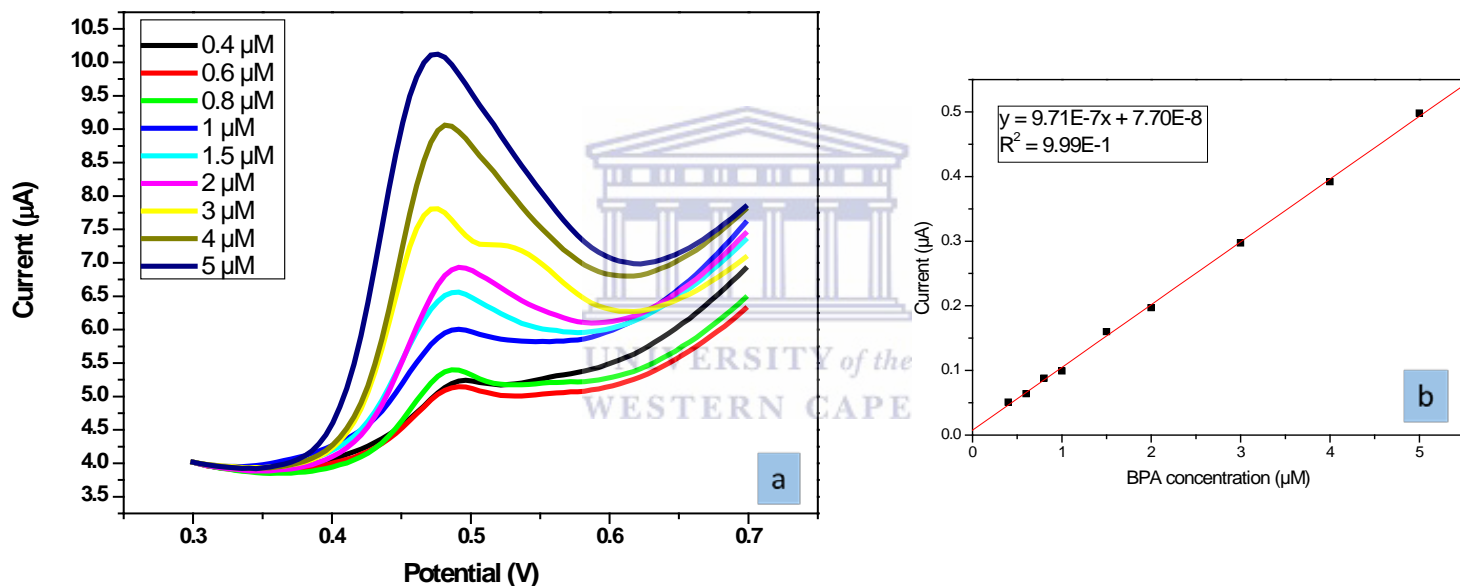


**Figure 6.24:** DPV voltammograms for rGO-SbNPs–PGE nanocomposite electrode, with the optimised parameters (a). The BPA concentrations range from 0.4  $\mu\text{mol L}^{-1}$  to 5.0  $\mu\text{mol L}^{-1}$ . linear dependence of the peak current with BPA concentration(b).

The detection limit of this method was found to be comparable to those reported in the literature. The analytical parameters obtained in this study and those reported previously is shown in Table

6.1. However lower detection limits have been reported but fouling problem as the main challenge for the analysis of BPA and phenols in general still exist [11], [12], [54]. The use of ERGO-SbNPs-PGE electrode involves no complex modification protocols and the fouling was completely eliminated by using single used electrodes.

**Table 6.1.** Comparison of the proposed method with some of the previously reported ones.

Electrode	Linear range ( $\mu\text{M}$ )	Detection limit ( $\mu\text{M}$ )	Reference
ETPGE-LP/SH	0.05-5.0	0.0031	[11]
EG	1.56-50	0.76	[13]
GCE-MWCNT	0.01-10	0.005	[37]
Graphene/GCE	0.05-1	0.046	[86]
MWCNT-SbNPs/GCE	0.5-5.0	0.005	[87]
ERGO-SbNPs-PGE	0.4-5.0	0.012	This study

\*ETPGE-LP/SH: sodium hydroxide in the preparation of electrochemically treated pencil graphite electrodes, EG: exfoliated graphite, GCE-MWCNT: glassy carbon electrode modified with carboxylated multi-walled carbon nanotubes, Graphene/GCE: graphene- modified Glassy carbon electrode, MWCNT-SbNPs/GCE: glassy carbon electrode modified with carbon nanotubes modified with antimony nanoparticles.

### 6.3.17. Analytical application of ERGO-SbNPs–PGE

The potential and suitability of ERGO-SbNPs–PGE was tested in the determination of BPA in real water sample. The ERGO-SbNPs–PGE was used for the quantification of BPA in tap water sample, prepared as described in the experimental section. Bisphenol A determinations were performed three times in tap water samples spiked with 0.2  $\mu\text{M}$  BPA using standard addition method (Figure 6.25). The recovery percentages between 95.2% and 102.8% for BPA in tap water were very satisfactory. The range of relative standard deviation of 1.8- 4 % was calculated for the oxidation peak of BPA in tap water samples showing less than 5 % error in the quantification of BPA in tap water sample using the ERGO-SbNPs-PGE.

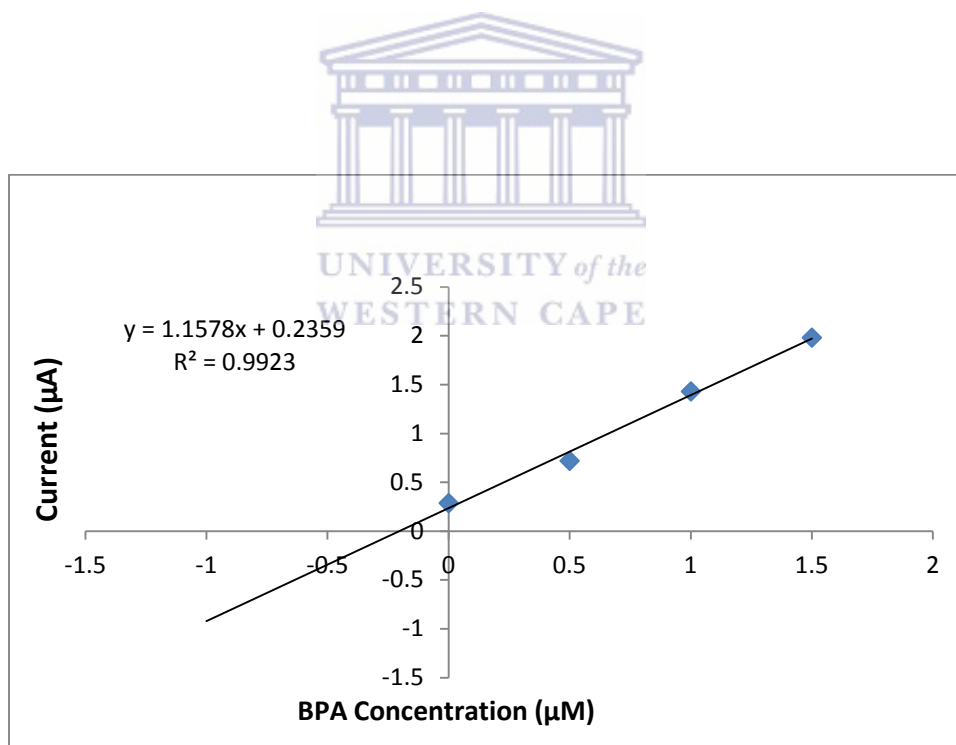


**Figure 6.25:** Linear dependence of the peak currents and BPA concentrations. Tap water sample spiked with 0.2  $\mu\text{M}$  BPA and 0.5  $\mu\text{M}$  BPA was added three times.

## **6.4. Electrochemically reduced graphene oxide gold nanoparticles pencil graphite electrode (ERGO-AuNPs-PGE)**

### **6.4.1. Electrochemical characterization of ERGO-AuNPs-PGE in Ferricyanide solution**

The electrochemical properties of electrochemically reduced graphene oxide gold nanoparticles pencil graphite electrode was evaluated in 0.1 M KCl solution containing 5 mM  $[\text{Fe}(\text{CN})_6]^{3-/4-}$ .

CV measurements in 5.0 mmol L<sup>-1</sup> of  $\text{K}_3[\text{Fe}(\text{CN})_6]$  were used to investigate the electrocatalytic effect of the ERGO-AuNPs nanocomposite with a scan rate of 50mV/s as shown in Figure 6.26. The oxidation and reduction peak have been increased significantly from bare PGE to ERGO-AuNPs-PGE and the difference between cathodic and anodic peaks ( $\Delta_{ep}$ ) has been decreased from 1.012 V at bare PGE to 0.18 V and 0.11 V at ERGO-PGE and ERGO-AuNPs-PGE respectively. These changes are attributed to the faster electron transfer and higher surface to volume ratio at ERGO-AuNPs-PGE [38,87,107].

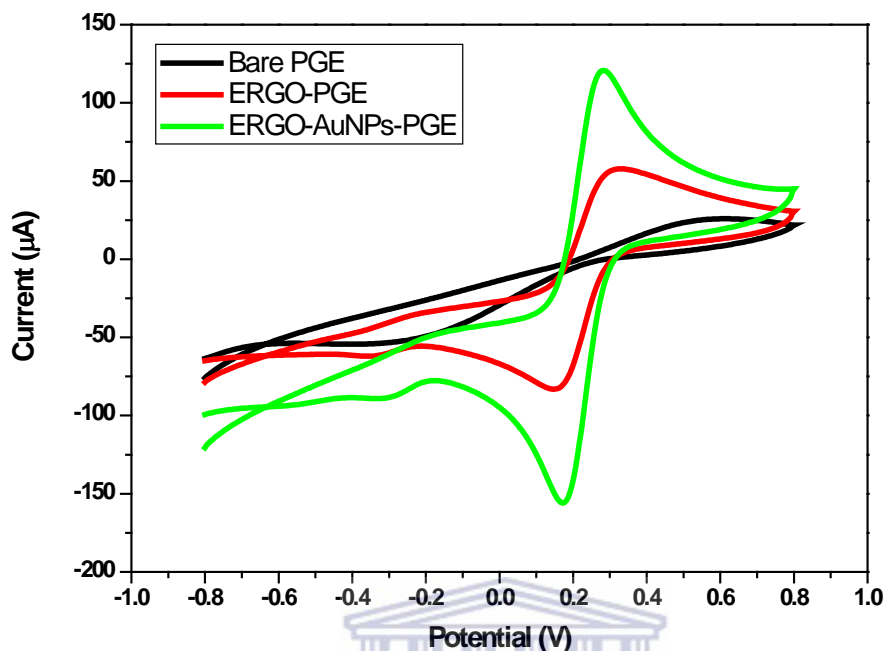


**Figure 6.26:** Cyclic voltammetry at bare PGE (black), ERGO-PGE in absence of AuNPs (red) and ERGO-AuNPs-PGE (green) in 5.0 mM  $\text{Fe}(\text{CN})_6$  in 0.1 M KCl solution.

#### 6.4.2. Impedimetric analysis

Figure 6.27 shows electrochemical impedance analysis of the bare PGE, ERGO-PGE, and ERGO-AuNPs-PGE in 0.1 M KCl solution containing 5 mM  $[\text{Fe}(\text{CN})_6]^{3-/4-}$ . The electrochemical properties of the film modified on the pencil graphite electrode are studied by using the associated equivalent circuit model. The semicircle parameters of the Nyquist plots of the bare PGE, ERGO-PGE, and ERGO-AuNPs-PGE correspond to the double layer capacity ( $C_{dl}$ ) of the film and the electron transfer resistance ( $R_{ct}$ ) [109–111]. A semicircle area ( $R_{ct} = 1971.9 \Omega$ ) is observed at bare PGE which is larger than ERGO film ( $R_{ct} = 458.94 \Omega$ ); this area has decreased at ERGO-AuNPs



film ( $R_{ct} = 224.04 \Omega$ ) in comparison to other two electrodes indicating the lower electron transfer resistance at ERGO-AuNPs film which improves the electron- transfer kinetics process as a faster one and more suitable for the electrocatalytic activities, respectively [110,112,113].

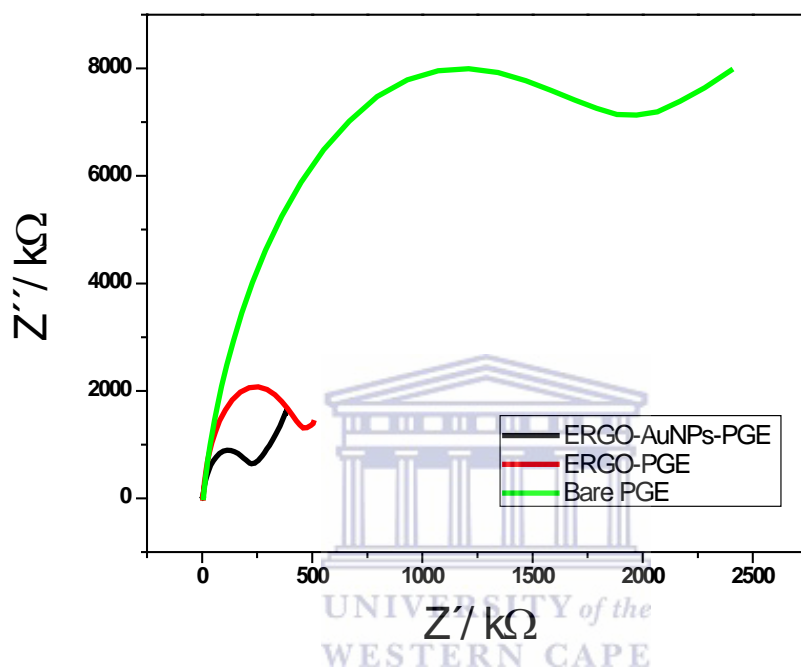


**Figure 6.27:** EIS response of the bare PGE (green), and ERGO-PGE (red), and ERGO-AuNPs-PGE (black) in 0.1 M KCl containing 5 mM  $[\text{Fe}(\text{CN})_6]^{3-/4-}$ .

### 6.4.3. The effect of scan rate

It is shown in Figure 6.28a the CV measurements of the 5 mM  $\text{K}_3\text{Fe}(\text{CN})_6$  at ERGO-AuNPs-PGE at different scan rates from 10 to 100  $\text{mV s}^{-1}$ . The linear relationship between the square root of the scan rate and oxidation and reduction peak current of  $\text{K}_3\text{Fe}(\text{CN})_6$  (Fig. 6.28b) indicates that the process is diffusion controlled[15]. Anodic and cathodic peak current versus the square root of the scan rate obtained a correlation of 0.9998 and 0.998, respectively.

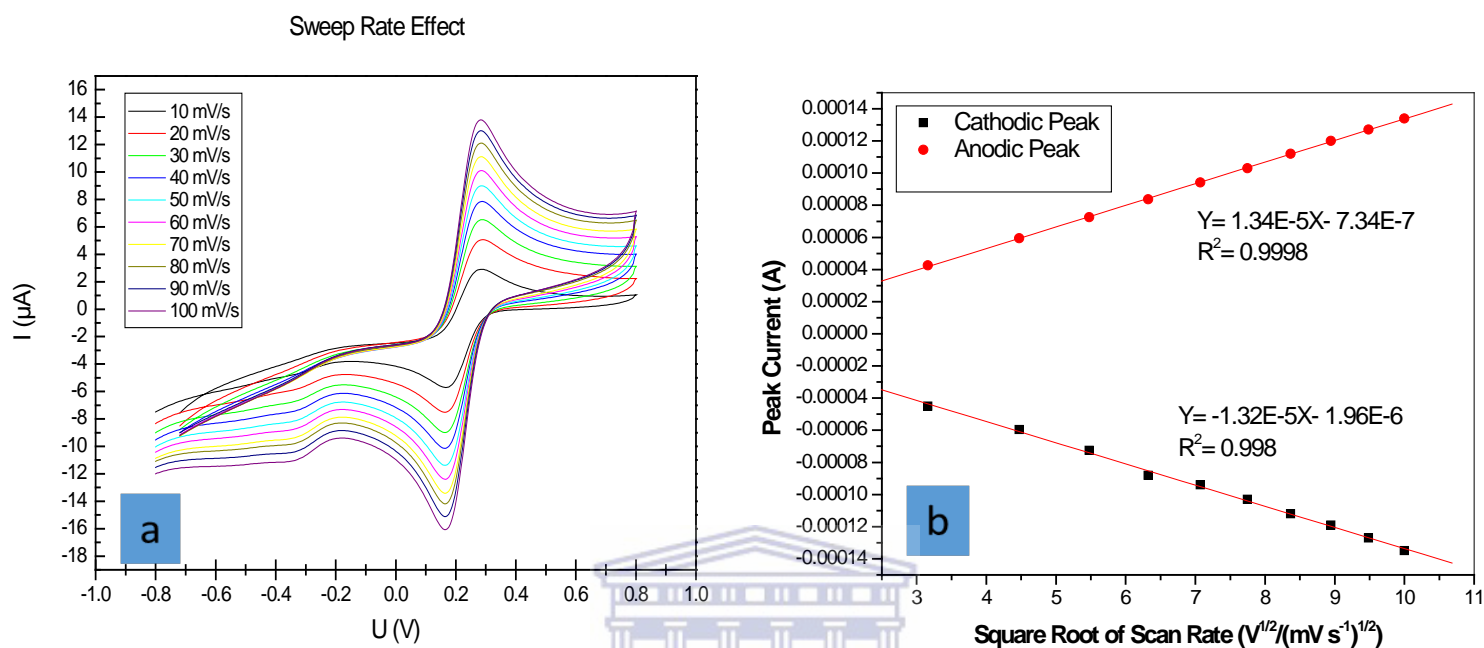


**Figure 6.28:** Cyclic voltammograms overlay at different scan rates from 10 to 100 mV s<sup>-1</sup> in 10 mL 0.1 M KCl solution containing 5.0 mM [Fe (CN)<sub>6</sub>]<sup>3-/4-</sup> at ERGO-AuNPs-PGE (a) and The plot of peak currents vs square root of scan rate (b).

#### 6.4.4. Influence of the number of GO-AuNPs electrodeposition cycles

The effect of the number of cycles to modify the pencil graphite electrode with GO-AuNPs on the oxidation peak of BPA was investigated in a 0.1 M phosphate buffer solution (pH 7) containing 50 µg L<sup>-1</sup> BPA (Figure 6.29). The optimum number of cycles of 5 was selected for the further analysis as the peak heights decreased after 5 cycles due to the ERGO-AuNPs film thickness causing less electron flow to the electrode surface.

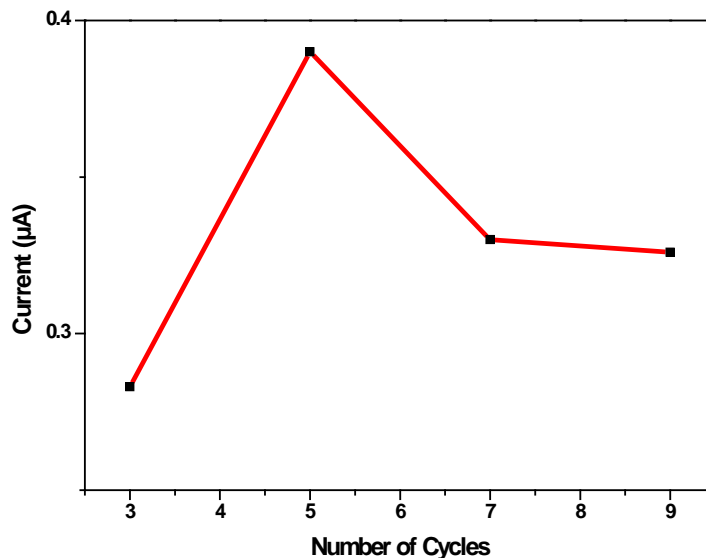
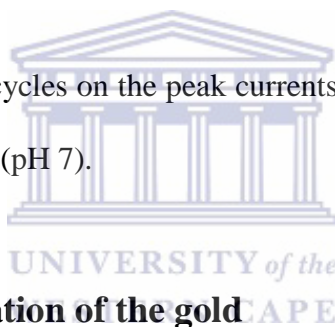


**Figure 6.29:** Effect of number of cycles on the peak currents of BPA at the ERGO-AuNPs-PGE in 0.1 M phosphate buffer solution (pH 7).



#### 6.4.5. Effect of the concentration of the gold

The influence of gold concentration in the GO-AuNPs solution before its electrodeposition onto the pencil graphite electrode was studied in a 0.1 M phosphate buffer solution (pH 7) containing  $50 \mu\text{g L}^{-1}$  BPA (Figure 6.30). It was observed in Figure 10 that the electrochemical response of BPA at ERGO-AuNPs-PGE changes with increasing the gold concentration in GO-AuNPs solution. A 15 ppm concentration of Au solution gives the highest oxidation peak current. The gold nanoparticles sizes probably enlarge with increasing the gold concentration in the solution and it causes the shorter oxidation peak heights at solution concentrations greater than 15 ppm of Au [80,81,108].

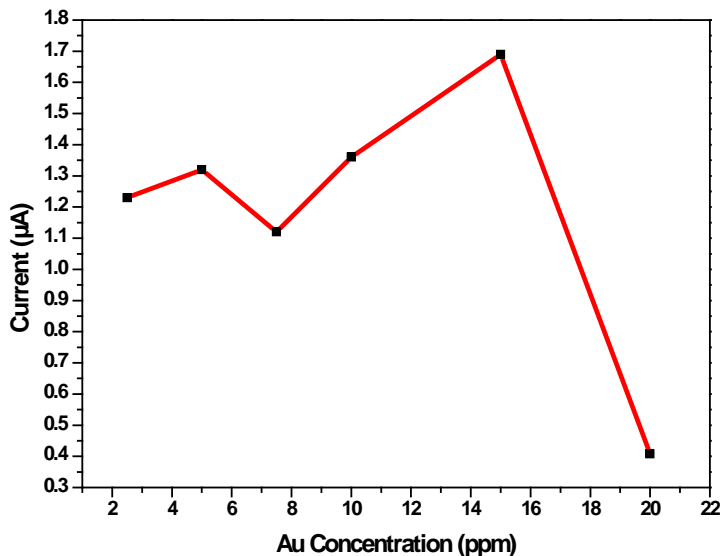
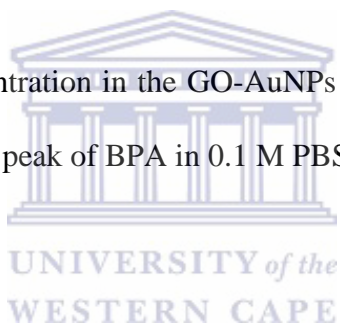


**Figure 6.30:** Effect of gold concentration in the GO-AuNPs solution for modification of pencil graphite electrode on the oxidation peak of BPA in 0.1 M PBS (pH 7) containing  $50 \mu\text{g L}^{-1}$  BPA.



#### 6.4.6. The effect of the electrodeposition time of GO-AuNPs

The effect of the electrodeposition time of GO-AuNPs varying from 30 s to 300 s for the modification of the pencil graphite electrode on the oxidation peak of BPA was investigated in a 0.1 M phosphate buffer solution (pH 7) containing  $50 \mu\text{g L}^{-1}$  BPA (Figure 6.31). The peak currents increased to a maximum at 120 s with increasing the electrodeposition time followed by the decrease in peak current with increasing the electrodeposition time more than 120 s suggesting surface saturation of the electrode. The optimal deposition time of 120 s was chosen for further analysis.

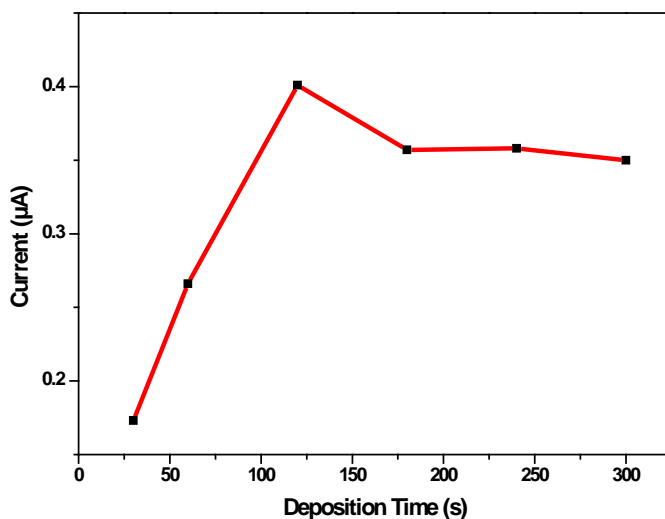
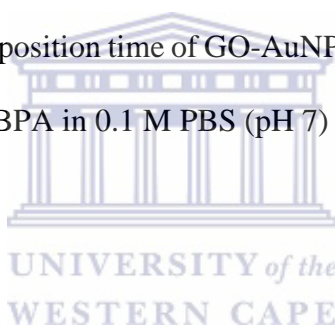
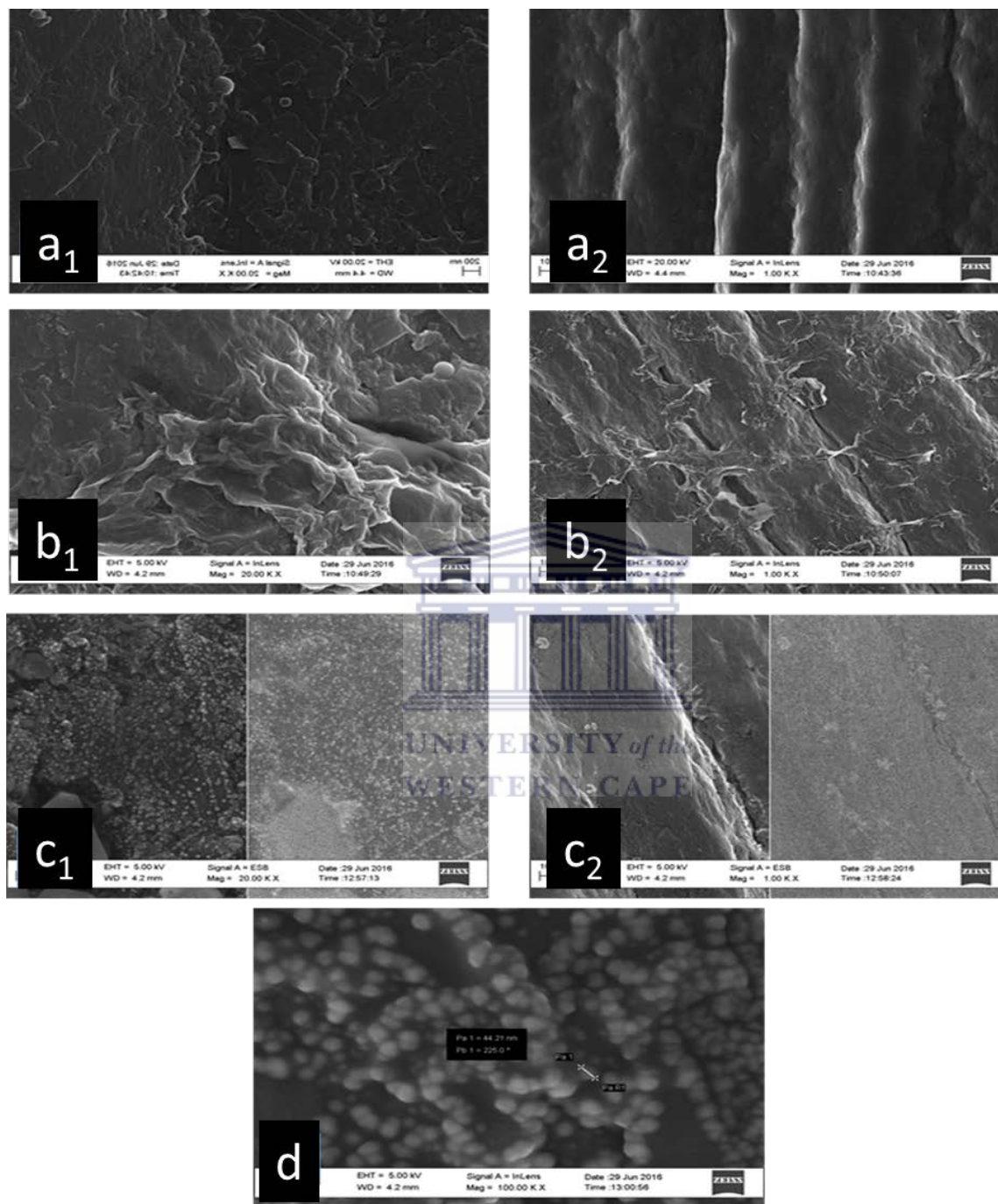


**Figure 6.31:** Effect of the electrodeposition time of GO-AuNPs for modification of pencil graphite electrode on the oxidation peak of BPA in 0.1 M PBS (pH 7) containing  $50 \mu\text{g L}^{-1}$  BPA.



#### **6.4.7. Microscopic Characterization of Electrodeposited Graphene- AuNPs Modified Pencil Electrode (ERGO-AuNPs-PGE)**

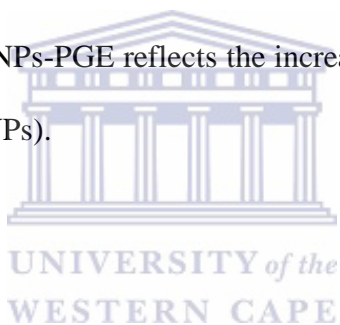
The high resolution scanning electron microscopy (HRSEM) images of the bare PGE, ERGO-PGE and ERGO-AuNPs-PGE surfaces are shown in Figure 6.32. Surface roughness with grooves on the surface along the direction of machining can be observed at the bare PGE surface (Figure 6.32a). Following the electrochemical reduction of graphene oxide, flakes of graphene sheets can be seen at the ERGO-PGE surface at high magnification (Fig 6.32b). Gold nanoparticles on top of the graphene sheets are observed at the ERGO-AuNPs-PGE (Figure 6.32c). The gold nanoparticles sizes varies from 20 to 50 nm (Fig 6.32d)



**Figure 6.32:** HRSEM images of bare PGE (a), EGO-PGE (b), and ERGO-AuNPs-PGE (c) at 20.00 k times magnification (1) and 1000 times magnification (2). HRSEM image of ERGO-AuNPs-PGE at 100.00 k times magnification (d).

#### **6.4.8. Effect of the ERGO-AuNPs nanocomposite surface on electrochemical oxidation of BPA**

The electrochemical response of BPA on the ERGO-AuNPs-PGE was evaluated in 0.1 mol L<sup>-1</sup> PBS pH 7, containing 50 μM BPA by differential pulse voltammetry (DPV) experiments with amplitude of 100 mV, step potential of 2 mV, and an effective scan rate of 5 mV s<sup>-1</sup>. The results are presented in Fig 6.33. The DPV voltammetry shows a negative shift for BPA oxidation peak on bare PGE at 542 mV to 461 mV and 416 mV on ERGO-PGE and ERGO-AuNPs-PGE, respectively. Moreover, the BPA oxidation peak on modified ERGO-AuNPs-PGE at 20.2 μA shows a 9 times bigger current than the bare PGE at 2.39 μA. The enhancement in the oxidation current peak of PBA at ERGO-AuNPs-PGE reflects the increase of the electroactive surface area by the formed hybrid (ERGO–AuNPs).



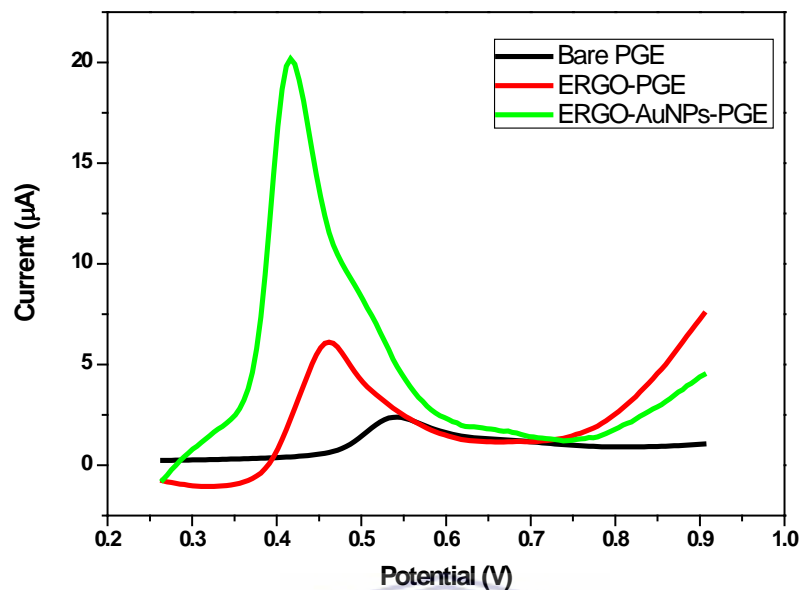
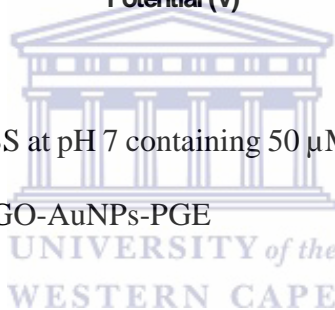


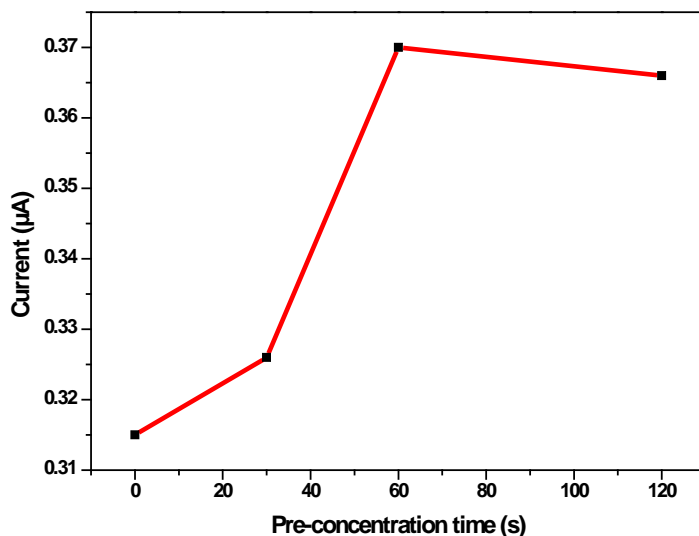
**Figure 6.33:** DPV of  $0.1 \text{ molL}^{-1}$  PBS at pH 7 containing  $50 \mu\text{M}$  BPA for the electrode (black) bare PGE, (red) ERGO-PGE, (green) ERGO-AuNPs-PGE



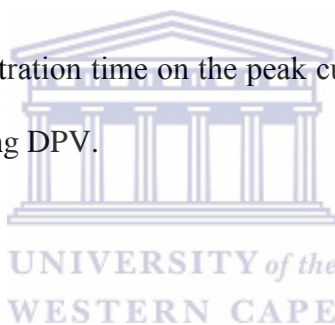
#### 6.4.9. Preconcentration time optimization

The pre-concentration time of BPA oxidation was optimized over the time interval from 0 to 120 seconds at ERGO-AuNPs-PGE using differential pulse voltammetry (Figure 6.34). As a longer pre-concentration time allowed for more analyte to be adsorbed onto the electrode, the peak current increased with increasing pre-concentration time. A pre-concentration time of 60 s was used for further measurements.





**Figure 6.34:** Effect of pre-concentration time on the peak current of 5.0  $\mu\text{M}$  BPA in 10 mL 0.1 M PBS at ERGO-AuNPs-PGE using DPV.



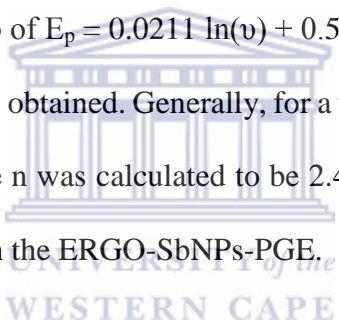
#### **6.4.10. Effect of scan rate on the electrocatalytic oxidation of BPA at ERGO-AuNPs-PGE**

Figure 6.35 shows the cyclic voltammograms of BPA at the ERGO-AuNPs-PGE when the scan rate ( $\nu$ ) varies from 10 to 100  $\text{mVs}^{-1}$ . As is shown in Fig 6.35 (a), the oxidation peak currents increased linearly in an irreversibly electrode process, indicating that the oxidation of BPA at the ERGO-AuNPs-PGE is adsorption-controlled [52,114,115]. Moreover, not linearity of the plot of the peak current ( $I_{pa}$ ) against the square root of scan rate ( $\nu^{1/2}$ ), confirms the adsorption-controlled BPA oxidation (Fig 6.35 (d)). The linear regression equations for oxidation peak ( $I_{pa}$ ) current is:  $I_{pa} = 0.478 \nu + 1.64$  with the correlation coefficients of 0.9984 (Fig 6.35 (b)). As

shown in Figure 6.35 (c) there is a linear relationship between the peak potential ( $E_p$ ) and the natural logarithm of scan rate ( $\ln v$ ) for the ERGO-AuNPs-PGE. As for an irreversibly electrode process, the number of electrons involved in the reaction can be estimated according to the Laviron's equation as follows:

$$E_p = E^{0'} + (RT/\alpha nF) [\ln (RTk_s/\alpha nF) - \ln v] \quad (\text{Eqn. 6.3})$$

Where  $\alpha$  is the electron transfer coefficient,  $k_s$  is the standard rate constant of the surface reaction,  $T$  is the temperature (298 K here),  $v$  is the scan rate,  $R$  the gas constant ( $8.314 \text{ JK}^{-1}\text{mol}^{-1}$ ),  $n$  is the electron transfer numbers,  $F$  the Faraday constant ( $96,480 \text{ C mol}^{-1}$ ) and  $E^{0'}$  the formal redox potential. The  $\alpha n$  value can be calculated from the slope of the linear regression equation of the linear plot of  $E_p$  with respect to  $\ln v$  of  $E_p = 0.0211 \ln(v) + 0.515$ ,  $R^2 = 0.998$ .  $RT/\alpha nF$  was 0.0248 here, then the value of  $\alpha n = 1.21$  was obtained. Generally, for a totally irreversible electron transfer,  $\alpha$  was assumed to be 0.5. Thus, the  $n$  was calculated to be 2.43 showing that two electrons were involved in the oxidation of BPA on the ERGO-SbNPs-PGE.



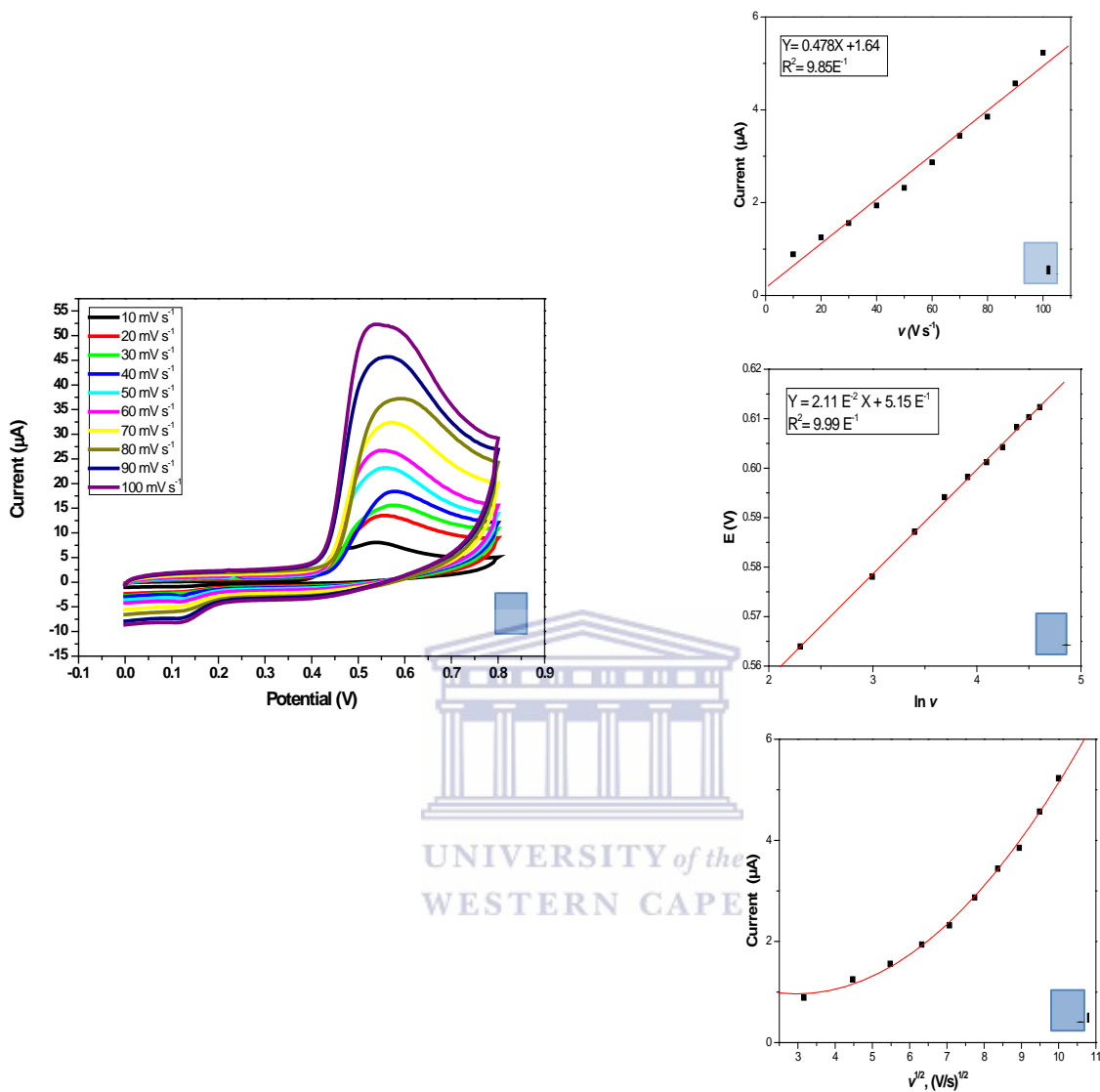


**Figure 6.35:** (a) Cyclic voltammetric responses of 10  $\mu\text{M}$  BPA at ERGO-AuNPs-PGE in 0.1 M PBS (pH= 7.0) at scan rates, (inner to outer) 10, 20, 30, 40, 50, 60, 70, 80, 90, 100  $\text{mVs}^{-1}$ . (b and d) The plots of peak currents vs scan rate and square root of scan rate, respectively. (c) The variation of peak potential vs  $\ln v$ .

### 6.4.11. pH optimization

The influence of pH on the oxidation peak current of BPA on ERGO-AuNPs-PGE was studied with pH ranging from 5 to 10 as shown in Figure 6.36. The oxidation peak at pH 7 showed the highest peak current. Thus pH 7 was selected as the optimum pH electrolyte for subsequent experiments. The linear shifting of the peak potential to more negative values with increasing pH with a slope of  $-61.24 \text{ mV/pH}$  which was close to the theoretical value  $57 \text{ mV/pH}$  indicates equal number of protons and electrons are involved in the BPA oxidation (a two-electron-two-proton process) [11,86,115].

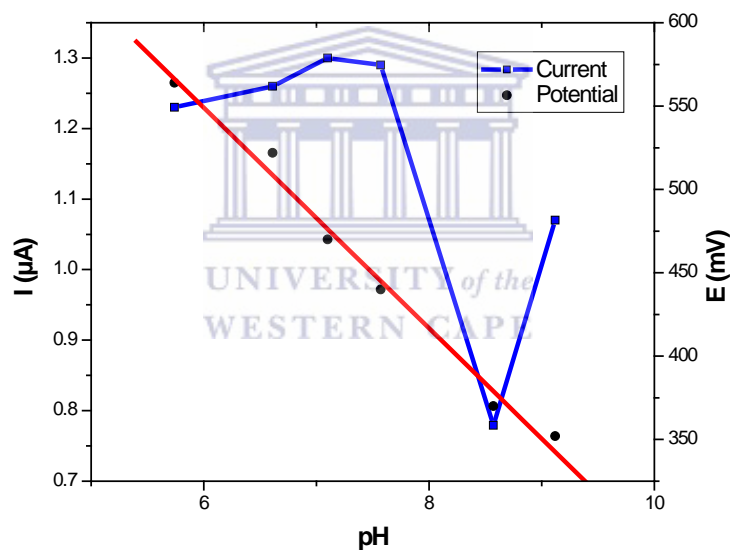


**Figure 6.36:** Effect of pH on the peak current of  $1.0 \mu\text{M}$  BPA in  $10 \text{ mL } 0.1 \text{ M}$  PBS at ERGO-AuNPs-PGE using DPV.

### 6.4.12. Interference studies

The influence of possible interfering molecules for the oxidation measurements of  $50 \mu\text{M}$  bisphenol A in the absence and presence of interfering molecules was studied using adsorptive

stripping differential pulse voltammetry (Figure 6.37). The interfering molecules that were examined were as following: 2, 2- Dimethoxyphenol, Potassium Chloride, 4- Hydroxyanisol 4-Methoxyphenol, sodium chloride, 4-cumylphenol. . No electroactivity and change in the voltammetric response was observed for 50  $\mu\text{M}$  BPA in the presence of a two-time excess concentration (100  $\mu\text{M}$ ) of electroinactive species except for 4-cumylphenol. The significant increasment observed in the oxidation peak current shows the interfering effect of 4-cumylphenol on response of the electrode towards BPA measurement.



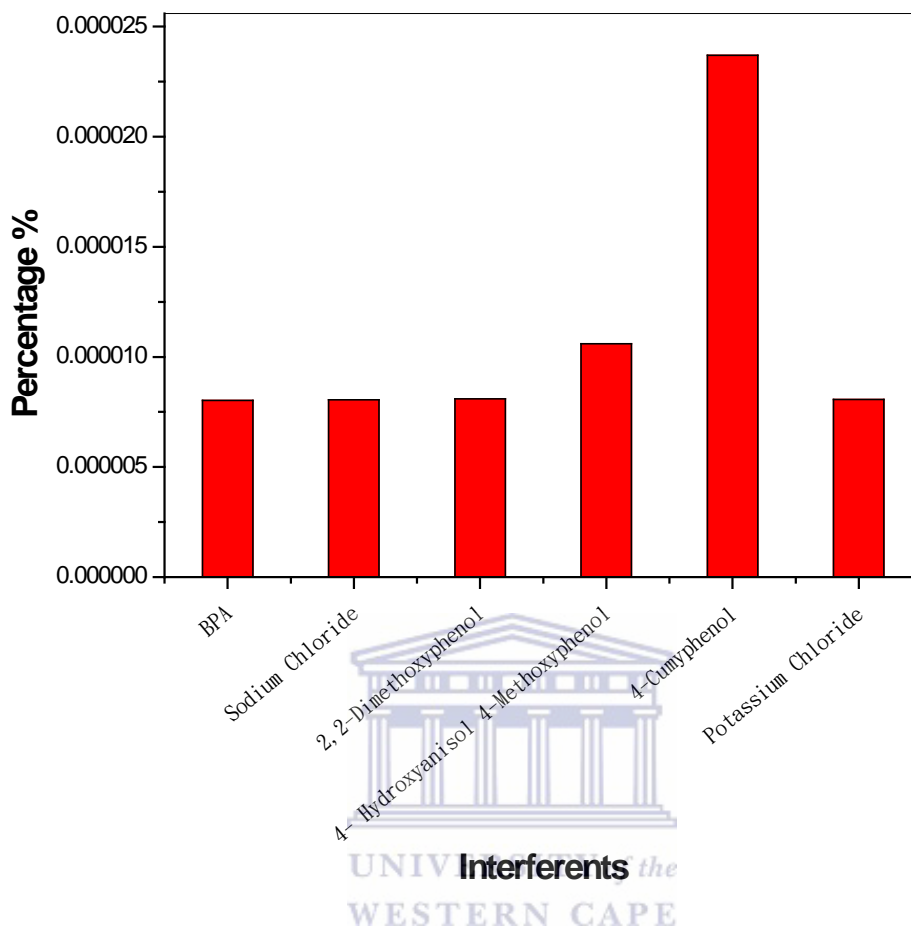


**Figure 6.37:** Percentages of the oxidation peak current of 50  $\mu\text{M}$  of the BPA in absence and presence of 100  $\mu\text{M}$  2, 2- Dimethoxyphenol, Potassium Chloride, 4- Hydroxyanisole 4- Methoxyphenol, sodium chloride, 4-cumylphenol.

### 6.4.13. Detection Limit

A linear relationship between the BPA concentration in the range of 0.4  $\mu\text{M}$  to 5.0  $\mu\text{M}$  and peak current with a correlation coefficient of 0.999 is observed (Figure 6.38). The standard deviation was calculated based on the linear regression equation of the average of calibration curves (n=5) as following:

$$I(\mu\text{A}) = 0.739 (\mu\text{A } \mu\text{mol L}^{-1}) [\text{BPA}] (\mu\text{mol L}^{-1}) + 0.141 (\mu\text{A}) \quad (\text{Eqn. 6.4})$$

Detection limit for biphenol A with ERGO-AuNPs-PGE was determined using following equation:

$$\text{D.L.} = 3\sigma/\text{slope} \quad (\text{Eqn. 6.5})$$

Where,

D.L., is the limit of detection

$3\sigma$ , is three times the standard deviation of the blanks

Slope, is the gradient (slope) of the calibration curve

The detection limit was found to be  $0.062 \mu\text{M}$  based on ten replications of the electrode's response in the blank solutions.

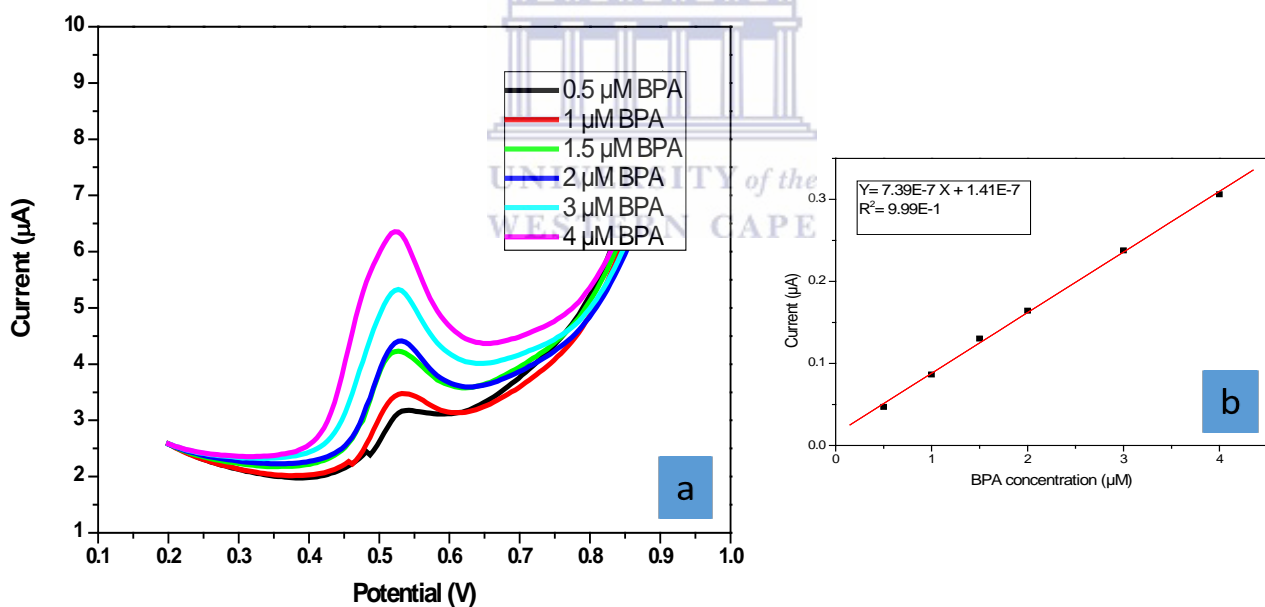


**Figure 6.38:** DPV voltammograms for ERGO-AuNPs-PGE with the optimised parameters (a). The BPA concentrations range from  $0.4 \mu\text{mol L}^{-1}$  to  $5.0 \mu\text{mol L}^{-1}$ . Linear dependence of the peak current with BPA concentration (b).

The calculated detection limit is comparable to those reported in the literature. The analytical parameters obtained in this study and those reported previously is shown in Table 6.2. However lower detection limits have been found in the reported literature but fouling problem as the main challenge for the determination of BPA [11], [12], [54] is eliminated using the single used ERGO-AuNPs-PGE.

**Table 6.2.** Comparison of the proposed method with some of the previously sensors.

Electrode	Linear range ( $\mu\text{M}$ )	Detection limit ( $\mu\text{M}$ )	Reference
GCE-MWCNT-AuNPs	0.02-0.2	0.0075	[38]
ssDNA/SWCNT/Au	1-3.8	0.045	[53]
PAMAM-AuNPs-NF/GCE	0.001-0.0103	0.005	[52]
AuNPs/GR based aptasenor	0.001-10	0.005	[10]
RGOM-GCE	0.01-200	0.004	[115]
GC/MWCNTs	4-8	0.084	[54]
ERGO-AuNPs-PGE	0.4-5.0	0.062	This study

\* GCE-MWCNT-AuNPs: nanotubes-gold nanoparticles modified glassy carbon electrode, ssDNA/SWCNT/Au: single-stranded DNA (ssDNA) wrapped CNTs on a gold substrate, PAMAM-AuNPs-NF/GCE: glassy carbon electrode modified with gold nanoparticles, silk fibroin, and PAMAM dendrimers, AuNPs/GR based aptasenor: An electrochemical aptasensor based on gold nanoparticles dotted graphene modified glassy carbon electrode for, RGOM-GCE: graphene/melamine nanoparticle-modified glassy carbon electrode, GC/MWCNTs: glassy carbon electrode modified with multi wall carbon nanotubes.



#### 6.4.14. Analytical application of ERGO-AuNPs-PGE

The ERGO-AuNPs-PGE was used to determine bisphenol A in real water samples using differential pulse adsorptive stripping voltammetry. Known concentration of bisphenol A was used to spiked 10 mL portion of tap water sample prepared as described in the experimental and determined using standard addition method (Figure 6.39). Recovery percentage of bisphenol A determination performed three times in tap water sample solutions spiked with 0.2  $\mu\text{M}$  BPA values in the range of 96.98 % to 103.5 % which found to be satisfactory. The range of relative standard deviation of 1.3- 4 % was calculated for the oxidation peak of BPA in tap water samples showing less than 5 % error in the quantification of BPA in tap water sample using the ERGO-AuNPs-PGE.

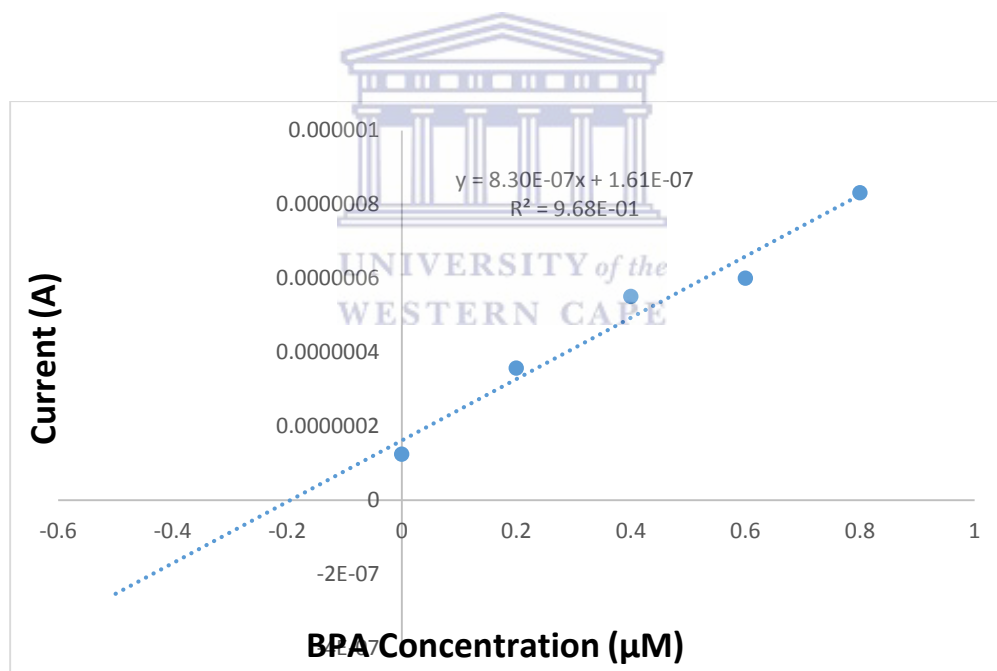


**Figure 6.39:** Linear dependence of the peak currents and BPA concentrations. Tap water sample spiked with 0.2  $\mu\text{M}$  BPA and 0.2  $\mu\text{M}$  BPA was added three times.

## 6.5. Conclusion

Modification of pencil graphite electrodes with a reduced graphene oxide metal nanocomposite for the detection of bisphenol A by differential pulse adsorptive voltammetry was characterized

electrochemically and microscopically. Improved detection limits were found to be comparable to other known carbon-based electrodes and below USEPA standards as well as accurate detection of BPA in tap water samples with a 5% error.



# CHAPTER SEVEN

## Conclusions and Future Work

This study demonstrates the need of finding sensitive and inexpensive techniques for the determination of bisphenol A by differential pulse adsorptive stripping voltammetry and clarifies the use of graphene-metal nanocomposite as a good coating material. A sensitive electrochemical sensor for determining bisphenol A was prepared based on the direct electrochemical reduction of colloidal graphene oxide metal nanocomposite at pencil graphite electrodes with the sensitivity comparable to that of the glassy carbon electrodes.

The pencil graphite electrode modified with graphene-antimony nanocomposite showed an improved detection limit of bisphenol A comparable to other known pencil graphite electrodes. The enhanced sensing capabilities of reduced graphene oxide antimony nanoparticles pencil graphite electrode was proved by the accurate detection of bisphenol A in tap water samples with a 5% error.

The assessment of the analytical application of the reduced graphene oxide gold nanoparticles pencil graphite electrode was conducted by recovery studies and real sample analysis with a low detection limit below the USEPA standard of BPA.

The future work includes the use of pencil graphite electrode modified with various graphene-metal nanocomposites to existing green approach. The electroanalytical use of graphene-metal nanocomposite pencil graphite electrodes has been encouraged based on the achieved results.

In future, the use of pencil graphite electrode as a substrate that offer good results comparable to common electrode substrates could be investigated for a wide range of applications. The pencil graphite substrate could be used for future studies as a low cost and disposable electrode.

# Bibliography

- [1] J.J. Heindel, S. Jobling, K.A. Kidd, R.T. Zoeller, Endocrine Disrupting Chemicals - 2012, 2012.
- [2] T. Doshi, S.S. Mehta, V. Dighe, N. Balasnor, G. Vanage, Hypermethylation of estrogen receptor promoter region in adult testis of rats exposed neonatally to bisphenol A, *Toxicology*. 289 (2011) 74–82. doi:10.1016/j.tox.2011.07.011.
- [3] U.S.E.P. Agency, U.S. Environmental Protection Agency 3/29/2010, (2011) 1–22.
- [4] G. Gatidou, N.S. Thomaidis, A.S. Stasinakis, T.D. Lekkas, Simultaneous determination of the endocrine disrupting compounds nonylphenol, nonylphenol ethoxylates, triclosan and bisphenol A in wastewater and sewage sludge by gas chromatography-mass spectrometry, *J. Chromatogr. A*. 1138 (2007) 32–41. doi:10.1016/j.chroma.2006.10.037.
- [5] J. Ou, L. Hu, L. Hu, X. Li, H. Zou, Determination of phenolic compounds in river water with on-line coupling bisphenol A imprinted monolithic precolumn with high performance liquid chromatography, *Talanta*. 69 (2006) 1001–1006. doi:10.1016/j.talanta.2005.12.003.
- [6] H. Fromme, T. Kuchler, T. Otto, K. Pilz, J. Müller, A. Wenzel, Occurrence of phthalates and bisphenol A and F in the environment, *Water Res.* 36 (2002) 1429–1438. doi:10.1016/S0043-1354(01)00367-0.
- [7] EFSA, Scientific Opinion on the risks to public health related to the presence of nickel in food and drinking water, *EFSA J.* 13 (2015) 4002. doi:10.2903/j.efsa.2015.4002.
- [8] J.H. Kang, F. Kondo, Y. Katayama, Human exposure to bisphenol A, *Toxicology*. 226 (2006) 79–89. doi:10.1016/j.tox.2006.06.009.
- [9] P. Smad, M.L. Slattery, J. Herrick, K. Curtin, W. Samowitz, R.K. Wolff, B.J. Caan, D.

- Duggan, J.D. Potter, U. Peters, NIH Public Access, 70 (2011) 1479–1485.  
doi:10.1158/0008-5472.CAN-08-1792.Increased.
- [10] L. Zhou, J. Wang, D. Li, Y. Li, An electrochemical aptasensor based on gold nanoparticles dotted graphene modified glassy carbon electrode for label-free detection of bisphenol A in milk samples, *FOOD Chem.* 162 (2014) 34–40.  
doi:10.1016/j.foodchem.2014.04.058.
- [11] A. Özcan, Synergistic Effect of Lithium Perchlorate and Sodium Hydroxide in the Preparation of Electrochemically Treated Pencil Graphite Electrodes for Selective and Sensitive Bisphenol A Detection in Water Samples, *Electroanalysis.* 26 (2014) 1631–1639. doi:10.1002/elan.201400082.
- [12] B. Sebez, B. Ogorevc, S.B. Hocevar, M. Veber, *Analytica Chimica Acta* Functioning of antimony film electrode in acid media under cyclic and anodic stripping voltammetry conditions, *Anal. Chim. Acta.* 785 (2013) 43–49. doi:10.1016/j.aca.2013.04.051.
- [13] T. Ndlovu, O.A. Arotiba, S. Sampath, R.W. Krause, B.B. Mamba, An exfoliated graphite-based bisphenol a electrochemical sensor, *Sensors (Switzerland).* 12 (2012) 11601–11611. doi:10.3390/s120911601.
- [14] X. Niu, W. Yang, G. Wang, J. Ren, H. Guo, J. Gao, *Electrochimica Acta* A novel electrochemical sensor of bisphenol A based on stacked graphene nanofibers / gold nanoparticles composite modified glassy carbon electrode, *Electrochim. Acta.* 98 (2013) 167–175. doi:10.1016/j.electacta.2013.03.064.
- [15] J. Wang, *ANALYTICAL ELECTROCHEMISTRY*, Third, John Wiley & Sons, 2006.
- [16] S.B. Hocevar, S. Ivan, B. Ogorevc, K. Vytr, Antimony Film Electrode for Electrochemical Stripping Analysis, 79 (2007) 8639–8643. doi:10.1021/ac070478m.

- [17] J. Wang, A. Kawde, E. Sahlin, R. September, A. September, Renewable pencil electrodes for highly sensitive stripping potentiometric measurements of DNA and RNA, (2000) 5–7.
- [18] K. Pokpas, S. Zbeda, N. Jahed, N. Mohamed, P.G. Baker, E.I.I. Sensorlab, Electrochemically Reduced Graphene Oxide Pencil-Graphite in situ Plated Bismuth-film Electrode for the Determination of Trace Metals by Anodic Stripping Voltammetry, *Int. J. Electrochem. Sci.* 9 (2014) 736–759. [www.electrochemsci.org](http://www.electrochemsci.org) (accessed September 14, 2016).
- [19] K. Pokpas, N. Jahed, O. Tovide, P.G. Baker, E.I. Iwuoha, Nafion-graphene nanocomposite in situ plated bismuth-film electrodes on pencil graphite substrates for the determination of trace heavy metals by anodic stripping voltammetry, *Int. J. Electrochem. Sci.* 9 (2014) 5092–5115.
- [20] S. Zbeda, K. Pokpas, S. Titinchi, N. Jahed, P.G. Baker, E.I. Iwuoha, Few-layer Binder Free Graphene Modified Mercury Film Electrode for Trace Metal Analysis by Square Wave Anodic Stripping Voltammetry, 8 (2013) 11125–11141.
- [21] H. Yang, C. Shan, F. Li, Q. Zhang, D. Han, L. Niu, Convenient preparation of tunably loaded chemically converted graphene oxide / epoxy resin nanocomposites from graphene oxide sheets through two-phase extraction †, (2009) 8856–8860. doi:10.1039/b915228h.
- [22] J. Huang, Y. Liu, H. Hou, T. You, Biosensors and Bioelectronics Simultaneous electrochemical determination of dopamine , uric acid and ascorbic acid using palladium nanoparticle-loaded carbon nanofibers modified electrode, 24 (2008) 632–637. doi:10.1016/j.bios.2008.06.011.
- [23] Y. Song, K. Cui, L. Wang, S. Chen, The electrodeposition of Ag nanoparticles on a type I collagen-modified glassy a hydrogen peroxide sensor, (2009). doi:10.1088/0957-

4484/20/10/105501.

- [24] J. Li, S. Guo, Y. Zhai, E. Wang, *Analytica Chimica Acta* High-sensitivity determination of lead and cadmium based on the Nafion-graphene composite film, 649 (2009) 196–201. doi:10.1016/j.aca.2009.07.030.
- [25] S. Otles, *Electroanalytical Techniques and Instrumentation in Food Analysis, Handb. Food Anal. Instruments.* (2008).
- [26] P. Kissinger and W. Heineman, No Title, *Laboratory Tech. Electroanal. Chem.* (1996).
- [27] C. Zoski, *Handbook of Electrochemistry*, Elsevier. (2007).
- [28] L.. Bard, A.J.; Faulkner, No Title, *Electrochem. Methods Fundam. Appl.* (2000).
- [29] J. Wang, *Stripping Analysis-Principles, Instrumentation and Application*, Inc. (1985).
- [30] P. Monk, No Title, *Fundam. Electro-Analytical Chem.* (2001).
- [31] J.P. Franke; R.A. De Zeeuw, *Differential Pulse Anodic Stripping Voltammetry as a Rapid Screening Technique for Heavy Metals Intoxications, Arch Toxicol.* 37 (1976) 47–55.
- [32] P.A. Eric, B. Charlotte, *Stripping Voltammetry for the determination of trace metal speciation and in-situ measurements of trace metal distribution in marine waters, Anal. Chim. Acta.* 400 (1999) 381–397.
- [33] D.W.M. Arrigan, *Voltammetric Determination of Trace Metals and Organics after Accumulation at Modified Electrodes*, 11 (1994) 1953–1966.
- [34] S. Gumaa, A. Zbeda, *Multilayer graphene modified metal film electrodes for the determination of trace metals by anodic stripping voltammetry*, (2013).
- [35] S. A. Ozkan, *Principles and Techniques of Electrochemical Stripping Methods for Pharmaceutically Active Compounds in Dosage Forms and Biological Samples, Curr. Pharm. Anal.* 5 (2009) 127–143.

- [36] K. Robert, K. Miloslav, Adsorptive stripping in trace analysis, *Pure Appl. Chem.* (1989) 97–112.
- [37] J. Li, D. Kuang, Y. Feng, Voltammetric determination of bisphenol A in food package by a glassy carbon electrode modified with carboxylated multi-walled carbon nanotubes, (2011) 379–386. doi:10.1007/s00604-010-0512-0.
- [38] X. Tu, L. Yan, X. Luo, S. Luo, Electroanalysis of Bisphenol A at a Multiwalled Carbon Nanotubes-gold Nanoparticles Modified Glassy Carbon Electrode, (2009) 2491–2494. doi:10.1002/elan.200900195.
- [39] W. Huang, Voltammetric Determination of Bisphenol A Using a Carbon Paste Electrode Based on the Enhancement Effect of Cetyltrimethylammonium Bromide ( CTAB ), *Bull. Korean Chem. Soc.* 26 (2005) 1560–1564.
- [40] J.R. Rochester, Bisphenol A and human health : A review of the literature, *Reprod. Toxicol.* 42 (2013) 132–155. doi:10.1016/j.reprotox.2013.08.008.
- [41] X. Wang, H. Zeng, Y. Wei, J. Lin, A reversible fluorescence sensor based on insoluble  $\beta$ -cyclodextrin polymer for direct determination of bisphenol A ( BPA ), 114 (2006) 565–572. doi:10.1016/j.snb.2005.06.020.
- [42] A. García-prieto, M.L. Lunar, S. Rubio, D. Pérez-bendito, Determination of urinary bisphenol A by coacervative microextraction and liquid chromatography – fluorescence detection, 0 (2008) 19–27. doi:10.1016/j.aca.2008.09.060.
- [43] X. Wang, H. Zeng, L. Zhao, J. Lin, Selective determination of bisphenol A ( BPA ) in water by a reversible fluorescence sensor using pyrene / dimethyl  $\beta$ -cyclodextrin complex, 556 (2006) 313–318. doi:10.1016/j.aca.2005.09.060.



- [44] Y. Ji, J. Yin, Z. Xu, C. Zhao, H. Huang, H. Zhang, C. Wang, determination of bisphenol A in environmental water and milk samples Preparation of magnetic molecularly imprinted polymer for rapid determination of bisphenol A in environmental water and milk samples, *Anal Bioanal Chem.* 395 (2009) 1125–1133. doi:10.1007/s00216-009-3020-5.
- [45] M.R. Hadjmohammadi, Determination of bisphenol A in Iranian packaged milk by solid-phase extraction and HPLC, (2010) 501–506. doi:10.1007/s00706-010-0297-1.
- [46] E.M. Malone, C.T. Elliott, D.G. Kennedy, L. Regan, Rapid confirmatory method for the determination of sixteen synthetic growth promoters and bisphenol A in bovine milk using dispersive solid-phase extraction and liquid chromatography – tandem mass spectrometry, *J. Chromatogr. B.* 878 (2010) 1077–1084. doi:10.1016/j.jchromb.2010.03.012.
- [47] R. Zhao, X. Wang, Highly sensitive determination of tetrabromobisphenol A and bisphenol A in environmental water samples by solid-phase extraction and liquid chromatography- tandem mass spectrometry, (2010) 1652–1657. doi:10.1002/jssc.201000010.
- [48] E. Herrero, R. Carabias, E. Rodr, *Analytica Chimica Acta* Use of a bisphenol-A imprinted polymer as a selective sorbent for the determination of phenols and phenoxyacids in honey by liquid chromatography with diode array and tandem mass spectrometric detection, 650 (2009) 195–201. doi:10.1016/j.aca.2009.07.043.
- [49] M. Zhao, Y. Li, Z. Guo, X. Zhang, A new competitive enzyme-linked immunosorbent assay (ELISA) for determination of estrogenic bisphenols, 57 (2002) 1205–1210.
- [50] X. Jin, G. Jiang, G. Huang, Determination of 4- tert -octylphenol, 4-nonylphenol and bisphenol A in surface waters from the Haihe River in Tianjin by gas chromatography – mass spectrometry with selected ion monitoring, 56 (2004) 1113–1119.

- doi:10.1016/j.chemosphere.2004.04.052.
- [51] C. Sánchez-brunete, E. Miguel, J.L. Tadeo, Determination of tetrabromobisphenol-A , tetrachlorobisphenol-A and bisphenol-A in soil by ultrasonic assisted extraction and gas chromatography – mass spectrometry, 1216 (2009) 5497–5503.  
doi:10.1016/j.chroma.2009.05.065.
- [52] H. Yin, Y. Zhou, S. Ai, R. Han, Electrochemical behavior of bisphenol A at glassy carbon electrode modified with gold nanoparticles , silk fibroin , and PAMAM dendrimers, (2010) 99–105. doi:10.1007/s00604-010-0396-z.
- [53] F.C. Moraes, T.A. Silva, I. Cesarino, S.A.S. MacHado, Effect of the surface organization with carbon nanotubes on the electrochemical detection of bisphenol A, Sensors Actuators, B Chem. 177 (2013) 14–18. doi:10.1016/j.snb.2012.10.128.
- [54] L.A. Goulart, F.C. De Moraes, L.H. Mascaro, Influence of the different carbon nanotubes on the development of electrochemical sensors for bisphenol A, Mater. Sci. Eng. C. 58 (2016) 768–773. doi:10.1016/j.msec.2015.09.073.
- [55] S. Poorahong, C. Thammakhet, P. Thavarungkul, W. Limbut, A. Numnuam, P. Kanatharana, Amperometric sensor for detection of bisphenol A using a pencil graphite electrode modified with polyaniline nanorods and multiwalled carbon nanotubes, Microchim. Acta. 176 (2012) 91–99. doi:10.1007/s00604-011-0698-9.
- [56] A.R. Reserved, Introduction to Nanoscience and Nanotechnology : A Workbook, (2005).
- [57] K. Klabunde, R. Richards, Nanoscale Materials in Chemistry, Inc. (2009).
- [58] T. Takagahara, K. Takeda, Theory of the Quantum Confinement Effect on Excitons in Quantum Dots of Indirect-gap Materials, Phys.Rev. B. 46 (1992) 15578–15581.
- [59] O.Arsenault, A Chemical Approach to Nanomaterials, Cambridge R. Soc. Chem. (2005).

- [60] B. Pollard, Growing Graphene via Chemical Vapor Deposition, Dep. Physics, Pomona Coll. (2011).
- [61] A.C. Neto, F. Guinea, N.M. Peres, Drawing conclusions from graphene, Phys. World. (2006). doi:10.1088/2058-7058/19/11/34.
- [62] J. Bunch, S. Verbridge, J. Alden, A. van der Zande, J. Parpia, H. Craighead, P. McEuen, Impermeable Atomic Membranes from Graphene Sheets, Nano Lett. 8 (2008) 2458–2462.
- [63] A.G. and K. Novoselov, The Rise of Graphene, Nat. Mater. 6 (2007) 183–191.
- [64] D. Demetriades, A. Economou, A. Voulgaropoulos, A study of pencil-lead bismuth-film electrodes for the determination of trace metals by anodic stripping voltammetry, 519 (2004) 167–172. doi:10.1016/j.aca.2004.05.008.
- [65] J.M. Raimond, M. Brune, Q. Compton, F. De Martini, C. Monroe, Electric Field Effect in Atomically Thin Carbon Films, 306 (2004) 666–670.
- [66] C. Willemse, K. Tlhomelang, N. Jahed, P. Baker, E. Iwuoha, Metallo-Graphene Nanocomposite Electrocatalytic Platform for the Determination of Toxic Metal Ions, Sensors. 11 (2011) 3970–3987.
- [67] B. Partoens, F.M. Peeters, From graphene to graphite: Electronic structure around the K point., Phys. Rev. B. 74 (2006) 075404. doi:10.1103/PhysRevB.74.075404.
- [68] S. Arar, Everything You Need to Know About the Future of Graphene, All About Circuits. (2016). <https://www.allaboutcircuits.com/news/everything-you-need-to-know-about-the-future-of-graphene/>.
- [69] C. Schonberger, Bandstructure of Graphene and Carbon Nanotubes: Exercise in Condensed Matter Physics, n.d.
- [70] O. Kharisov, Graphenes, One of the hottest Areas in the Nanotechnology: Attention of

- Chemists is Needed, *Open Inorg. Chem. J.* 2 (2008) 39–49.
- [71] L.A. Falkovsky, Optical properties of graphene and IV-VI semiconductors, *Phys.-Usp.* 51 (2008) 887. doi:10.1070/PU2008v051n09ABEH006625.
- [72] B. Brodie, Sur le poids atomique du graphite, *An, Chim. Phys.* 59 (1860) 466–472.
- [73] W.S. Hummers, R.E. Offeman, Preparation of Graphitic Oxide, 1958.  
<https://pubs.acs.org/sharingguidelines> (accessed August 21, 2018).
- [74] L. Staudenmaier, Verfahren zur darstellung der graphitsaure, *Ber. Dtsch. Chem Ges.* 31 (1898) 1481–1499.
- [75] A. Reina, S. Thiele, X. Jia, S. Bhaviripudi, S. Mildred, Growth of Large-area Single- and Bi-layer Graphene by Controlled Carbon Precipitation on Polycrystalline Ni Surfaces, (n.d.) 1–27.
- [76] H. Jin, J. Meyer, S. Roth, Growth and properties of few-layer graphene prepared by chemical vapor deposition, 8 (2009) 0–6. doi:10.1016/j.carbon.2009.11.030.
- [77] M. Voutilainen, E.T. Seppälä, P. Pasanen, M. Oksanen, Graphene and Carbon Nanotube Applications in Mobile Devices, 59 (2012) 2876–2887.
- [78] N. Shang, P. Wang, Platinum Integrated Graphene for Methanol Fuel Cells, (2010) 15837–15841.
- [79] P. Reunchan, S. Jhi, Metal-dispersed Porous Graphene for Hydrogen Storage, *Appl. Phys. Lett.* 98 (2011) 093103-093103-3.
- [80] H. Wang, L. Cui, Y. Yang, H.S. Casalongue, Mn<sub>3</sub>O<sub>4</sub> - Graphene Hybrid as a High-Capacity Anode Material for Lithium Ion, (2010) 13978–13980.
- [81] Y. Shao, J. Wang, H. Wu, J. Liu, I.A. Aksay, Y. Lin, Graphene Based Electrochemical Sensors and Biosensors : A Review, (2010) 1027–1036. doi:10.1002/elan.200900571.

- [82] S. Guo, E. Wang, Synthesis and electrochemical applications of gold nanoparticles, 598 (2007) 181–192. doi:10.1016/j.aca.2007.07.054.
- [83] M. Begon, A.C. Garcia, Metal-Nanoparticles Based Electroanalysis, (2002) 1225–1235.
- [84] T.M. Day, P.R. Unwin, N.R. Wilson, J. V Macpherson, Electrochemical Templating of Metal Nanoparticles and Nanowires on Single-Walled Carbon Nanotube Networks, (2005) 10639–10647.
- [85] I. Cesarino, F.H. Cincotto, S.A.S. Machado, A synergistic combination of reduced graphene oxide and antimony nanoparticles for estriol hormone detection, Sensors Actuators, B Chem. 210 (2015) 453–459. doi:10.1016/j.snb.2015.01.013.
- [86] B. Ntsendwana, B.B. Mamba, S. Sampath, O.A. Arotiba, Electrochemical Detection of Bisphenol A Using Graphene- Modified Glassy Carbon Electrode, Int. J. Electrochem. Sci. 7 (2012) 3501–3512.
- [87] F.C. Moraes, I. Cesarino, V. Cesarino, L.H. Mascaro, S.A.S. MacHado, Carbon nanotubes modified with antimony nanoparticles: A novel material for electrochemical sensing, Electrochim. Acta. 85 (2012) 560–565. doi:10.1016/j.electacta.2012.08.123.
- [88] E. Svobodová, L. Baldrianová, S.B. Ho, I. Švancara, Electrochemical Stripping Analysis of Selected Heavy Metals at Antimony Trioxide-Modified Carbon Paste Electrode, 7 (2012) 197–210.
- [89] A. Erdem, H. Karadeniz, A. Caliskan, Single-Walled Carbon Nanotubes Modified Graphite Electrodes for Electrochemical Monitoring of Nucleic Acids and Biomolecular Interactions, (2009) 464–471. doi:10.1002/elan.200804422.
- [90] M. Muti, S. Sharma, A. Erdem, Electrochemical Monitoring of Nucleic Acid Hybridization by Single-Use Graphene Oxide-Based Sensor, (2011) 272–279.

doi:10.1002/elan.201000425.

- [91] L. Chen, Y. Tang, K. Wang, C. Liu, S. Luo, *Electrochemistry Communications Direct* electrodeposition of reduced graphene oxide on glassy carbon electrode and its electrochemical application, *Electrochem. Commun.* 13 (2011) 133–137.  
doi:10.1016/j.elecom.2010.11.033.
- [92] G. Nanosheets, H. Guo, X. Wang, Q. Qian, F. Wang, X. Xia, *ARTICLE A Green Approach to the Synthesis of*, 3 (2009) 2653–2659.
- [93] C. Su, A. Lu, Y. Xu, F. Chen, A.N. Khlobystov, L. Li, *High-Quality Thin Graphene Films from Fast Electrochemical Exfoliation*, (2011) 2332–2339. doi:10.1021/nn200025p.
- [94] Y. Shao, J. Wang, M. Engelhard, C. Wang, Y. Lin, *Facile and controllable electrochemical reduction of graphene oxide and its applications †*, (2010).  
doi:10.1039/b917975e.
- [95] *Analytical I, Characterization of Materials by FT-IR*, n.d.
- [96] P. Griffiths, *Fourier Transform Infrared Spectrometry*, *Science* (80-. ). 222 (1983) 297–302.
- [97] W. Zachariasen, *A General Theory of X-Ray Diffraction in Crystals*, *Acta Cryst.* 23 (1967) 558–564.
- [98] N. Colthup, *Introduction to Infrared and Raman Spectroscopy*, Elsevier. (1990).
- [99] C. Bosch-Navarro, E. Coronado, C. Martí-Gastaldo, J.F. Sánchez-Royoc, M.G. Gómezc, *Influence of the pH on the synthesis of reduced graphene oxide under hydrothermal conditions*, *Nanoscale*. (2012).
- [100] D. Marcano, D. Kosynkin, J. Berlin, A. Sinitskii, Z. Sun, A. Slesarev, L. Alemany, W. Lu, J. Tour, *Improved Synthesis of Graphene Oxide*, *ACS Nano*. 4 (2010) 4806–4814.

- [101] W. Chen, L. Yan, Preparation of Graphene by a Low-temperature Thermal Reduction at Atmosphere Pressure, *Nanoscale*. 2 (2010) 559–563.
- [102] A. Bourlinos, D. Gournis, D. Petridis, T. Szabo, A. Szeri, I. Dekany, Graphite Oxide: Chemical Reduction to Graphite and Surface Modification with Primary Aliphatic Amines and Amino Acids, *Langmuir*. 19 (2003) 6050–6055.
- [103] S. Stankovich, D. Dikin, R. Piner, K. Kohlhaas, A. Kleinhammes, Y. Jia, Y. Wu, S. Nguyen, R. Ruoff, Synthesis of Graphene-based Nanosheers via Chemical Reduction of Exfoliated Graphite Oxide, *Carbon N. Y.* (2007) 1558–1565.
- [104] Y. Zhu, S. Murali, W. Cai, X. Li, J.W. Suk, J.R. Potts, R.S. Ruoff, Graphene and graphene oxide: Synthesis, properties, and applications, *Adv. Mater.* (2010).  
doi:10.1002/adma.201001068.
- [105] F.Y. Ban, S.R. Majid, N.M. Huang, H.N. Lim, Graphene Oxide and Its Electrochemical Performance, 7 (2012) 4345–4351.
- [106] M. Del Prado Lavin-Lopez, A. Romero, J. Garrido, L. Sanchez-Silva, J.J. Valverde, Influence of Different Improved Hummers Method Modifications on the Characteristics of Graphite Oxide in Order to Make a More Easily Scalable Method, (2016).  
doi:10.1021/acs.iecr.6b03533.
- [107] R. Paper, *Electrochemical Biosensors - Sensor Principles and Architectures*, (2008) 1400–1458.
- [108] V. Determination, P. Ii, P. Clara, J. Bastos-arrieta, N. Serrano, D. Manuel, Ag Nanoparticles Drop-Casting Modification of, (n.d.). doi:10.3390/s17061458.
- [109] E. Casero, A.M. Parra-Alfambra, M.D. Petit-Domínguez, F. Pariente, E. Lorenzo, C. Alonso, Differentiation between graphene oxide and reduced graphene by electrochemical

- impedance spectroscopy (EIS), *Electrochem. Commun.* 20 (2012) 63–66.  
doi:10.1016/j.elecom.2012.04.002.
- [110] B. Devadas, M. Rajkumar, Electrochemically reduced graphene oxide/neodymium hexacyanoferrate modified electrodes for the electrochemical detection of paracetamol, *Int. J. Electrochem. Sci.* 7 (2012) 3339–3349.  
<http://www.electrochemsci.org/papers/vol7/7043339.pdf>.
- [111] S. Eloul, C. Batchelor-McAuley, R.G. Compton, Thin film-modified electrodes: a model for the charge transfer resistance in electrochemical impedance spectroscopy, *J. Solid State Electrochem.* 18 (2014) 3239–3243. doi:10.1007/s10008-014-2662-1.
- [112] J. Kudr, L. Richtera, L. Nejd, K. Xhaxhiu, P. Vitek, B. Rutkay-Nedecky, D. Hynek, P. Kopel, V. Adam, R. Kizek, Improved electrochemical detection of zinc ions using electrode modified with electrochemically reduced graphene oxide, *Materials (Basel)*. 9 (2016) 1–12. doi:10.3390/ma9010031.
- [113] R.N. Vyas, B. Wang, Electrochemical analysis of conducting polymer thin films, *Int. J. Mol. Sci.* 11 (2010) 1956–1972. doi:10.3390/ijms11041956.
- [114] F. Electrode, Direct Electrochemical Detection of Bisphenol A Using a Highly Conductive Graphite Nanoparticle, (2017). doi:10.3390/s17040836.
- [115] R. Shen, W. Zhang, Y. Yuan, G. He, H. Chen, Electrochemical detection of bisphenol A at graphene/melamine nanoparticle-modified glassy carbon electrode, *J. Appl. Electrochem.* 45 (2015) 343–352. doi:10.1007/s10800-015-0792-5.